Synthesis and New Characterization Method of Silicalite-1 Membranes for Gas Separation

Shaaima Al-Akwaa

Thesis submitted to the University of Ottawa
in partial fulfillment of the requirements for the Degree of Master
of Applied Science in Chemical Engineering

Department of Chemical and Biological Engineering
Faculty of Engineering
University of Ottawa

STATEMENT OF CONTRIBUTIONS OF COLLABORATORS AND/OR CO-AUTHORS

I hereby declare that the work presented here is my own effort, and I am the sole author of this thesis. I performed all the experiments and analysis unless stated otherwise under the scientific supervision of Dr. F. Handan Tezel, and Dr. Boguslaw Kruczek. I have acknowledged other sources of information and assistance in analyses where applicable. My research project supervisors Dr. F. Handan Tezel, and Dr. Boguslaw Kruczek provided the editorial and scientific reviews of this research.

In Chapter 2, Dr. David Carter and I fabricated the membranes and performed gas permeation experiments. Dr. Carter put the idea forward, which I modified and completed the assessment.

In Chapter 3, the membranes' fabrication and conducting permeation experiments were done by Dr. David Carter and I. The original idea of the characterization of defect-containing membranes was proposed by Dr. Carter. However, I refined the idea and generated most of the experimental data. More importantly, instead of focusing on transport diffusivities, which depend on the experimental pressure, I went one step further and determined the corresponding corrected diffusivities. The latter is the zeolite's intrinsic properties. Minimal variation of corrected diffusivity of a given gas regardless of the original membrane performance and the experimental feed pressure proves the new characterization method's validity.

In Chapter 4, Dr. David Carter and I fabricated the membranes. Dr. Carter, James Penny and I conducted permeation experiments. I proposed the third set of gas permeation tests after sealing the glazed ends of the membrane with Torrseal epoxy. I also developed the new set of rate equations, the solution of which gives the modified structural parameters of the membrane.

ABSTRACT

Zeolite membranes have great potential in gas separation applications because of their unique selective properties. The main challenge is in synthesizing defect-free zeolite membranes. In this study, we synthesized silicalite-1 zeolite membranes on ceramic supports composed of Al_2O_3 and TiO_2 using the pore-plugging method. We investigated the effect of the fill-level in the autoclave during the synthesis on the membrane performance. In particular, we were interested in determining the conditions at which the defects' contribution to the total transport is minimized. We adopted and further developed the approach proposed by Carter (2019) to quantify the permeance contribution through defects. Comparing the membrane performance before and after calcination, we proposed several modifications to the original analysis of Carter (2019). Knowing the defect transport contribution, we determined the corrected diffusivity, an intrinsic property of zeolite crystals at a given temperature, of several adsorbed gases on silicalite-1 crystals.

The defect's contribution decreased as the autoclave fill-level increased from 94 to 98%. A further increase in the autoclave fill-level introduced more defects and caused the autoclave lid to rupture. Despite the differences in the membranes' performance arising from the autoclave fill-level, the corrected diffusivities of CO_2, CH_4, and N_2 in silicalite-1 showed minimal variation from membrane to membrane. This proves the validity of the proposed characterization method. Moreover, the reported corrected diffusivities are comparable to the literature's values, found using other characterization methods. However, none of the previously used methods is as simple and straightforward as the one we further developed in this study.

RÉSUMÉ

Les membranes zéolites ont beaucoup de potentiel dans les applications de séparation de gaz en raison de leurs propriétés sélectives uniques. Le principal défi consiste à synthétiser des membranes de zéolite sans défaut. Dans cette étude, nous avons synthétisé des membranes de zéolite silicalite-1 sur des supports céramiques composés d'Al_2O_3 et TiO_2 en utilisant la méthode de synthèse “colmatage des pores (pore plugging)”. Nous avons étudié l'effet du niveau de remplissage dans l'autoclave pendant la synthèse des membranes sur leurs performances. En particulier, nous étions intéressés à déterminer les conditions de synthèse dans lesquelles la contribution des défauts au transport total au travers des membranes est minimisée. Nous avons adopté et développé davantage l'approche proposée par Carter (2019) pour quantifier la contribution des défauts à la perméance des membranes. En comparant les performances de la membrane avant et après calcination, nous avons proposé plusieurs modifications à l'analyse originale de Carter (2019). En connaissant la contribution des défauts au transport membranaire, nous avons pu déterminer la diffusivité corrigée, qui est une propriété intrinsèque des cristaux de zéolite à une température donnée, de plusieurs gaz adsorbés sur des cristaux de silicalite-1.

La contribution des défauts au transport membranaire a diminué à mesure que le niveau de remplissage de l'autoclave augmentait de 94 à 98%. Une augmentation supplémentaire du niveau de remplissage de l'autoclave a introduit plus de défauts et a provoqué la rupture du couvercle de l'autoclave. Malgré les différences de performances des membranes résultant du niveau de remplissage de l'autoclave, les diffusivités corrigées du CO_2, du CH_4 et du N_2 dans la silicalite-1 ont peu variées d'une membrane à l'autre. Cela renforce la validité de la méthode de caractérisation proposée. De plus, les diffusivités corrigées rapportées dans cette étude sont comparables aux valeurs que l’on retrouve dans la littérature, qui ont été obtenus en utilisant d'autres méthodes de caractérisation. Cependant, aucune des méthodes précédemment utilisées n'est aussi simple et directe que celle que nous avons développée davantage dans cette étude.

ACKNOWLEDGMENTS

Foremost I would like to express my deep gratitude for my supervisors Dr. Handan Tezel and Dr. Boguslaw Kruczek for their support and guidance through this journey. Your passion and enthusiasm kept me constantly engaged in my research, and I consider myself fortunate to have you as my supervisors.

My gratitude also extends to the technical and administrative staff in the department of Chemical and Biological Engineering in University of Ottawa: James MacDermid, Gerard Nina, Franco Ziroldo, Francine Pétrin, Sylvie Saindon and Frantz Célestin.

I would like to thank my sister, Nora for sharing this journey with me. My family and friends back home for their endless support and encouragement, Yunes, Muaadh, Tsneem, Alaa, Haya, Maryam, Thekra, Rouqiah, Shayma, Duaa and Rahma. My friends at the department of Chemical and Biological Engineering, Asma, Hilal, Nilofar, Amir, Sophia, David, Najmeh, Sean, Curtis, Fahad, Tanushree, Azra, Didem, Mohammed and Chris. And a special thank you to Charbel for translating my thesis abstract to French.

DEDICATION

I would like to dedicate this thesis to my parents Bushra and Ahmed for their unconditional love and support. I am forever in debt to you…

TABLE OF CONTENTS

LIST OF FIGURES

LIST OF TABLES

Chapter 1

Global Introduction

1.1. INTRODUCTION

With the increased demand for energy, large amounts of greenhouse gases are released into the atmosphere as fossil fuels remain to be one of the main sources of energy. These gases act as heat traps, causing an increase in global temperatures. The two main gases known to have an immense impact are CO_2 and CH_4 [2]. Therefore, the main method to combat climate change is to cut the emissions from their sources and find cleaner energy sources. While many efforts are put towards increasing energy efficiency, the focus in the short-term is on the separation and sequestration of CO_2 [3].

Gas separation processes include absorption, cryogenic distillation, adsorption and membrane separation [3][4]. Absorption's main cost goes to regenerating the solvent, as it requires high temperatures [3]. Also, the flue gas components can degrade the solvent, increasing the cost to replace it [3]. However, a lot is known about the process, and it provides high purities of CO_2 [3]. Cryogenic distillation is energy-intensive, as it requires low temperatures and high pressures to liquefy carbon dioxide. The liquefied product is of very high purity and is ready for transportation or sequestration [2]. Adsorption requires a minimum of two simultaneous operating units for adsorption and regeneration. Regeneration could occur by PSA (pressure swing adsorption) or TSA (temperature swing adsorption). However, the pressure and temperature required are not as large as the previous two processes. The CO_2 purity largely depends on the adsorbent used. Membrane separation mainly requires a compressor and a membrane module [3]. Compared to the previously mentioned processes that require multiple units, membrane separation is the simplest. There are also no moving parts in the process, making it compact. However, the main drawback of the membrane system is the trade-off between purity and quantity. Membranes are used in this study for their great potential in gases separation.

Membranes are semi-permeable barriers that preferentially transport one type of molecules from a feed gas mixture. To achieve separation, they are placed in housing modules to segregate the streams. The stream passing through the membrane is called the permeate, as shown in Figure 1.1. Depending on the membrane's selectivity, the required

product is collected either at the permeate or the retentate side. The membrane's performance is measured by permeance, which is the flux normalized by the pressure differential across the membrane. The selectivity is defined as the ratio of the permeances of gases tested. For pure and binary component tests, the selectivity is identified as ideal selectivity and perm-selectivity, respectively.

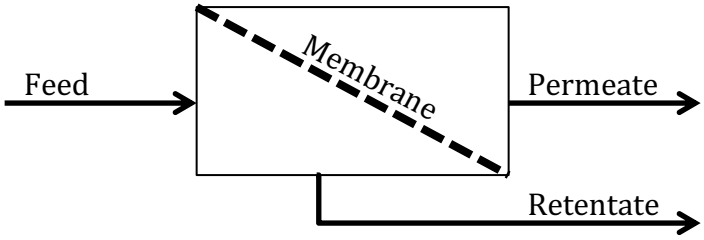

Figure 1.1. Schematic representation of a membrane cell with the inlet stream (feed) and the outlet streams (permeate and retentate).

There are three types of membranes, organic, mixed matrix and inorganic. Organic (polymeric) membranes are cheaper, have good selectivity and permeance, are easy to synthesize and are mechanically stable [4]. However, they are not resilient at high temperatures [4]. Gas transport in organic membranes is governed by a solution-diffusion mechanism. Mixed matrix membranes (MMM) combine the properties of organic and inorganic materials. The permeance and perm-selectivity are enhanced by adding inorganic materials as fillers to the polymers [5]. Nonetheless, MMM use is restricted by the polymer's thermal and chemical limitations [1].

Inorganic membranes include activated carbons, MOFs (metal-organic frameworks) and zeolites. They are more resilient under harsher conditions compared to organic membranes. Gas separation by inorganic membranes is achieved by molecular sieving and/or selective adsorption. Activated carbons have broad pore size distributions, and therefore separation is attained only by adsorption. MOFs consist of inorganic cores and organic linkers, forming three-dimensional structures [6]. However, they are usually less stable than zeolites [6]. Their flexible structure allows the pore size distribution to vary [7]. On the other hand, zeolites have a very narrow pore size distribution. They are made out of aluminosilicates, which are thermally [7][6] and chemically stable [8]. However, zeolites are not mechanically stable on their own as membranes. Therefore, they are deposited on supports that are made out of metal, glass or ceramic materials.

For the application of CO_2 removal from humid flue gas, the membrane needs to be hydrophobic, chemically and mechanically stable. To get high performing systems, the zeolite in the membrane needs to be hydrophobic to prevent water from blocking the pores. The size and shape of the pores depends on the basic units that make-up the structure. Over 253 frameworks have been reported by the Structure Commission of the International Zeolite Association [9]. Silicalite-1 has an MFI framework that is build up by SiO_4 rings. The MFI structure belongs to the pentasil zeolite family; since its main building blocks are 5-membered oxygen rings [6]. These rings form channels with 10-membered oxygen rings, as shown in Figure 1.2 [6]. The structure has straight and zigzag channels with pore sizes of 5.3 x 5.6 Å and 5.1 x 5.5 Å, respectively [10]. Silicalite-1 is a hydrophobic zeolite analogous to ZSM-5 in its MFI structure and has a Si/Al ratio greater than 1000 [6]. This reduction in aluminum cations gives Silicalite-1 its hydrophobic nature.

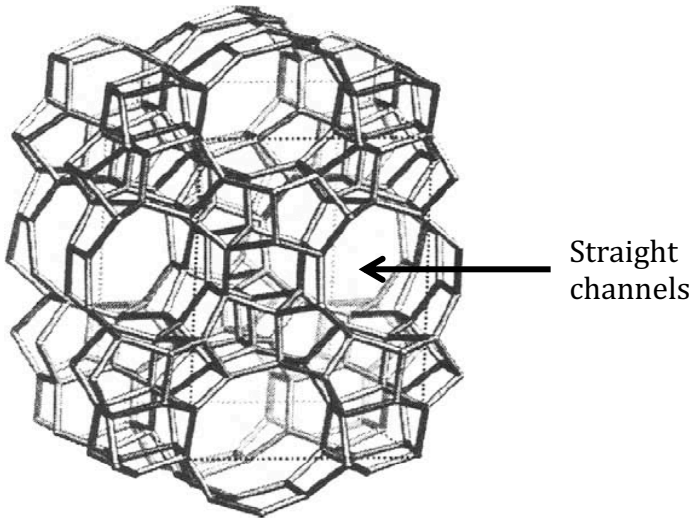

Figure 1.2. MFI framework viewed along the plane [010], showing the straight channels [10].

Silicalite-1 has an average pore size of 5.5 Å, and therefore, CO_2 with a kinetic diameter of 3.3 Å can easily penetrate through these pores. Also, the adsorption affinity of silicalite-1 towards carbon dioxide is high compared to other gases. Therefore CO_2 travels through the zeolite pores by surface diffusion. This transport dramatically depends on the adsorption isotherm and the molecule's mobility. Contrary to polymeric membranes, zeolite membranes have higher perm-selectivity values than the ideal selectivity for carbon dioxide and nitrogen, which is due to their competitive adsorption. Adsorbed carbon

dioxide molecules block the adsorption sites preventing other gasses from entering the membrane. Figure 1.3 shows the adsorption isotherms of some of the common gases found in flue gas by silicalite-1 crystals at 22℃. The adsorption of CO_2, CH_4 and N_2 gases by silicalite-1 is by physisorption. Consequently, the membrane can be regenerated by an increase in temperature or a decrease in pressure.

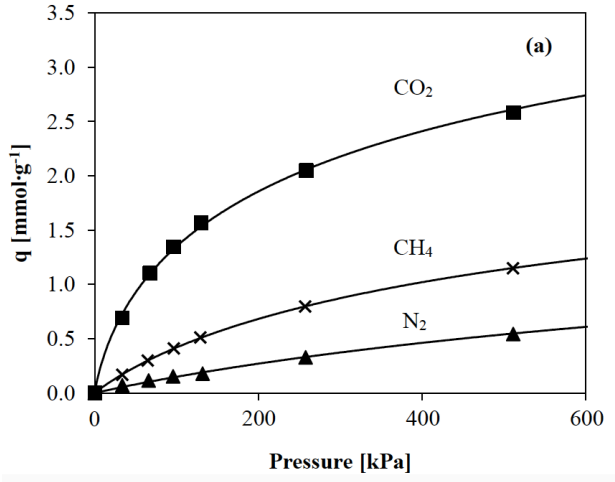

Figure 1.3. Adsorption isotherm for single-component gases on silicalite-1 crystals at T=22℃ [11].

Since silicalite-1 is not mechanically stable as a membrane, it requires support. Porous ceramic supports have a closer thermal expansion coefficient to aluminosilicates compared to metal supports. The two common shapes for membrane supports are tubular and flat. The tubular module has a high volume to area ratio. Therefore, tubular ceramic supports are used in this study. Even though ceramic tubular modules are expensive, they can withstand high pressures and large flow rates [12].

Zeolite membranes are synthesized hydrothermally in an autoclave. There are two main types of synthesis procedures: pore plugging and secondary growth. The former, as the name suggests, deposits zeolite crystals within the ceramic support plugging its pores. Whereas, the latter focuses on forming a zeolite layer above the ceramic support. Pore plugging is a simple one-step process compared to, secondary growth where the crystals are first seeded then deposited on the surface of the support to allow for growth. The one-step process in pore plugging includes filling a Teflon lined autoclave with a precursor solution containing silica and baking it with tubular ceramic supports. The amount of

precursor solution in the Teflon beaker or the autoclave fill-level determines the overhead volume. The effect of varying the autoclave fill-level during the synthesis is investigated in this thesis. Another advantage of pore plugging is the size restriction of the defect pores. The defect pores are limited by the support pore size thus, the resulting membrane contains relatively smaller defects. Consequently, in this study we synthesize silicalite-1 membranes by pore-plugging.

Current challenges with zeolite membranes include the high cost of the membranes and presence of defects within the membrane. For zeolite membranes to be commercialized their cost needs to be reduced by ten-folds [12][13][14]. The defects present within the selective layer decrease the membrane selectivity as they offer a low resistance pathway for gases to transport. Defects form when the pores of the support are not plugged with zeolite crystals which, is mainly due to two reasons: incomplete plugging of the membrane support during synthesis and difference in thermal expansion of the zeolite crystal and support [15][16][17]. Using support that has a similar thermal expansion coefficient to the zeolite can reduce the latter's effect and slow the rate of heating or cooling applied to the membrane during calcination. A thermal break is introduced during hydrothermal synthesis to allow the precursor solution to diffuse back to the support [17]. This is to ensure the availability of precursor solution for further crystal growth.

The hypothesis of this thesis is that the autoclave fill-level during hydrothermal synthesis affects the membrane's quality and performance. Thus, four batches with different fill-levels were synthesized, and their performances were assessed. The main objective of this thesis is to minimize the defects in silicalite-1 membranes prepared on tubular support using pore-plugging procedure with a thermal break. To further assess the defects in the membrane, the characterization model developed by a former PhD student [1] is used to obtain structural parameters and diffusivity values. The model was further developed to acquire intrinsic properties of silicalite-1 zeolite namely, corrected transport diffusivities. In addition, the effect of different sealants used to connect the membrane to the housing module is investigated. Finally, one of the critical outcomes of this work is modifying the previously developed model for the characterization of defect-containing membranes. That allowed us to understand the limits of the model, for further development.

1.2. THESIS STRUCTURE

The thesis consists of 5 chapters, with the current one as the first.

Chapter 2- *Effect of autoclave fill level during membrane fabrication on the quality of silicalite-1 membranes*

This chapter studies the effect of autoclave fill level during synthesis of silicalite-1 membrane. Four batches with four membranes were fabricated. The membranes were assessed on their performance by calculating their permeances and selectivity. Four gases were used for the analysis; nitrogen, helium, carbon dioxide and methane. This chapter was presented as an oral presentation during the 69th Canadian Chemical Engineering Conference held in Halifax, NS in 2019.

Chapter 3- *The New Characterization Method of Defect-containing Zeolite Membranes.*

This chapter arises from the characterization method proposed by Dr. David Carter, which was adapted and modified in this research. The method requires two sets of gas permeation tests with two gases, before and after membrane calcination, and the knowledge of adsorption isotherms of the two gases on the zeolite that forms the membrane. The method distinguishes the transport through the zeolite crystals from the defect transport. Consequently, it allows the determination of membrane structural parameters and the corrected diffusivity of gases, which is an intrinsic property of zeolites. This chapter has been submitted to the Journal of Membrane Science.

Chapter 4- *Modification of In-Situ Characterization Model*

This chapter presents another modification of the characterization method proposed by Dr. Carter. Recognizing that membrane defects could also originate from the membrane seal, the third set of gas permeation tests was proposed. These tests were performed after sealing the membrane's glazed ends using a Torrseal epoxy. The existence of defects in the glazed ends of the membranes was confirmed experimentally. However, solving the resulting set system of equations did yield reasonable structural parameters. In some cases, negative values were obtained. The third set of gas permeation tests required another membrane module, which was designed and manufactured for this purpose.

Chapter 5- *Conclusion*

This chapter presents the overall summary of the previously presented chapters, contributions to original work and recommendations.

Appendix I- Tabulated permeances of all pure gases

Appendix II- Postulated modified characterization models

Appendix III- Process hazard analysis

1.3. NOMENCLATURE

Abbreviations

N_2	Nitrogen
CO_2	Carbon Dioxide
CH_4	Methane
MMM	Mixed Matrix Membrane
MFI	Mordenite Framework Inverted
MOF	Metallic Organic Framework
MFC	Mass Flow Controller
PSA	Pressure Swing Adsorption
TSA	Temperature Swing Adsorption

1.4. REFERENCES

[1] D. Carter, Fabrication and Characterization of Silicalite-1 Membranes for the Separation of the Greenhouse Gases, (2019). Ph.D. thesis, University of Ottawa, Ottawa

[2] M. Pera-Titus, Porous inorganic membranes for CO2 capture: Present and prospects, Chem. Rev. 114 (2014) 1413–1492. https://doi.org/10.1021/cr400237k.

[3] D. Aaron, C. Tsouris, Separation of CO2 from flue gas: A review, Sep. Sci. Technol. 40 (2005) 321–348. https://doi.org/10.1081/SS-200042244.

[4] M. Songolzadeh, M. Soleimani, M. Takht Ravanchi, R. Songolzadeh, Carbon dioxide separation from flue gases: A technological review emphasizing reduction in greenhouse gas emissions, Sci. World J. 2014 (2014) 34. https://doi.org/10.1155/2014/828131.

[5] J. Caro, M. Noack, Zeolite membranes - Recent developments and progress, Microporous Mesoporous Mater. 115 (2008) 215–233. https://doi.org/10.1016/j.micromeso.2008.03.008.

[6] J. Kärger, D.M. Ruthven, D.N. Theodorou, Diffusion in Nanoporous Materials, Hoboken: John Wiley & Sons, Weinheim, (2012).

[7] N. Rangnekar, N. Mittal, B. Elyassi, J. Caro, M. Tsapatsis, Zeolite membranes - a review and comparison with MOFs, Chem. Soc. Rev. 44 (2015) 7128–7154. https://doi.org/10.1039/c5cs00292c.

[8] M.P. Bernal, J. Coronas, M. Menéndez, J. Santamaría, Separation of CO2/N2 mixtures using MFI-type zeolite membranes, AIChE J. 50 (2004) 127–135. https://doi.org/10.1002/aic.10012.

[9] C. IZA Structure, Database of zeolite structures, Available Http//Www. Iza-Structure. Org/Databases/Accessed June. 25 (2012) 2017. http://www.iza-structure.org/databases/.

[10] L.B. McCusker, D.H. Olson, C. Baerlocher, Atlas of Zeolite Framework Types, in: C. Baerlocher, W.M. Meier, D.H.B.T.-A. of Z.F.T. Olson (Eds.), Atlas Zeolite Framew. Types, Elsevier, Amsterdam, 2007: pp. 184–185. https://doi.org/10.1016/B978-0-444-53064-6.X5186-X.

[11] D.A. Kennedy, D. Carter, S. Wilson, B. Kruczek, F.H. Tezel, Pore plugging synthesis and characterization of silicalite-1 membranes using tubular TiO2 supports: Effect of support pore size on membrane performance, Can. J. Chem. Eng. 96 (2018) 1597–1611. https://doi.org/10.1002/cjce.23095.

[12] R. Baker, Membrane Technology and Applications, 3rd ed., Wiley, New York, (2012).

[13] N. Mittal, Process Modeling and Techno-Economic Analysis of Zeolite Membrane Separation Processes, (2018). Ph.D. thesis, University of Minnesota, Minneapolis.

[14] G.W. Meindersma, A.B. De Haan, Economical feasibility of zeolite membranes for industrial scale separations of aromatic hydrocarbons, Desalination. 149 (2002) 29–34. https://doi.org/10.1016/S0011-9164(02)00687-2.

[15] M. Pan, Y.S. Lin, Template-free secondary growth synthesis of MFI type zeolite membranes, Microporous Mesoporous Mater. 43 (2001) 319–327. https://doi.org/10.1016/S1387-1811(01)00212-8.

[16] J. Dong, Y.S. Lin, M.Z.C. Hu, R.A. Peascoe, E.A. Payzant, Template-removal-associated microstructural development of porous-ceramic-supported MFI zeolite membranes, Microporous Mesoporous Mater. 34 (2000) 241–253. https://doi.org/10.1016/S1387-1811(99)00175-4.

[17] Y. Li, M. Pera-Titus, G. Xiong, W. Yang, E. Landrivon, S. Miachon, J.A. Dalmon, Nanocomposite MFI-alumina membranes via pore-plugging synthesis: Genesis of the zeolite material, J. Memb. Sci. 325 (2008) 973–981. https://doi.org/10.1016/j.memsci.2008.09.030.

CHAPTER 2

Effect of Autoclave Fill-Level during Membrane Fabrication on the Quality of Silicalite-1 Membranes

S. Al-Akwaa, D. Carter, F.H. Tezel, B. Kruczek

University of Ottawa, Department of Chemical and Biological Engineering

161 Louis Pasteur, Ottawa, Ontario, CANADA, K1N 6N5

ABSTRACT

In this research, the effect of increasing the autoclave fill level during the hydrothermal synthesis of silicate-1 zeolite membranes using the pore-plugging method, was investigated. Four autoclave fill levels ranging from 94% to 99% were studied. The membrane performance was assessed based on N_2 and He permeances and their ratio, determined before and after membrane calcination, and after additional sealing of the calcined membranes with an epoxy. The quality of the membranes improved as the autoclave fill level increased from 94% to 98%. However, a further increase to 99% led to the autoclave lid's rupturing and more defects than at the 98% level, particularly in the resulting membranes' glazed ends. Despite the defects due to incomplete pore plugging and partial deterioration of the membranes' glazed ends, all membranes after calcination were nitrogen selective. This indicates gas transport in the resulting membranes was dominated by surface diffusion of nitrogen and Knudsen diffusion of helium in the silicalite-1 crystals forming the selective layer of the membrane.

Keywords: Zeolite, Silicalite-1, Membranes, Pore-plugging synthesis, Autoclave fill-level

HIGHLIGHTS

- Effect of autoclave fill-level during synthesis on membrane performance.
- An autoclave fill level of 98% leads to the best quality of membranes.

2.1. INTRODUCTION

Zeolite membranes have gained worldwide attention in the previous years due to their interesting abilities in liquid and gas separation [1][2]. Silicalite-1 is a zeolite that has a narrow pore size distribution and an ability to selectively adsorb gas species. Silicalite-1 has an MFI framework with elliptical 5.3 x 5.6 Å straight channels interconnected to 5.1 x 5.5 Å sinusoidal channels [3]. For gas separation, zeolite crystals are used as pellets in adsorption beds or are grown on membrane supports. Adsorption beds operate in a semi-batch process that requires at least two beds. At the same time, membranes operate in a continuous process that is easy to install and scale-up.

Zeolite membranes require porous support, as they cannot be self-supported. A common practice is to deposit and grow crystals on porous supports. The porous support provides mechanical stability, while the zeolite layer provides selective properties. Different types of porous supports have been reported in the literature. The main types include stainless steel and alumina [4][5]. TAMI Industries (Nyons, France) porous supports consist of three layers an active layer, intermediate layer and porous support. The active layer contains titanium and zirconium oxides, which generally do not integrate into the zeolite structure [6][7].

In-situ pore plugging and secondary growth are two main methods for the synthesis of silicalite-1 membranes [8]. Pore plugging is a one-step process where the membrane support is immersed in a precursor solution containing silica gel. By hydrothermal synthesis, the crystals deposit within the supports' pores and grow, thereby plugging the pores. Secondary growth is a two-step process where the crystals are first made and used as seeds. The crystals are dispersed on the support and allowed to grow and form a zeolite layer. The resulting difference between these two methods is the selective layer. It is within the support for the former, whereas, it is on top for the latter, as shown in Legend:

Figure 2.1. Below the active layer of the porous support the pore size is too large for the crystals to grow and plug the pore. Thus the depth of the selective layer can be controlled and it is estimated to be the depth of the active layer.

The main challenge of silicalite-1 membranes, and zeolite membranes, in general, is the presence of intercrystalline non-zeolite pores that lower the membrane selectivity.

These defects originate from incomplete growth of crystals [7] and the difference in thermal expansion between the support and the crystals during calcination [4][9][10]. A template is used during synthesis to direct the structure of the crystals. It also binds to the crystals, thereby blocking the pores. Therefore, the template must be removed in a thermal process, often referred to as calcination, which requires a temperature of 500°C or higher. Many studies have reported template-free synthesis using the secondary growth method [8][11]. Secondary growth is the most commonly used method. However, the pore plugging method, developed by Dalmon's group [12][13], has many advantages. Pore plugging provides mechanical resistance to the membrane and ensures the confinement of any defects or cracks to the pores' size. The zeolite layer thickness is controlled by the thickness of the active layer of the support. It is practically impossible to plug large pores located below the active layer, and the growth on top of the active layer is limited to a few microns [14]. In other words, since the crystal growth is limited to the active layer of the support, the thickness of the selective layer cannot exceed that of the active layer. Therefore, with TAMI's ceramic support, the membrane's maximum thickness ranges from 3 to 10 µm [14]. In contrast, using secondary growth method, the thickness can vary from 0.5 µm [15][16] to more than 40 µm [17].

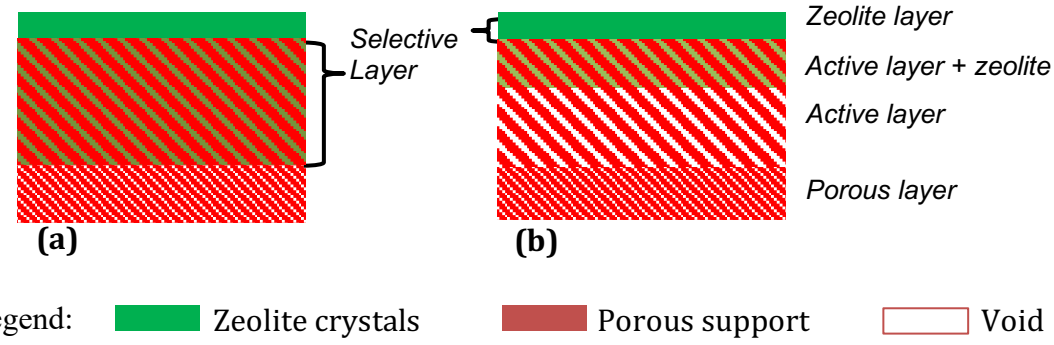

Figure 2.1. Illustration of the selective layer in porous support by TAMI Industries of a membrane synthesized by **(a)** Pore-plugging **(b)** Secondary growth method.

In previous research, the effect of different parameters on the zeolite membrane performance was studied. These include pore size of the support [7][14], zeolite film thickness [16], synthesis temperature [18], calcination rate [16], precursor composition [19] and template material [19]. However, the effect of the autoclave fill-level during

hydrothermal synthesis has not been reported. We hypothesize that at high autoclave fill-levels, the crystals deposit and grow more effectively, reducing the number of defects due to incomplete crystal growth. More specifically, by increasing the autoclave fill-level, the overhead space available for the vapours to occupy decreases. Thus the pressure and temperature increase. In turn, gas solubility might also increase, shifting the precursor solution's equilibrium [20]. Four membrane batches were synthesized at different autoclave-fill levels, and their gas permeation performance was asssessed.

2.2. THEORETICAL BACKGROUND

Figure 2.2 illustrates three types of flow transport that are present when gases permeate across zeolite membranes. The type of flow depends on the type and size of the pore and the permeating specie. In general, as shown by Equation (2.1), the total gas permeation is a combination of different transport mechanisms. Before calcination, the template binds to the zeolite structure and blocks the zeolite pathway. However, after calcination, the template is assumed to be removed entirely, and the zeolite channels open [8]. Consequently, any gas permeation across the membrane before it is calcined indicates the presence of the defects. Since the defects are relatively large, gas can permeate by the viscous flow and Knudsen diffusion simultaneously. The viscous flow occurs when the collisions between gas molecules are more frequent than those between gas molecules and the pore walls. When the opposite occurs, Knudsen diffusion prevails. As seen in Equation (2.2), the viscous flow is non-selective as all gas molecules move at the same average velocity. The Knudsen diffusion flux is selective and proportional to the inverse square root of the molecular weight of the permeating gas as shown in Equation (2.2). After calcination, the zeolite pores are open, and the adsorption sites become available. In the zeolite pores, the adsorbed gas molecule hops from one adsorption site to the other, and this process is referred to as a surface diffusion [21]. The surface diffusion is controlled by the mobility of the gas (diffusivity) and equilibrium affinity of the adsorbent. Equilibrium adsorption isotherms of a gas describe the latter. Figure 2.3 presents the adsorption isotherms of CO_2, CH_4 and N_2 on silicalite-1 crystals at 22^oC where the experimental data points are fit using Sips model by Kennedy et al. [7].

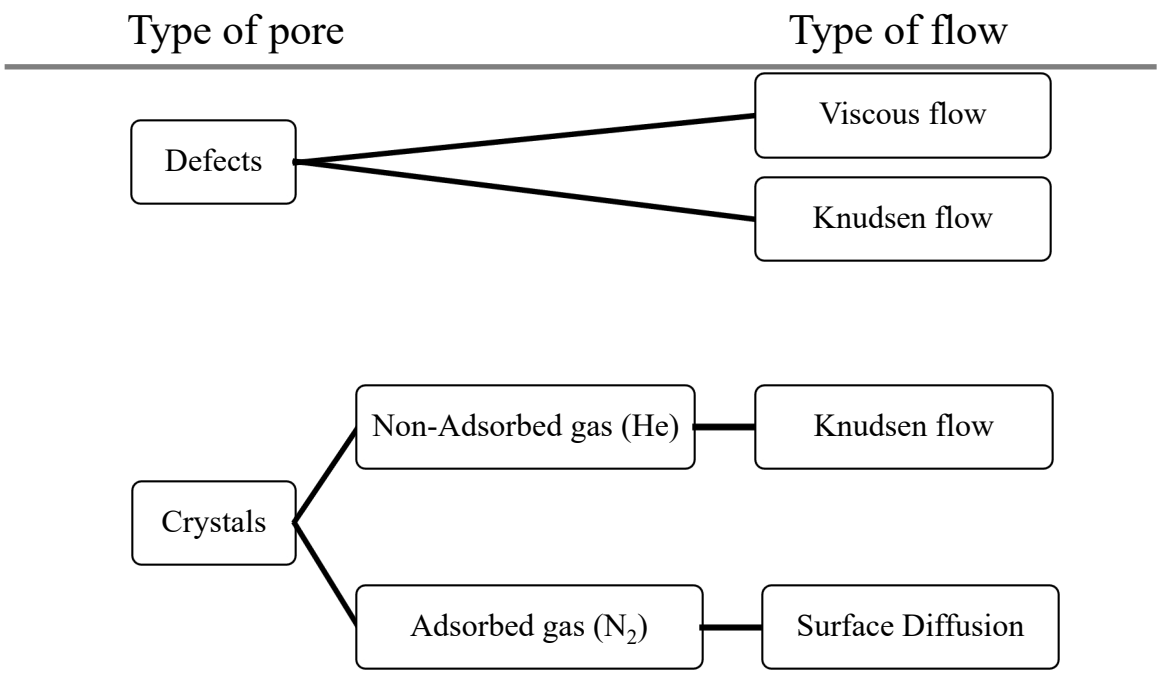

Figure 2.2. Different types of flow corresponding to pore type.

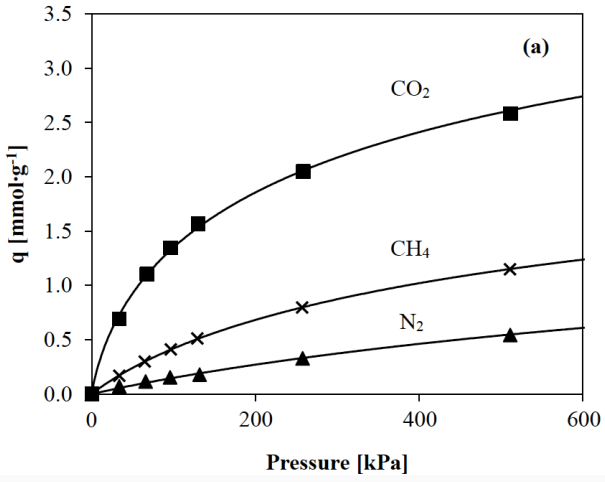

Figure 2.3. Adsorption isotherm for single-component gases on silicalite-1 crystals at T= 22°C [7].

Gas transport through zeolite pores can occur by surface or Knudsen diffusion, or a combination of both. The mechanism of gas transport depends on the affinity of the adsorbent to the gas molecule and the type and size of the zeolite pore. Therefore, to analyze a membrane, single gas permeation experiments are done with two gases; non-

adsorbed and adsorbed gas to silicalite-1. In the case of silicalite-1, helium does not get adsorbed at ambient temperatures and therefore, it can be used as a non-adsorbed gas [22]. On the other hand, as seen in Figure 2.3, nitrogen is adsorbed on silicalite-1, and therefore, it can be used as an adsorbing gas.

The total permeance could be divided into the zeolite permeance (P_z) and defect permeance (P_d). The zeolite permeance can be further split into surface diffusion permeance ($P_{z,SD}$) and Knudsen diffusion permeance ($P_{z,K}$). Similarly, the defect permeance can be split into viscous flow permeance ($P_{d,v}$) and Knudsen diffusion permeance ($P_{d,K}$).

$$P_i = P_z + P_d = P_{z,SD} + P_{z,K} + P_{d,K} + P_{d,v} \tag{2.1}$$

Using rate equations for each mode of gas transport, Equation (2.1) can be re-written as [23]:

$$P_i = \underbrace{y\left(\frac{q_h - q_l}{p_h - p_l}\right)\rho D_T}_{\text{Surface diffusion}} + \underbrace{\frac{y d_z}{3}\sqrt{\frac{8}{\pi MRT}} + \frac{x d_d}{3}\sqrt{\frac{8}{\pi MRT}}}_{\text{Knudsen}} + \underbrace{x {d_d}^2\left(\frac{p_h + p_l}{64\mu RT}\right)}_{\text{Viscous}} \tag{2.2}$$

where, $y = \varepsilon_z / l_z$ the void fraction of the crystals over the effective length of the crystal pore, p_h and p_l are the pressures at the high and low pressure sides, respectively, q_h and q_l are the quantities adsorbed at p_h and p_l, respectively, ρ is the density of the zeolite, D_T is the transport diffusion, $x = \varepsilon_d / l_d$ is similar to y but for defect pores, d_d is the defect pore diameter, μ is the viscosity of gases, R is the gas constant, T is the absolute temperature, and M is the molecular weight of the gas. Note that viscous flow has the summation of the high and low pressures to account for the expansion of the gas moving down the pressure gradient.

2.3.EXPERIMENTAL

2.3.1. Membrane Fabrication

The membrane synthesis protocol is adapted from a previous study by Carter [23]. The membranes were produced in batches of four. A 6 cm Filtanium™ tubular ceramic membrane support (TAMI Industries, Nyons, France) was first glazed using a

homogeneous solution formed by mixing 2:1 weight ratio of Aremco 617 glaze (Aremco Products Inc, Valley Cottage, NY, USA) and water. The glazing solution was applied evenly on the axial faces and radial surface 1 cm from the ends. The application of a glazing solution was facilitated by attaching the membrane supports to a rotating motor. A heating lamp was used to speed up the drying process. Once the membrane supports were glazed, they were cured using the following program. First, they were heated at the rate of 2^{o}C/min up to 300 ^{o}C. After two hour-period at 300 ^{o}C, they were further heated to 875 ^{o}C and kept at that temperature for one hour. Then, they were let to cool down to ambient temperature. The process was repeated to apply five coatings of the glaze.

To synthesize silicalite-1 crystals, we first prepared a precursor solution. 12 g of 99.8 % pure silica (Sigma-Aldrich, Oakville, ON, Canada) was mixed with 10 mL of deionized water and 90 mL of 1 M tetrapropylammonium hydroxide (TPAOH) solution (Sigma-Aldrich, Oakville, ON, Canada) inside of a Teflon (polytetrafluoroethylene) beaker. The resulting solution had the following molar composition 1.00 (SiO_2): 0.45 (TPAOH): 27.8 (H_2O). The mixture was placed on a magnetic stirrer at speed 7 on Corning magnetic stirrer for 72 hours. Once the solution became homogenous, it was centrifuged for 30 minutes at a speed of 4000 rpm. A 125 mL Teflon beaker and membrane cradle were wiped with the TPAOH solution to remove any impurities. The outer surface of the membrane supports was wrapped with Teflon tape and placed inside the cradle. The cradle was used to ensure the vertical orientation of the supports during the synthesis [24]. The precursor solution was added and left for 6 hours with the membrane supports. The solution was then topped off to the required level and placed in an autoclave where hydrothermal synthesis took place. A summary of the synthesis protocol is shown in Figure 2.4. The heating program consisted of two stages, where the cooling and heating rate was at 1^{o}C/min. The first stage is heating to 170 ^{o}C and a holding period of 12 hours and then cooling off for another 12 hours. This break promotes crystal growth allowing replenishing the pores with silica. The second stage included heating to 170^{o}C and a holding period of 72 hours. After the autoclave was completely cooled off, the membranes were taken out of the oven and placed in deionized water to remove any unused TPAOH. This step was repeated until the pH of the water was neutral. Subsequently, the water was removed by drying the membranes in a Vulcan 3-550 oven.

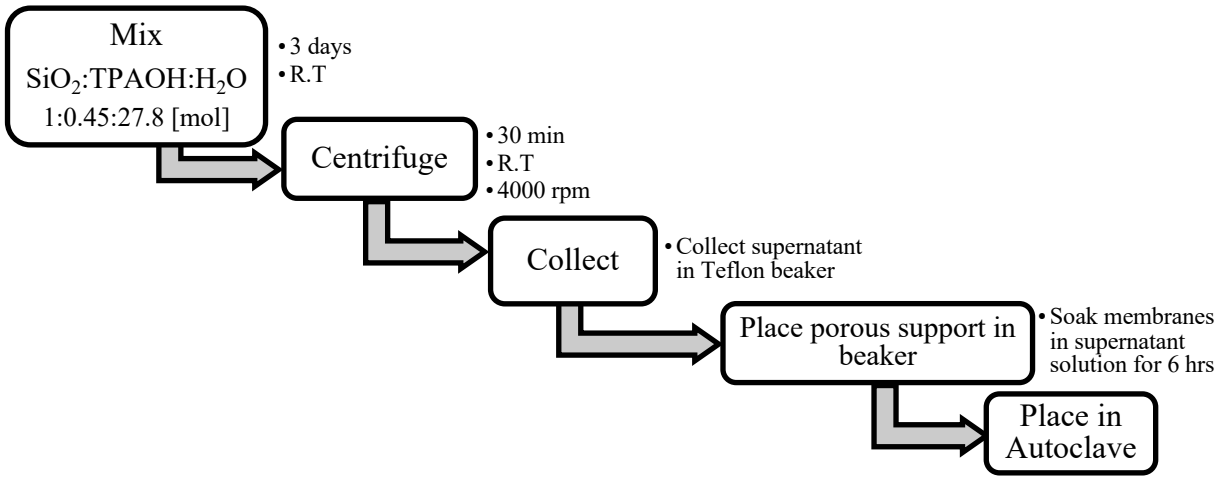

Figure 2.4. Block diagram summarizing the synthesis protocol

The zeolite crystals were deposited in the tubular ceramic support's inner surface, where the active layer was located. During synthesis, the Teflon tape was wrapped around the support's outer surface to prevent silicalite-1 crystals from growing on the outer surface. After synthesis, the tape was removed, but parts of it stuck to the Aremco 617 glazing.

To study autoclave fill–level effects, four different fill-levels, 94, 97, 98 and 99%, were selected. At the 99% level, the autoclave lid ruptured, indicating the autoclave could not withstand the resulting pressure. It would be interesting to know the exact pressure in the autoclave vessel at that point. However, because of the lack of thermodynamic data of TPAOH, the corresponding pressure could not be estimated. Previous attempts to measure the pressure directly inside the vessel were not successful [23].

2.3.2. Membrane modules

The membranes were tested with different gases using two different membrane modules. In the first module (Figure 2.5), the glazed membrane ends (the axial and radial surfaces) formed a seal to prevent the gases from bypassing the selective layer during permeation experiments. The compressive graphite gaskets separated the retentate flow from the permeate flow. Two sets of gas permeation tests (before and after calcination) were performed in the first membrane module. It has been postulated that Aremco 617 could degrade during the hydrothermal synthesis due to the presence of TPAOH at a relatively high temperature and pressure. Consequently, after the two sets of permeation tests, the membranes were removed from the module to seal the glazed

sections with a Torrseal epoxy (Agilent Technologies Inc., Santa Clara, CA, USA). The Torrseal epoxy is a vacuum sealant, which does not emit VOCs, and can withstand temperatures up to 120°C. To perform gas permeation tests with Torrsealed membranes, we used the second membrane module (Figure 2.6), in which the membrane was connected to stainless steel tubes at either end by the Torrseal epoxy.

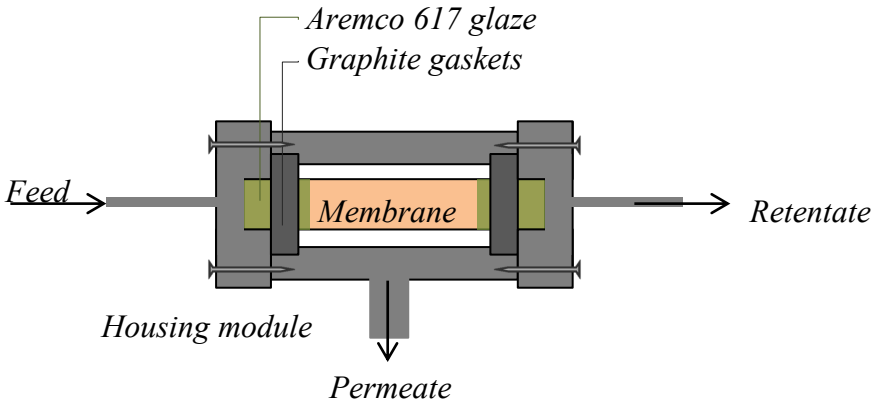

Figure 2.5. Schematic of module 1 with Aremco 617 glazing and graphite gaskets

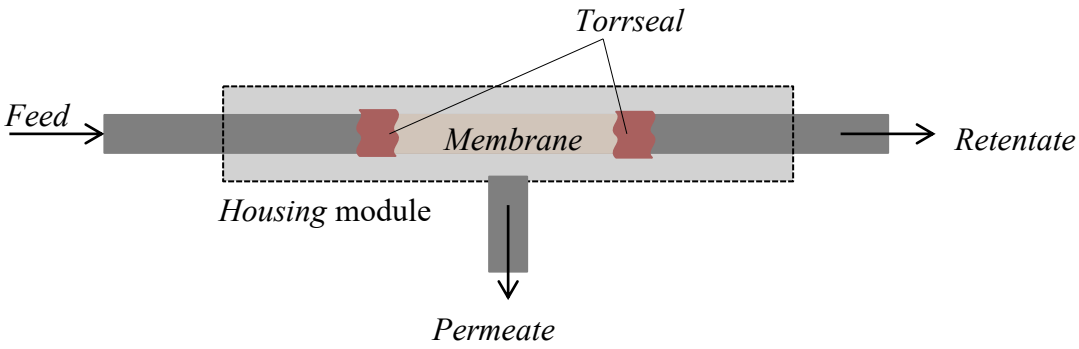

Figure 2.6. Schematic of module 2 with Torrseal epoxy

A coding system to distinguish between different membranes is used. In particular, the fill-level in the autoclave, the type of module (graphite, G or Torrseal, T), the stage at which the membranes were tested (dried, D or calcined, C) and the number of the membrane in a batch. For instance, M94TC1 is membrane 1 from the batch with a fill-level of 94%, the type of sealant used is Torrseal, the membrane is calcined (C), and X will be inserted in the naming when unidentified.

2.3.3 Experimental Procedure

A dry membrane was first installed in the module shown in Figure 2.5 and tested with He and N_2 at three different feed pressures 0.6, 2.0 and 3.3 atm. The membrane was then uninstalled and placed in a programmable oven for calcination at 500℃ with a heating program shown in Figure 2.7. After calcination, it was reinstalled in the same module, and the gas permeation tests were repeated. Following that, the membrane was again removed from the first module, and Torseal was applied on the glazed surfaces and SS tubes. It was then followed by the third set of gas permeation runs with He and N_2 using the module shown in Figure 2.6. An outline for the single gaspermeation experiments is shown in Figure 2.8.

(a) Drying **(b)** Calcination

Figure 2.7. Heating program for **(a)** drying and **(b)** calcination of the membranes

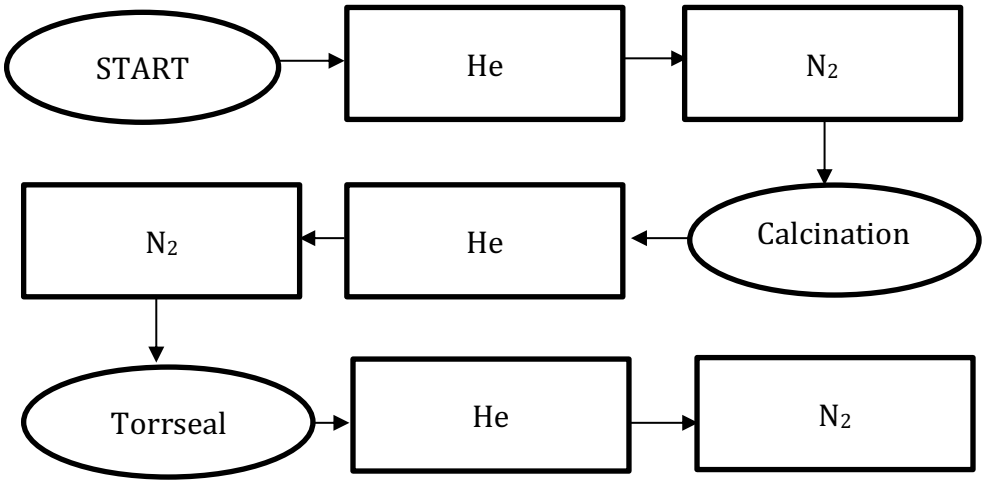

Figure 2.8**.** Gas permeation experiment outline

Figure 2.9 presents a schematic diagram of a gas permeation system. Our testing systems allowed both single and mixed gas permeation experiments; however, we focused only on single gas permeation tests in this project. The feed/retentate flow rate was by the valve V2 and measure using a bubble flow meter F2. The permeation rate was measured using a bubble flow meter F2. The outlets from the bubble flow meters F1 and F2 run into a fume hood. Since we were interested in single gases rather than gas mixtures, the feed gas was delivered to the system either through a mass flow controller MFC1 or MFC2. Although we did not require a gas chromatograph GC, the gas permeation line runs through the GC, which led to backpressure at the permeate side of the membrane. The higher the feed pressure, the higher the permeation rate and the higher the backpressure. In some initial gas permeation runs, the backpressure was as high as 10 psig. We replaced the original 1/16" tubing in the permeate line by 1/4" tubing and bypassed the GC, which practically eliminated the backpressure. In other words, regardless of the feed pressure, the permeate pressure was practically equal to the atmospheric pressure. The membrane module was installed inside an enclosure, in which the temperature is controlled over a range of 21°C - 22°C.

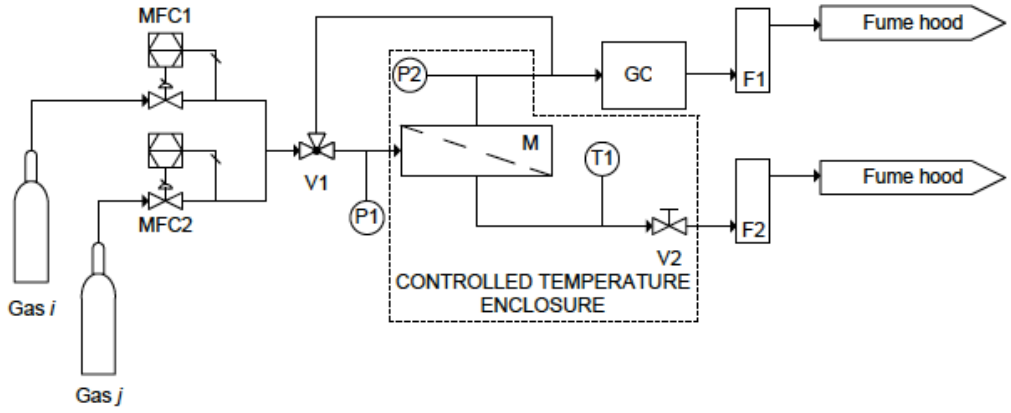

Figure 2.9. Process flow diagram for the setup used to test pure and binary components retrieved from Carter, 2019 [23].

2.3.4. Gas Permeation Experiment Analysis

The membranes were assessed based on their performance in gas permeation tests. A steady-state gas permeation rate was used to calculate membrane permeance (P_i) for different gasses using:

$$P_i = \frac{J_i}{\Delta p_i} \tag{2.3}$$

where J_i the molar flux, Δp_i is the partial pressure difference across the membrane, which for single gases is simply the pressure difference between the feed (p_h) and permeate-side (p_l). The ideal selectivity ($\propto_{i/j}$) represent a ratio of gas permeances determined in separate gas permeation tests:

$$\propto_{i/j} = \frac{P_i}{P_j} \tag{2.4}$$

where P_i and P_j are the permeance for gases *i* and *j*, respectively.

2.4. RESULTS AND DISCUSSION

2.4.1. Single gas permeation experiments before and after calcination

Figure 2.10 shows the results of representative samples from each batch of different autoclave fill-levels. For uncalcined membranes, the permeance of He is greater than that of N_2. Since before calcination, the template is bond to the crystals, the only open pores to permeation are defects. Consequently, defect permeance appears to decrease as the autoclave fill-level increases from 94% to 98%. However, as the autoclave fill level increases further to 99%, the defect permeance slightly increases.

The gas transport through the defects can occur by a combination of Knudsen diffusion and viscous flow. Since the viscous flow is non-selective, the fact that He permeance is higher than N_2 indicates that Knudsen diffusion must contribute to the defect transport. The permeances of both He and N_2 increase with feed pressure. According to Equation (2.3), the Knudsen permeance is independent of feed pressure, but the viscous flow permeance increases with pressure. Consequently, in addition to Knudsen diffusion, the viscous flow must also contribute to the defect transport in membranes depicted in Figure 2.10.

The Knudsen diffusion occurs when collisions between gas molecules and pore walls are more frequent than the collisions between gas molecules themselves. Consequently, Knudsen diffusion is favoured in small defect pores at a given pressure while the viscous flow in large defect pores. In other words, knowing the relative contribution of Knudsen diffusion and viscous flow to the total permeation rate provides information about the size of the defect pores. There are two ways to graphically assess these contributions. The most straightforward way is the comparison of He and N_2 permeances. The more significant the difference between the He and N_2 permeances, the greater the relative contribution of Knudsen diffusion. The second measure is the slope of the gas permeance as a function of feed pressure: the higher the slope, the more significant the contribution of viscous flow to the total gas permeation. Therefore, the membrane depicted in Figure 2.10 (c) (98% autoclave fill level) has the highest contribution of the Knudsen diffusion to the total permeance. In contrast, the membrane depicted in Figure 2.10 (a) (94% autoclave fill level) has the lowest Knudsen diffusion contribution to the total gas permeation through the defects. The contribution of Knudsen diffusion to the total defect permeance coincides with the size of the defects. More specifically, the smaller the pore size of defects, the more significant the Knudsen diffusion's contribution. Therefore, it appears that as the defect permeation increases, it is primarily because of relatively large defects in which viscous flow is the dominating gas transport mechanism.

After membrane calcination, there is a very significant increase in gas permeance of both He and N_2 regardless of the autoclave fill level. The calcination step opens the pores of silicalite-1 crystals, making them accessible to both He and N_2 for permeation. However, the increase in N_2 permeance is more significant than that in He. He is a non-adsorbed gas; consequently, its transport in silicalite-1 pores is limited to Knudsen diffusion. On the other hand, gas transport of N_2 in silicalite-1 at ambient temperature occurs by both Knudsen diffusion and surface flow; the latter must be more significant than the former. It is because all membranes in Figure 2.10 become nitrogen selective. If Knudsen diffusion of N_2 in silicalite-1 pores were significant, the calcined membranes would remain He-selective. The reverse in membrane selectivity after calcination also indicates that surface diffusion permeance of N_2 in 0.55 nm-pore size silicalite-1 crystals

must be considerably greater than Knudsen diffusion permeance of He in the same crystals. According to Equation (2.3), Knudsen permeance is directly proportional to the pore's diameter. On the other hand, surface diffusion permeance is independent of the pore size.

Assuming that all TPAOH is removed after calcination, the corresponding increase in N_2 permeance could be used to measure the number of crystals formed during hydrothermal synthesis. Applying this assumption to Figure 2.10, it appears that the number of crystals increases with the autoclave fill-level from 94% to 98%. However, when the fill level increases further to 99%, the number of crystals decreases but remains greater than for the 97% autoclave fill level. It is important to emphasize that the relationship between the autoclave fill level and the number of crystals is the opposite of the relationship between the autoclave fill level and the defect permeance. Regardless of the autoclave fill level, the porous support used to synthesize membranes by the pore-plugging method was the same. In other words, the space in which crystal could be formed was the same in all cases. Consequently, the more crystals were formed in the support's active layer, the less free space (defects) remained.

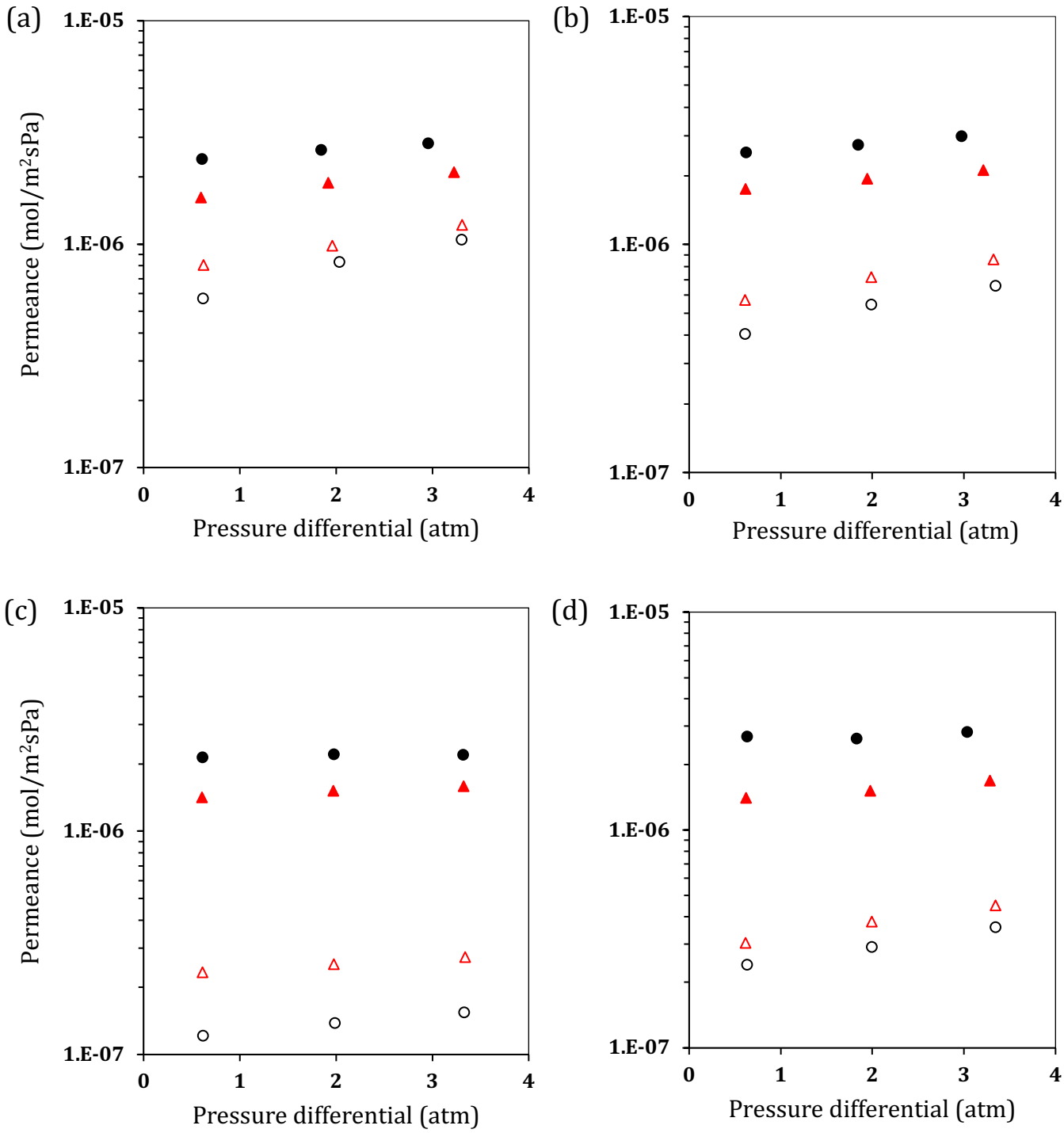

Figure 2.10. Permeance with respect to pressure differential for four membranes with autoclave fill levels in ascending order **(a)** M94GX3 **(b)** M97GX1 **(c)** M98GX2 **(d)** M99GX3. The solid points (He ● and N_2 ▲) are for after calcination, and the hollow points (He ○ and N_2 △) are before calcination of the membrane.

The selected representative from each batch of the autoclave fill level are quantified for all membranes synthesized in this research. The summary is presented in Table 2.1. The first column presents the N_2 permeance of dried membrane (i.e. before membrane calcination) at three different pressure gradients, corresponding to the low, medium and high feed pressures. The second column presents the corresponding ideal N_2/He selectivity of the membranes before calcination. For all membranes, the defect N_2 permeance and the corresponding ideal N_2/He selectivity increase with the pressure. However, the ideal N_2/He selectivity is less than unity in all cases, confirming that all membranes are He-selective before calcination. The fact that the ideal N_2/He selectivity increases with pressure but remains lower than unity confirms the expected increase in the viscous flow contribution as the feed pressure increases. Considering the average values for a given type of membrane at all feed pressure, the previously mentioned relationship between the autoclave fill level and defect permeance is evident. The average N_2 defect permeance for the autoclave fill levels of 94%, 97% and 98% decreases from 9.2 x 10^{-7} to 4.6 x 10^{-7} and 2.1 x 10^{-7} mol s^{-1} m^{-2} Pa^{-1}. However, for the 99% autoclave fill level, the N_2 defect permeance increases to 3.8 x 10^{-7} mol s^{-1} m^{-2} Pa^{-1}. Therefore, it appears that while we were not able to synthesize defect-free membranes in this research, the autoclave fill level of 98% minimized their presence in the synthesized membrane. Not only that, these membranes showed the lowest average ideal N_2/He selectivity before calcination, indicating the lowest contribution of viscous flow to the defect permeance and thus the smallest average pore size of the defects among the four autoclave fill levels.

Columns 3 and 4 in Table 2.1 present the total N_2 permeance after membrane calcination and the corresponding ideal N_2/He selectivity, which now becomes higher than unity. Columns 5 presents the relative increase in the N_2 permeance after calcination, and column 6, the corresponding relative increase in the ideal N_2/He selectivity. As previously discussed, the relative increase in the N_2 permeance after calcination is a measure of the number of crystals formed during hydrothermal synthesis. As expected, the relationship between the autoclave fill level and the relative increase in the N_2 permeance is the opposite of that between the autoclave level the defect permeance. More specifically, the average relative increases in the N_2 permeance for the autoclave fill levels of 94%, 97% and 98% are 2.9, 8.6 and 11.8, respectively. However, when the autoclave fill level increases to 99%,

the relative increase in the N_2 permeance drops to 7.6. It is therefore evident that the autoclave fill level of 98% appears to be the optimum among the four autoclave fill levels considered in this study.

One could expect that the optimum autoclave fill level should lead to the highest ideal N_2/He selectivity after membrane calcination. However, considering the values listed in column 4 of Table 2.1, it is not the case. In general, there is little variation in the ideal N_2/He selectivities, which range from 1.4 for the autoclave fill levels of 94% and 98% to 1.8 for the autoclave fill level of 99%. We assumed that before calcination TPAOH is present only in silicalite-1 crystal. However, it is possible that some TPAOH also exists in small gaps (defects) between the crystals in the active layer. These gaps would also open during membrane calcination. However, unlike the pores inside silicalite-1 crystals, the dominating gas transport mechanism in these gaps would be Knudsen diffusion.

Column 6 in Table 2.1 presents the relative ideal N_2/He selectivity after calcination. The latter is the ratio of the ideal selectivities after and before calcination. Similar to the absolute ideal N_2/He selectivities in column 4, there is a little variation with the autoclave fill level. However, the trend of the relative ideal N_2/He selectivity with the autoclave fill level is the same as that for the relative N_2 permeance. More specifically, as the autoclave fill level increases from 94% to 97% and 98%, the relative ideal N_2/He selectivity increases from 1.6 to 2.3 and 2.4. However, when the fill level increases to 99%, the relative ideal N_2/He selectivity drops to 2.2.

Table 2.1.Permeance[1] and ideal selectivity of nitrogen over helium for dried and calcined membranes synthesized at four different autoclave fill-levels (94%, 97%, 98%, 99%).

Membrane	Pressure	Dried		Calcined		$\frac{P_{N_2}^*}{P_{N_2}}$	$\frac{\alpha_{N_2/He}^*}{\alpha_{N_2/He}}$
		P_{N_2}	$\alpha_{N_2/He}$	$P_{N_2}^*$	$\alpha_{N_2/He}^*$		
M94GX1	ΔP_{low}	7.03	0.81	23.0	1.39	3.3	1.7
	ΔP_{medium}	10.1	0.84	25.4	1.36	2.5	1.6
	ΔP_{high}	13	0.88	28.3	1.33	2.2	1.5
M94GX2	ΔP_{low}	5.72	0.71	24.1	1.49	4.2	2.1
	ΔP_{medium}	8.33	0.84	26.4	1.40	3.2	1.7
	ΔP_{high}	10.5	0.86	28.4	1.35	2.7	1.6

M94GX3	ΔP_{low}	6.75	0.87	21.1	1.44	3.1	1.6
	ΔP_{medium}	9.22	0.90	23.8	1.36	2.6	1.5
	ΔP_{high}	11.7	0.91	26.9	1.31	2.3	1.4
$\bar{x} \mp s.d.$		**9.15±2.42**	**0.85±0.06**	**25.3±2.5**	**1.38±0.06**	**2.9±0.6**	**1.6±0.2**
M97GX1	ΔP_{low}	4.05	0.71	25.3	1.45	6.2	2.0
	ΔP_{medium}	5.46	0.76	27.4	1.41	5.0	1.9
	ΔP_{high}	6.58	0.77	29.9	1.41	4.5	1.8
M97GX2	ΔP_{low}	1.53	0.52	24.0	1.55	15.7	3.0
	ΔP_{medium}	1.67	0.51	25.5	1.56	15.3	3.1
	ΔP_{high}	1.89	0.54	26.4	1.53	14.0	2.8
M97GX3	ΔP_{low}	5.2	0.70	33.4	1.43	6.4	2.0
	ΔP_{medium}	6.95	0.76	36.4	1.41	5.2	1.9
	ΔP_{high}	8.36	0.77	38.2	1.35	4.6	1.8
$\bar{x} \mp s.d.$		**4.63±2.51**	**0.67±0.11**	**29.6±5.2**	**1.45±0.07**	**8.6±4.9**	**2.3±0.5**
M98GX1	ΔP_{low}	2.42	0.57	20.2	1.15	8.3	2.0
	ΔP_{medium}	2.87	0.6	20.8	1.28	7.2	2.1
	ΔP_{high}	3.27	0.62	24.8	1.38	7.6	2.2
M98GX2	ΔP_{low}	1.21	0.52	21.4	1.51	17.7	2.9
	ΔP_{medium}	1.39	0.55	22.1	1.46	15.9	2.7
	ΔP_{high}	1.54	0.56	22.0	1.38	14.3	2.5
$\bar{x} \mp s.d.$		**2.12±0.86**	**0.57±0.04**	**21.9±1.6**	**1.36±0.13**	**11.8±4.6**	**2.4±0.3**
M99GX1	ΔP_{low}	3.33	0.77	24.4	1.83	7.3	2.4
	ΔP_{medium}	4.75	0.82	26.0	1.71	5.5	2.1
	ΔP_{high}	5.93	0.85	27.6	1.63	4.7	1.9
M99GX3	ΔP_{low}	2.42	0.80	26.8	1.91	11.1	2.4
	ΔP_{medium}	2.91	0.76	26.3	1.73	9.0	2.3
	ΔP_{high}	3.59	0.79	28.2	1.68	7.9	2.1
$\bar{x} \mp s.d.$		**3.82±1.30**	**0.8±0.0**	**26.6±1.3**	**1.75±0.10**	**7.6±2.3**	**2.2±0.2**

[1] All permeances in [10^{-7} × mol·s^{-1}·m^{-2}·Pa]

2.4.2. Effect of sealing glazed ends of the membrane

Glazing of the membrane's ends was necessary to prevent the gases from bypassing the selective layer during permeation experiments. Since the proper application of the Aremco 617 glaze required a 1-hour exposure to 875°C, the glazing had to be done before hydrothermal synthesis of silicalite-1 crystal. The latter are not thermally stable at such high temperatures. Consequently, the support membranes' glazed ends were exposed to a

harsh environment, particularly to TPAOH, during hydrothermal synthesis. Moreover, the removal of the Teflon tape from the outer surface of the membrane (used to prevent the deposition of crystals) after hydrothermal synthesis was challenging. And some of the Teflon tape was stuck to the glazing. Although no visible cracks were observed, the process of tape removal could lead to invisible, micro defects in the glazed layer. Therefore, after finishing the gas permeation tests discussed in the previous section, the membrane was removed from the module (Figure 2.5) to seal the glazed ends with a Torrseal epoxy. Then, the Torrsealed membrane was reinstalled in another membrane module (Figure 2.6) to repeat the gas permeation tests with He and N_2. Table 2.2 summarizes the gas permeation results of Torssealed membranes and provides a comparison with non-Torrsealed membranes.

Table 2.2. Permeance[1] and ideal selectivity of nitrogen over helium membranes of membranes with Torrsealed glazed end synthesized at four different autoclave fill-levels (94%, 97%, 98%, 99%).

Membrane	Pressure	$P_{N_2}{}^{**}$	$\frac{P_{N_2}{}^{**}}{P_{N_2}{}^{*}}$	$\alpha_{N_2/He}{}^{**}$	$\frac{P_{He}{}^{**}}{P_{He}{}^{*}}$	$\frac{\alpha_{N_2/He}{}^{**}}{\alpha_{N_2/He}{}^{*}}$
M94TC1	ΔP_{low}	20.9	0.91	1.77	0.71	1.28
	ΔP_{medium}	21.4	0.84	1.78	0.64	1.31
	ΔP_{high}	22.2	0.78	1.83	0.57	1.37
M94TC2	ΔP_{low}	15.4	0.64	1.56	0.61	1.05
	ΔP_{medium}	16.2	0.61	1.45	0.60	1.03
	ΔP_{high}	16.6	0.58	1.39	0.57	1.03
M94TC3	ΔP_{low}	17.5	0.83	2.01	0.59	1.40
	ΔP_{medium}	17.6	0.74	2.00	0.50	1.47
	ΔP_{high}	17.8	0.66	1.99	0.43	1.52
$\bar{x} \mp s.d.$		**18.4±0.25**	**0.73±0.12**	**1.75±0.24**	**0.58±0.08**	**1.27±0.19**
M97TC1	ΔP_{low}	22.4	0.89	1.54	0.83	1.07
	ΔP_{medium}	23.7	0.86	1.50	0.81	1.07
	ΔP_{high}	25.3	0.85	1.46	0.82	1.04
M97TC2	ΔP_{low}	21.7	0.90	1.67	0.84	1.08
	ΔP_{medium}	22.4	0.88	1.67	0.82	1.07
	ΔP_{high}	23.3	0.88	1.65	0.82	1.08
M97TC3	ΔP_{low}	30.0	0.90	1.65	0.78	1.15
	ΔP_{medium}	31.3	0.86	1.66	0.73	1.18

	ΔP_{high}	31.7	0.83	1.49	0.75	1.10
$\bar{x} \mp s.d.$		**25.8±0.41**	**0.87±0.02**	**1.59±0.09**	**0.80±0.04**	**1.09±0.05**
M98TC1	ΔP_{low}	21.4	1.06	1.45	0.84	1.26
	ΔP_{medium}	22.0	1.06	1.48	0.91	1.16
	ΔP_{high}	22.2	0.90	1.43	0.87	1.03
M98TC2	ΔP_{low}	18.3	0.86	1.61	0.80	1.07
	ΔP_{medium}	18.7	0.85	1.52	0.81	1.04
	ΔP_{high}	19.5	0.89	1.48	0.82	1.08
$\bar{x} \mp s.d.$		**20.4±1.74**	**0.93±0.10**	**1.50±0.07**	**0.84±0.04**	**1.11±0.09**
M99TC1	ΔP_{low}	20.4	0.84	2.37	0.65	1.29
	ΔP_{medium}	20.6	0.79	2.27	0.60	1.33
	ΔP_{high}	20.5	0.74	2.20	0.55	1.35
M99TC3	ΔP_{low}	21.8	0.81	2.30	0.68	1.20
	ΔP_{medium}	22.2	0.84	2.32	0.63	1.34
	ΔP_{high}	22.0	0.78	2.28	0.58	1.36
$\bar{x} \mp s.d.$		**21.3±0.08**	**0.80±0.04**	**2.29±0.06**	**0.62±0.05**	**1.31±0.06**

[1] All permeances in [10^{-7} × mol·s^{-1}·m^{-2}·Pa]

Except for a couple of permeation runs with one of the membranes synthesized at the autoclave fill level of 98%, the N_2 permeance of the Torrsealed membrane (column 1) is smaller than that of the corresponding non-Torrsealed membranes. The magnitude of the permeance decrease, i.e. the relative permeance after Torrsealing, is shown in column 2 for N_2 and in column 4 for He. The results in Table 2.2 confirm the presence of defects in the membrane seal. However, these defects are not catastrophic, which is indicated by the magnitude of N_2 and He's relative permeance. Even without Torrsealing, the membranes were N_2-selective, indicating that the surface diffusion was the dominating transport mechanism after membrane calcination. It is important to emphasize that our membranes were relatively short (6 cm). If longer membranes were used, e.g. 1 m, the contribution of defects from the glazed ends to the total gas permeance would decrease. Nevertheless, the problem with the deterioration of Aremco 617 glaze during hydrothermal synthesis and the remnants of the Teflon tape on the ends are challenges that needs to be addressed.

In general, a decrease in He permeance after Torrsealing is more significant than in N_2. As a result, the ideal N_2/He selectivity after Torrsealing (column 3) increases. The magnitude of this increase is shown in column 5, where the relative ideal N_2/He selectivity

after Torrsealing is presented. Since the decrease in He's permeance is more significant than that of N_2, gas transport in the glazed ends defects must be a combination of Knudsen diffusion and viscous flow. In other words, the pore size of these defects should be in the same order of magnitude as the defects in the zeolite membrane.

The relative N_2 permeance (column 2) represents the number of defects generated in the membrane's glazed ends. The smaller the relative N_2 permeance, the more defects generated during hydrothermal synthesis. As the autoclave fill level increases from 94% to 97% and 98%, the relative N_2 permeance increases from 0.73 to 0.87 and 0.93. However, as the autoclave fill level increases to 99%, the relative N_2 drops to 0.80. Therefore, except for the highest autoclave fill level, it appears that increasing the fill level in the autoclave not only facilitates crystal formation in the pore-plugging synthesis, which minimizes the defect transport but also minimizes deterioration of the glazed ends of the membrane.

As previously mentioned, at the 99% fill level, the autoclave lid ruptured, indicating the autoclave could not withstand the resulting pressure. Since the thermodynamic data for TPAOH is not available, and we could not measure the pressure directly in the autoclave, the pressure at this condition in the autoclave is unknown. The membranes synthesized at the highest autoclave fill level of 99% may be also affected by the lead rapture. On the one hand, it is evident that increasing the fill level improves the membrane's quality. On the other hand, 98% fill-level likely represents the limit for the autoclave.

2.5. CONCLUSION

We investigated the effect of the autoclave fill level on the performance of silicalite-1 membranes synthesized by the pore-plugging method, before and after membrane calcination. Also, we repeated the performance tests after sealing the glazed ends of the membrane with a Torrseal epoxy. We assessed membrane performance based on N_2 and He permeances as well as their ratio.

The quality of the membranes improves as the autoclave fill level increases. Although we were not able to prepare defect-free membranes, the contribution of the defects was minimized at the 98% autoclave fill level. We also discovered that the defects originated not only from incomplete pore-plugging but also from deterioration of the glazed ends of the membrane during hydrothermal synthesis. Finally, there is a limit to

which the autoclave can be filled. In our case, it was 98%. A further increase to 99% led to the rupturing of the autoclave lead and in more defects, particularly in the glazed ends of the resulting membranes.

2.6. NOMENCLATURE

A	$[m^2]$	Membrane area
$\propto_{i/j}$	$[-]$	Ideal selectivity of component i over component j for uncalcined membranes
$\propto_{i/j}{}^{*}$	$[-]$	Ideal selectivity of component i over component j for calcined membranes using module with Aremco 617 and graphite gaskets
$\propto_{i/j}{}^{**}$	$[-]$	Ideal selectivity of component i over component j for calcined membranes using module with torrseal epoxy
d	$[m]$	Diameter
D_T	$[m^2.s^{-1}]$	Transport diffusion
ε	$[-]$	Void fraction
J_i	$[mol \cdot s^{-1}m^2]$	Molar flux
l	$[m]$	Length
M	$[kg.mol^{-1}]$	Molecular weight
P_i	$[mol \cdot s^{-1}m^{-2}Pa^{-1}]$	Permeance of component i when membrane is uncalcined
$P_i{}^{*}$	$[mol \cdot s^{-1}m^{-2}Pa^{-1}]$	Permeance of component i when membrane is calcined and tested using module with Aremco 617 and graphite gaskets
$P_i{}^{**}$	$[mol \cdot s^{-1}m^{-2}Pa^{-1}]$	Permeance of component i when membrane is calcined and tested using module with torrseal epoxy
Δp_i	$[Pa]$	Partial pressure differential
p	$[Pa]$	Pressure
ΔP_{low}	$[kPa]$	Partial pressure at low pressure differential

ΔP_{medium}	$[kPa]$	Partial pressure at medium pressure differential
ΔP_{high}	$[kPa]$	Partial pressure at high pressure differential
ρ	$[kg.m^{-3}]$	Zeolite density
q	$[mmol \cdot g^{-1}]$	Quantity of amount adsorbed
R	$[Pa.m^3.K^{-1}mol^{-1}]$	Gas constant
R.T	[K]	Room temperature
$s.d.$	$[m^{-1}]$	Standard Deviation
T	$[K]$	Temperature
μ	$[Pa.s^{-1}]$	Viscosity
x	$[m^{-1}]$	Lumped parameter of porosity over effective length of defect
$\bar{x}$	$[-]$	Average
y	$[m^{-1}]$	Lumped parameter of porosity over effective length of zeolite

Subscripts

d	Defect
h	At high pressure side
l	At low pressure side
i,j	Component
K	Knudsen flow
SD	Surface Diffusion
T	Transport
z	Zeolite crystal

Abbreviations

CH_4	Methane
CO_2	Carbon Dioxide
F-	Bubble Flow Meter
GC	Gas Chromatography
He	Helium

M-	Membrane cell
MFC	Mass Flow Controller
MFI	Mordenite Framework Inverted
N_2	Nitrogen
P-	Pressure Transducer
rpm	Round per minute
T-	Thermocouple
TPAOH	Tetra Propyl Ammonium Hydroxide
V-	Valve

2.7. REFERENCES

[1] J. Caro, M. Noack, Zeolite membranes - Recent developments and progress, Microporous Mesoporous Mater. 115 (2008) 215–233. https://doi.org/10.1016/j.micromeso.2008.03.008.

[2] A. Julbe, Zeolite membranes - A short overview, Elsevier B.V., 2005. https://doi.org/10.1016/s0167-2991(05)80009-6.

[3] L.B. McCusker, D.H. Olson, C. Baerlocher, Atlas of Zeolite Framework Types, in: C. Baerlocher, W.M. Meier, D.H.B.T.-A. of Z.F.T. Olson (Eds.), Atlas Zeolite Framew. Types, Elsevier, Amsterdam, 2007: pp. 184–185. https://doi.org/10.1016/B978-0-444-53064-6.X5186-X.

[4] M.P. Pina, R. Mallada, M. Arruebo, M. Urbiztondo, N. Navascués, O. De La Iglesia, J. Santamaria, Zeolite films and membranes. Emerging applications, Microporous Mesoporous Mater. 144 (2011) 19–27. https://doi.org/10.1016/j.micromeso.2010.12.003.

[5] M. Kazemimoghadam, T. Mohammadi, Synthesis of MFI zeolite membranes for water desalination, Desalination 206 (2007) 547–553. https://doi.org/10.1016/j.desal.2006.04.063.

[6] P. Ferreira, A. Ferreira, J. Rocha, M.R. Soares, Synthesis and structural characterization of zirconium silicates, Chem. Mater. 13 (2001) 355–363. https://doi.org/10.1021/cm0007196.

[7] D.A. Kennedy, D. Carter, S. Wilson, B. Kruczek, F.H. Tezel, Pore plugging synthesis and characterization of silicalite-1 membranes using tubular TiO2 supports: Effect of support pore size on membrane performance, Can. J. Chem. Eng. 96 (2018) 1597–1611. https://doi.org/10.1002/cjce.23095.

[8] M. Pan, Y.S. Lin, Template-free secondary growth synthesis of MFI type zeolite membranes, Microporous Mesoporous Mater. 43 (2001) 319–327. https://doi.org/10.1016/S1387-1811(01)00212-8.

[9] J. Dong, Y.S. Lin, M.Z.C. Hu, R.A. Peascoe, E.A. Payzant, Template-removal-associated microstructural development of porous-ceramic-supported MFI zeolite membranes, Microporous Mesoporous Mater. 34 (2000) 241–253. https://doi.org/10.1016/S1387-1811(99)00175-4.

[10] E.R. Geus, H. van Bekkum, Calcination of large MFI-type single crystals, Part 2: Crack formation and thermomechanical properties in view of the preparation of zeolite membranes, Zeolites. 15 (1995) 333–341. https://doi.org/10.1016/0144-2449(94)00034-P.

[11] F. Banihashemi, L. Meng, A.A. Babaluo, Y.S. Lin, Xylene Vapor Permeation in MFI Zeolite Membranes Made by Templated and Template-Free Secondary Growth of Randomly Oriented Seeds: Effects of Xylene Activity and Microstructure, Ind. Eng. Chem. Res. 57 (2018) 16059–16068. https://doi.org/10.1021/acs.iecr.8b01373.

[12] S. Miachon, E. Landrivon, M. Aouine, Y. Sun, I. Kumakiri, Y. Li, O.P. Prokopová, N. Guilhaume, A. Giroir-Fendler, H. Mozzanega, J.A. Dalmon, Nanocomposite MFI-alumina membranes via pore-plugging synthesis. Preparation and morphological characterisation, J. Memb. Sci. 281 (2006) 228–238. https://doi.org/10.1016/j.memsci.2006.03.036.

[13] Y. Li, M. Pera-Titus, G. Xiong, W. Yang, E. Landrivon, S. Miachon, J.A. Dalmon, Nanocomposite MFI-alumina membranes via pore-plugging synthesis: Genesis of the zeolite material, J. Memb. Sci. 325 (2008) 973–981. https://doi.org/10.1016/j.memsci.2008.09.030.

[14] M. Tawalbeh, Silicalite-1 Membranes Synthesis, Characterization, CO2/N2 Separation and Modeling, (2013) 308. Ph.D. Thesis, University of Ottawa, Ottawa

[15] J. Hedlund, F. Jareman, A.J. Bons, M. Anthonis, A masking technique for high quality MFI membranes, J. Memb. Sci. 222 (2003) 163–179. https://doi.org/10.1016/S0376-7388(03)00285-0.

[16] C. Andersson, Factors affecting MFI membrane quality, (2007). Ph.D. Thesis, Luleå University of Technology, Luleå

[17] E. Dinçer, A. Çulfaz, H. Kalipçilar, Effect of seeding on the properties of MFI type zeolite membranes, Desalination. 200 (2006) 66–67. https://doi.org/10.1016/j.desal.2006.03.244.

[18] T. Mohammadi, S. Asarehpour, M. Samei, Effects of Synthesis Temperature and Support Material on CO2 and CH4 Permeation through SAPO-34 Membranes, Sep. Sci. Technol. 47 (2012) 2320–2330. https://doi.org/10.1080/01496395.2012.677924.

[19] B. Soydas, Characterization of Zeolite Membranes by Gas Permeation, (2009). Ph.D. Thesis, Middle East Technical University, Ankara

[20] L. Tosheva, B. Mihailova, V. Valtchev, J. Sterte, Silicalite-1 macrostructures – preparation and structural features, Microporous Mesoporous Mater. 39 (2000) 91–101. https://doi.org/10.1016/S1387-1811(00)00179-7.

[21] W.J.W. Bakker, L.J.P. Van Den Broeke, F. Kapteijn, J.A. Moulijn, Temperature Dependence of One-Component Permeation through a Silicalite-1 Membrane, AIChE J. 43 (1997) 2203–2214. https://doi.org/10.1002/aic.690430907.

[22] P. Malbrunot, D. Vidal, J. Vermesse, R. Chahine, T.K. Bose, Adsorbent helium density measurement and its effect on adsorption isotherms at high pressure, Langmuir. 13 (1997) 539–544. https://doi.org/10.1021/la950969e.

[23] D. Carter, Fabrication and Characterization of Silicalite-1 Membranes for the Separation of the Greenhouse Gases, (2019). Ph.D. Thesis, University of Ottawa, Ottawa

[24] X. Xu, Y. Bao, C. Song, W. Yang, J. Liu, L. Lin, Microwave-assisted hydrothermal synthesis of hydroxy-sodalite zeolite membrane, Microporous Mesoporous Mater. 75 (2004) 173–181. https://doi.org/10.1016/j.micromeso.2004.07.019.

Chapter 3

The New Characterization Method of Defect-containing Zeolite Membranes

S. Al-Akwaa, D. Carter, F.H. Tezel, B. Kruczek*

University of Ottawa, Department of Chemical and Biological Engineering

161 Louis Pasteur, Ottawa, Ontario, CANADA, K1N 6N5

To be submitted to: Journal of Membrane Science

ABSTRACT

Synthesis of defect-free zeolite gas separation membranes is challenging. In addition to the desired transport by surface and Knudsen diffusion through the zeolite pores, the undesired transport by Knudsen and viscous flows through the defects are typically present to a different extent. In this paper, we propose a method to assess the extent of the undesirable defect-transport in zeolite membranes, which is essential for the fine-tuning of membrane synthesis protocols. Also, knowing the contribution of the undesirable defect transport allows determining the corrected diffusivity of gases in the zeolite crystals incorporated in the membrane. The latter is the intrinsic property of the zeolite. The method relies on the gas permeation tests with not-adsorbed and adsorbed gases before and after calcination of the membrane. The adsorption isotherms of the gases with the zeolite crystals incorporated into the membrane are also required.

We tested the proposed characterization method using silicalite-1 zeolite membranes prepared by a pore-plugging method inside porous TiO_2 support. The validity of the parameters, which characterize the crystal and defect transport, were verified by comparing the experimental and predicted permeances of He, N_2, CO_2 and CH_4 at different pressures. Also, the calculated corrected diffusivity values of CO_2 and CH_4 in the silicalite crystals of $1.69 \cdot 10^{-8} m^2 s^{-1}$ and $6.51 \cdot 10^{-8}\ m^2 s^{-1}$, respectively, are comparable to the values reported in the literature.

Keywords: Zeolites, Silicalite, Membranes, Knudsen diffusion, Surface diffusion

HIGHLIGHTS

- Determination of gas transport properties of defect containing zeolite membranes
- Quantification of crystal and defect transport contributions to total gas transport
- Prediction of gas permeances of He, N_2, CO_2 and CH_4 at different pressures
- Calculation of corrected diffusivity of N_2, CO_2 and CH_4 in silicalite-1 zeolite

3.1. INTRODUCTION

Zeolite particles have an extraordinary ability to separate gas mixtures due to differences in the adsorption-diffusion behaviour of guest molecules inside their highly ordered pore networks at modest temperatures and pressures [1]. For the continuous separation of gas mixtures, zeolites can be used as membranes, and the general advantages of separating mixtures using membranes realized if a thin and continuous layer of zeolite crystals can be assembled [2,3]. Despite these advantages, a significant barrier to the adoption of zeolitic membranes is that their performance is compromised by the unoccupied regions, which surround the zeolite crystals of the membrane. These regions are henceforth referred to as defects. They can be attributed to experimental factors such as incomplete zeolite crystal growth, or the different rates of linear expansion for zeolite crystals and the membrane support during heating and cooling.

Both the number of defects and the size of defects affect membrane performance, and therefore numerous techniques have been developed to quantify these characteristics in novel membranes. These techniques have been summarized recently by Maghsoudi [4], and include polymer sphere permeation experiments, the bubble point method, and permporometry. These techniques require dedicated equipment, exposing the membrane to solid and/or liquid materials, as well as the consideration of the regeneration conditions that are required to restore membrane performance for gas separation applications. Although these limitations can be overcome at the lab scale, they are often not scalable for larger membranes. Technological advances in 3D laser microscopy show promise to be used as an alternative method to determine defect characteristics; however, the resolution of this technology is not yet sufficient enough to discriminate between differently sized Knudsen defects [5,6].

The most basic parameter that is determined experimentally is the gas permeance (P):

$$P = \frac{P'}{L} = \frac{J}{p_h - p_l} \tag{3.1}$$

where J is the steady-state permeation flux, p_h and p_l are the pressures at the high and low-pressure sides of the membrane, respectively, P' is the membrane permeability, and L is the membrane thickness. In the case of zeolite membranes, the thickness of the selective layer is rarely known, which is why permeance rather than permeability is reported. Knowing the permeances of different gases allows assessing membrane's ideal selectivity:

$$\alpha = \frac{P_i}{P_j} \tag{3.2}$$

where the subscripts i and j refer to the more and the less permeable gases, respectively. The two gases that are used to determine α are typically a small molecule, which can pass through the narrow channels of the zeolite (such as He, H_2, or N_2), and a larger molecule, which is excluded from the zeolite's pores (such as SF_6). Membranes containing few defects will, therefore, be selective for the smaller gas molecule, which will be able to permeate through both defects and the zeolite channel network. In contrast, the larger molecule will be transported through the defects only. For silicalite membranes, selectivities of $\alpha(N_2/SF_6)$ up to 108 at 298 K, and $\alpha(H_2/SF_6)$ of 136 and 155 at 298 K have been reported in the literature [7–9]. Although these ideal selectivities can be used to rank newly fabricated membranes effectively, they do not allow to characterize defect-containing membranes fully. Furthermore, adsorption of SF_6 by silicalite crystals has been found to induce crystal expansion, which affects the physical structure of the membrane [7,10]. Given this behaviour, characterized membranes may not have the same properties as they did before characterization.

Novel membranes can also be characterized by the Maxwell-Stefan (MS) model, which does not require the use of dedicated materials or equipment as required for permporometric or bubble point characterization methods. In the MS model, the diffusivity of gas molecules is determined with consideration of adsorption phenomena and isotherm data, which can be used to predict the performance of membranes at untested conditions. This model and its variations have been used for several different gas and membrane combinations by several research groups [11–13]. The Maxwell-Stefan model does not, however, discriminate between the transport of gases through defects and the selective layer of the

membranes. Therefore, MS diffusivities are reliable when there are no defects in the membrane. A simpler model that can be used in combination with transient permeation values to determine MS diffusivities has been proposed by Gardner et al. [14]. Similarly to the MS model, this model is best suited for defect-free membranes. Kangas et al. [15] have alternatively proposed characterizing defective membranes with the MS model combined with permporometric analysis; however, this type of investigation is very rigorous.

Some noteworthy alternatives to the MS model have been developed by other researchers and are pertinent to this study. Caravella et al. [16] proposed a model which combined surface diffusion and Knudsen diffusion transport through the zeolitic pores of NaY membranes and was followed up by Zito et al. [17] for silicalite membranes. This model does not, however, allow the characterization of defects that are present in addition to the zeolite crystals which make up the membrane. Also, Jareman et al. [18] combined defect sizes determined by permporometry with flux equations, which consider substrate effects. The resulting model is well suited for applications where substrate effects are likely to be present, and permporometry analysis can be conducted but is less desirable for applications where this is not possible.

Recently, we have characterized silicalite zeolite membranes, prepared by a pore plugging method on titanium oxide supports, by a combination of single gas permeation tests with He, N_2, CH_4 and CO_2 at different feed pressures, and dynamic adsorption experiments on zeolite crystals collected from an autoclave in which the zeolite membranes were synthesized [19]. Based on the fact that permeances of He and N_2 were independent of pressure, we concluded that the membranes were defect-free, or the defects were minimal so that viscous flow through the defects was negligible. Using N_2, CH_4 and CO_2 permeances along with the respective isotherms of these gases on silicalite crystals, the effective diffusivity values of N_2, CH_4 and CO_2 in the synthesized membranes were determined. However, these effective diffusivity values were subject to unquantified morphological attributes of the membrane structure. Therefore, they could not be compared to diffusivities determined by others. On the other hand, since the resulting N_2/CH_4 and N_2/CO_2 diffusivity coefficient ratios were independent of the morphological attributes of the membrane, they were compared with the respective values determined from dynamic adsorption experiments. The latter represent the maximum values for a given pair of gases and the zeolite. The ratios determined from gas permeation experiments were slightly smaller than those determined from the dynamic adsorption experiments [19]. It was, therefore, concluded that not all gas transport proceeded through the zeolite crystal channels of the membrane. Knowing the difference between the diffusivity

ratios from the dynamic adsorption experiments and steady-state permeation experiments could help us calculate the contribution of the defect transport in the membrane. However, this approach is cumbersome as it requires two different types of experiments, dynamic adsorption and steady-state permeation.

The objective of this paper is to develop a method to distinguish between the crystal and defect transport in zeolite membranes based on He and N_2 gas permeation experiments before and after membrane calcination. The method will be demonstrated using silicalite zeolite membranes prepared by a pore-plugging method inside porous TiO_2 support. The proposed method also requires the knowledge of the adsorption isotherms of tested gases with the silicalite zeolite crystals incorporated in the membrane, which is widely available in the literature. Knowing the contribution of the undesirable defect transport in the zeolite membrane will allow determining the corrected diffusivity of tested gases in zeolite crystals, which represent intrinsic transport properties. The latter will be compared with the literature values determined by other methods..

3.2. THEORETICAL BACKGROUND

The transport of gas molecules through zeolite membranes proceeds through two pathways. These pathways are firstly, the defined pore network of the zeolite crystals, and secondly, defects, which surround the zeolite crystals. In the former transport pathway, gas molecules are transported by surface diffusion or Knudsen diffusion, subject to the physicochemical properties of the gas molecules and the zeolite's pore characteristics. In the latter transport pathway, gas molecules are transported by Knudsen and/or viscous flow subject to the size of the defect pathways in comparison to the size of the gas molecules.

In the regime of surface diffusion, gas molecules are adsorbed into the zeolite's pores as described by their isotherms at the experimental conditions and diffuse in the direction of decreasing surface occupancy, by continuously adsorbing and desorbing through the zeolite pore network [20,21]. Transport by Knudsen diffusion results from more frequent collisions between gas molecules and pore walls, leading to the separation of gas mixtures based on molecular mass differences [20,21]. When gas molecules collide more frequently with other gas molecules than they collide with pore walls, the regime of viscous flow occurs, in which all gas molecules move with the same velocity.

The proposed method is based on single gas permeation tests performed before and after calcination of the membrane. The critical assumption of the proposed characterization method is that before membrane calcination, zeolite crystalline pathways are not accessible to penetrating gas molecules because they are filled with the template used during the synthesis of the zeolite membrane [8,22–25]. Consequently, before calcination, gas molecules can only permeate through the defects, in which gas transport occurs by a combination of Knudsen diffusion and viscous flow. The contributions of each transport mode depends on the pore size of the defects. The size and the shape of defects are not uniform; however, for the modelling purposes, the defects can be assumed to be straight cylinders of diameter (d_d) and the effective length (l_d). There are *n* defects per unit volume of the membrane so that the volume fraction of the defects in the membrane ε_d is simply:

$$\varepsilon_d = n\frac{\pi}{4}d_d^2 l_d \tag{3.3}$$

It can be shown that the total gas flux through an uncalcined membrane that is the defect flux (J_d) is given by [17]:

$$J_d = \left\{\frac{\varepsilon_d}{l_d}d_d^2\frac{(p_h+p_l)}{64\mu RT} + \frac{\varepsilon_d}{l_d}d_d\frac{1}{3}\sqrt{\frac{8}{\pi MRT}}\right\}(p_h - p_l) \tag{3.4}$$

where: *T* is the absolute temperature, *R* is the universal gas constant, and μ and *M* are the dynamic viscosity and the molecular weight of the gas, respectively. Dividing Equation (3.4) by the pressure difference leads to:

$$P_d = P_{d,v} + P_{d,K} = \frac{\varepsilon_d}{l_d}d_d^2\frac{(p_h+p_l)}{64\mu RT} + \frac{\varepsilon_d}{l_d}d_d\frac{1}{3}\sqrt{\frac{8}{\pi MRT}} \tag{3.5}$$

where P_d is the total defect permeance, which is the sum of the defect permeance due to the viscous flow ($P_{d,v}$) and the defect permeance due to Knudsen diffusion ($P_{d,K}$). There are three unknowns in Equation (3.4): ε_d, d_d, and l_d. Combining ε_d and l_d into a lumped term $x = \varepsilon_d / l_d$, Equation (3.5) is re-written as:

$$P_d = xd_d^2\frac{(p_h+p_l)}{64\mu RT} + xd_d\frac{1}{3}\sqrt{\frac{8}{\pi MRT}} \tag{3.6}$$

Therefore, performing single gas permeation tests with two different gases at the same conditions (T, p_h, p_l) should allow determination of d_d and x. One could choose any two gases differing significantly by the molecular weight, but we selected helium and nitrogen as the test cases. Knowing d_d and x determined at a given T, p_h, and p_l, one should be able to predict P_d at any other T, p_h, p_l. Out of these three operating conditions, the easiest to control is p_h. Therefore, the validity of the proposed method can be verified by comparing the experimental and calculated J_d (or P_d) at different p_h while keeping p_l and T constant.

After membrane calcination, it is assumed that the template is completely removed from the pores of zeolite crystals, and these pores become accessible to permeating gases. Moreover, it is assumed that calcination does not affect ε_d. The advantage of using He as one of the testing gases comes from the fact that it is practically not adsorbed by zeolites at ambient temperature [26–28]. Therefore, the transport through the zeolite pores is governed exclusively by Knudsen diffusion. Consequently, the total helium permeance after calcination (P_{He}) is given by:

$$P_{\mathrm{He}} = P_{\mathrm{He},d} + P_{\mathrm{He},z} = \left\{ x d_d^2 \frac{(p_h + p_l)}{64 \mu_{He} RT} + x d_d \frac{1}{3} \sqrt{\frac{8}{\pi M_{\mathrm{He}} RT}} \right\} + y d_z \frac{1}{3} \sqrt{\frac{8}{\pi M_{\mathrm{He}} RT}} \quad (3.7)$$

where $P_{\mathrm{He},d}$ and $P_{\mathrm{He},z}$ are the helium permeances due to transport through the defects and zeolite, respectively, d_z is the effective zeolite pore size, and y is equivalent to x for the zeolite pores, i.e. $y = \varepsilon_z / l_z$ in which ε_z is the volume fraction of pores in zeolite crystals and l_z is the effective length of zeolite pores. Typically, for a given zeolite d_z is known. For silicalite crystals d_z = 0.55 nm [22]. Therefore, knowing x and d_d from single gas permeation tests of the uncalcined membrane and using a reliable value of d_z allows determining the lumped parameter y in Equation (3.7).

In a more general case, the permeating gas can be adsorbed in zeolite crystal. Consequently, surface diffusion becomes another mode of transport across the membrane, and Equation (3.7) becomes:

$$P = P_d + P_z = \left\{ x d_d^2 \frac{(p_h + p_l)}{64 \mu RT} + x d_d \frac{1}{3} \sqrt{\frac{8}{\pi MRT}} \right\} + y d_z \frac{1}{3} \sqrt{\frac{8}{\pi MRT}} + y \left(\frac{q_h - q_l}{p_h - p_l} \right) \rho D_T \quad (3.8)$$

where q is the surface loading, D_T is the transport (surface) diffusivity in zeolite crystals and ρ is the zeolite density. Equation (3.8) requires the adsorption isotherm, $q = f(p)$, of the permeating gas in zeolite

crystals incorporated into the support of the membrane, which can be determined in parallel adsorption experiments or can be taken from the literature. Equation (3.8) implies a parallel transport of an adsorbed gas in zeolite crystals by the Knudsen diffusion and surface diffusion. However, as argued by Caravella et al. [16], the surface and Knudsen diffusion mechanisms inside zeolite crystals are not independent of each other. The adsorbed phase affects the pore size, porosity and tortuosity for Knudsen diffusion inside the crystals. As a result, the value of y determined from Equation (3.7) is applicable for the surface diffusion contribution, but not for the Knudsen diffusion contribution in Equation (3.8). The latter is significantly reduced by the adsorbed phase [16]. In the case of silicalite zeolite crystals at ambient temperature, the Knudsen contribution for CO_2 and CH_4 in the zeolite crystals is practically negligible [17], and consequently, Equation (3.8) reduces to:

$$P = P_d + P_z = \left\{ x d_d^2 \frac{(p_h + p_l)}{64 \mu RT} + x d_d \frac{1}{3} \sqrt{\frac{8}{\pi MRT}} \right\} + y \left(\frac{q_h - q_l}{p_h - p_l} \right) \rho D_T \tag{3.9}$$

Knowing x and d_d from gas permeation experiments with the uncalcined membrane, y from the gas permeation experiment with He after membrane calcination, Equation (3.8) can be used to determine D_T or a lumped $D_T\rho$, if ρ is not available, for CO_2 and CH_4 in silicalite crystals at ambient temperature. We will use Equation (3.9) also to calculate D_T of N_2 even though the contribution of Knudsen diffusion in silicalite crystals ambient temperature is not negligible [17].

The transport diffusivity D_T is a function of the amount adsorbed (q) and the temperature [29]:

$$D_T = D^0 \exp\left(-\frac{E_{D,S}}{RT} \right) = D_0 \frac{\Delta \ln p}{\Delta \ln q} \tag{3.10}$$

Equation (3.10) is known as the Darken equation, in which D^0 is the limiting diffusivity, which is independent of temperature, $E_{D,S}$ is the activation energy for surface diffusion, and D_0 is the corrected diffusivity, which is independent of the amount adsorbed. Knowing D_T, p_h, p_l, and the corresponding adsorption isotherm, one can calculate the corrected diffusivity [20]:

$$D_0 = D_T \frac{\ln q_h - \ln q_l}{\ln p_h - \ln p_l} \tag{11}$$

Since the corrected diffusivity is independent of the amount adsorbed, it is considered an intrinsic parameter for zeolite crystals [29].

3.3. MATERIAL AND METHODS

The selection of a system to demonstrate the validity of the proposed characterization method follows from our previous work. The synthesized silicalite-1 membranes were characterized by single gas permeation tests. For the current work, we synthesized and tested new silicalite membranes.

3.3.1. Membrane Fabrication Procedure

Silicalite zeolite membranes were synthesized using the pore-plugging method [21,30,31] on 6 cm long Filtanium^{TM} tubular ceramic membrane supports (TAMI Industries, Nyons, France). The membrane supports' active layers were composed of TiO_2, and contained an active layer pore size of 0.45 μm. Before the zeolite synthesis, both axial faces and the outer surface of the membrane support 1 cm from each end were glazed using the Aremco 617 glaze solution (Aremco Products Inc, Valley Cottage, NY, USA), to seal the ends. After applying a layer of the glaze solution, the support was dried at 573 K for 2 hours, followed immediately by curing at 1148 K for 1 hour, with 1 $K \cdot min^{-1}$ heating and cooling ramps. A total of 5 coats of glaze were applied.

Silicalite zeolite membranes were fabricated inside the active layer of the glazed membrane supports according to the interrupted hydrothermal synthesis method, which has been reported by Miachon et al. [30]. The molar composition of the solution and other synthesis parameters are shown in Table 3.1. The precursor solution was composed of 99.8% purity silicon dioxide (SiO_2), 20 wt% tetrapropyl ammonium hydroxide (TPAOH), and deionized water (H_2O). SiO_2 and TPAOH were purchased from Sigma (Oakville, ON, Canada). The crystal growth during hydrothermal synthesis depends on the temperature and pressure, which affect the solubility and diffusivity of solute molecules [32]. The temperature during all syntheses was 443 K, while the pressure was indirectly controlled by a void volume (free volume) in the autoclave. The latter varied from 1 % to 6%. After synthesizing silicalite-1 crystals, each membrane was held at 373 K for 20 hours to dry, and at 773 K for 4 hours to calcine. The heating and cooling rates for drying and calcination were 1 $K \cdot min^{-1}$.

Table 3.1. Selected properties of the synthesis parameters for the membranes M1 and M2 that have been fabricated in this study. Interruption time begins when the oven starts to cool down at the end of hold time 1, and ends when the oven commences heating up to the hold temperature for hold time 2.

Precursor solution molar ratio SiO_2:TPAOH:H_2O	Heating ramps	Cooling ramps	Hold Temp.	Hold Time 1	Interruption Time	Hold Time 2	Free Volume
[mol]	[K·min^{-1}]	[K·min^{-1}]	[K]	[h]	[h]	[h]	[%]
1 : 0.45 : 27.8	1	1	443	12	11	72	1 - 6

3.3.2. Gas Permeation Experiments

A process flow diagram (PFD) showing the experimental setup used to conduct gas permeation experiments is shown in Figure 3.1. The heart of the testing system is a membrane module, which connects the glazed ends of the tubular ceramic supported membrane to the stainless steel process lines. In the present study, a gas-tight seal between these materials has been achieved using single-use compressible graphite gaskets. These gaskets are positioned concentrically over the glazed ends of the tubular membrane and form an airtight seal when they expand radially due to axial compression from the membrane module flanges. The membrane module, shown in Figure 3.1, has been made in house at University of Ottawa, using stainless steel stock, brass flange bolts, and compressible graphite from McMaster Carr (Elmhurst, IL, USA). Compared to epoxies and elastomeric or fluorinated polymers, the graphite used in this study can be heated up to temperatures higher than 750 K without releasing any vapours or gasses that could poison the zeolite crystals.

The configuration of the experimental setup allows pure gases to be fed to the membrane at chosen constant feed flow rates using mass flow controllers MFC1 and MFC2. For feed flow rates below 1,000 ml(STP)·min^{-1}, MFC1, the mass flow controller made by Bronkhorst (Burlington, ON, Canada) was used, whereas MFC2, the mass flow controller made by MKS (Andover, MA, USA) with a range of 0 – 10 l(STP)·min^{-1} was used when higher feed flow rates were required. The flow rates of the permeate and retentate streams were then measured using bubble flow meters F1 and F2. The pressures on the feed side (high-pressure side) and the permeate side (low-pressure side) were measured with pressure transducers P1 and P2, respectively. The pressure transducers, purchased from Cole Parmer, (Montreal, QC, Canada),

had operating ranges of 0 – 250 psig and 0 – 10 psig for P1 and P2, respectively. Additionally, the gas temperature was measured in-line using a K type thermocouple T1 from Omega (Laval, QC, Canada). He (99.999% purity), N_2 (99.998% purity), CH_4 (99.99% purity), and CO_2 (99.99% purity), which were used as test gases, were purchased from Messer (Mississauga, ON, Canada).

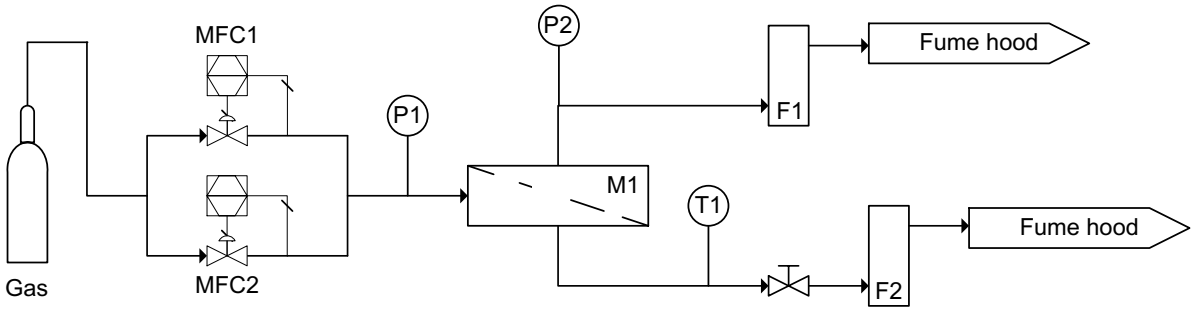

Figure 3.1. The schematic showing the experimental setup used in this investigation. MFC1 and MFC2 are mass flow controllers, P1 and P2 are pressure transducers, M is the module containing the membrane, T1 is a temperature thermocouple, and F1 – F2 are the bubble flow meters.

Pure gas permeation experiments were conducted at three different feed pressures of 170, 300 and 450 kPa absolute. The permeate side of the membrane was open to the atmosphere. However, since some of the gases needed to be vented into the fume hood for safety considerations, the permeate side pressure was greater than the atmospheric pressure, ranging from 109 kPa to 175 kPa absolute depending on the gas permeation rate.

The membranes were tested with single gases before and after calcination. The membranes were first tested before calcination using He and N_2. After calcination, they were retested with these gases, as well as with CH_4 and CO_2. The testing with calcined membranes was carried out in the following order: He, N_2, CH_4, CO_2. Then a test with He at one pressure was repeated to rule out potential contamination of the membranes with residual impurities of tested gases, in particular CH_4 and CO_2.

3.3.3. Parameters for the proposed method

In addition to experimentally measured gas permeances of uncalcined and calcined zeolite membranes, the proposed characterization method relies on adsorption parameters, which can be determined by independent adsorption experiments or are available in the literature. In this paper, we

relied on the adsorption parameters of silicalite zeolite powder determined experimentally in our lab and reported previously [19,33,34].

Single gas adsorption isotherms of N_2, CH_4 and CO_2 on silicalite zeolite crystals are adequately described using the Langmuir model [34,35]:

$$q = q^s \frac{bp}{1+bp} \tag{3.11}$$

where q is the equilibrium adsorption capacity of zeolite at pressure p, q^s is the maximum adsorption capacity of zeolite at the isotherm temperature, and b is the affinity constant [19]. The values of these constants for the gases considered in this study are summarized in Table 3.2.

Table 3.2. Parameters required for demonstration of the proposed characterization method using silicalite zeolite membranes at temperature 295 K. The adsorption properties are taken from Kennedy et al. [19].

Property		He	N_2	CH_4	CO_2
M	[kg·mol^{-1}]	0.004	0.028	0.016	0.044
μ	[Pa·s^{-1}]	1.973 x 10^{-5}	1.755 x 10^{-5}	1.096 x 10^{-5}	1.473 x 10^{-5}
q^s	[mol·kg^{-1}]	-	1.371	1.986	3.280
b	[Pa^{-1}]	-	1.263 x 10^{-6}	2.645 x 10^{-6}	7.135 x 10^{-6}

3.4. RESULTS

3.4.1. Experimental gas permeances

Table 3.3 summarizes the experimentally determined gas permeances, before and after calcination, calculated using Equation (3.1) based on steady-state permeation fluxes. In total, seven membranes were tested, but only three with all gases. Figure 3.2 presents a sample of permeation results for one membrane graphically. To better illustrate the effect of feed pressure and calcination, Figure 3.2 is split into part a), which presents gas permeances, and part b), which presents the ideal selectivity of selected pairs of gases.

Table 3.3. Summary of experimentally determined gas permeances (P_e)*

Memb.	p_h** [kPa]	$He^{(1)}$		$N_2^{(1)}$		$He^{(2)}$		$N_2^{(2)}$		$CH_4^{(2)}$		$CO_2^{(2)}$	
		p_l [kPa]	P_e	p_l [kPa]	P_e	p_l [kPa]	P_e	p_l [kPa]	P_e	p_l [kPa]	P_e	p_l [kPa]	P_e
M1	171	108	4.31	108	3.33	109	13.3	108	24.4	110	51.7	112	39.8
	307	109	5.79	109	4.75	112	15.2	127	26.0	135	50.7	140	35.7
	445	115	6.95	116	5.93	122	16.9	152	27.6	165	49.6	173	34.3
M2	171	110	7.72	109	6.75	109	14.7	108	21.1	109	42.3	110	33.0
	310	109	10.3	109	9.22	113	17.5	124	23.8	135	43.5	137	32.5
	450	123	12.9	121	11.7	125	20.6	150	26.9	164	45.2	171	33.2
M3	171	109	3.03	108	2.42	108	14.0	109	26.8	109	54.2	110	39.4
	310	108	3.81	109	2.91	110	15.2	122	26.3	131	50.4	133	35.7
	450	109	4.52	109	3.59	117	16.8	144	28.2	157	49.5	158	32.8
M4	170	108	8.06	109	5.72	109	16.2	108	24.1	-	-	-	-
	309	109	9.86	107	8.33	112	18.8	123	26.4	-	-	-	-
	448	113	12.2	115	10.5	122	21.0	145	28.4	-	-	-	-
M5	171	109	5.73	108	4.05	109	17.5	108	25.3	-	-	-	-
	310	109	7.21	108	5.46	112	19.5	123	27.4	-	-	-	-
	447	110	8.59	109	6.58	122	21.2	146	29.9	-	-	-	-
M6	171	108	2.97	109	1.53	109	15.5	108	24.0	-	-	-	-
	309	108	3.26	109	1.67	111	16.3	121	25.5	-	-	-	-
	449	108	3.50	108	1.89	118	17.3	140	26.4	-	-	-	-
M7	171	109	7.39	108	5.20	108	23.3	108	33.4	-	-	-	-
	309	109	9.18	109	6.95	116	25.9	130	36.4	-	-	-	-
	444	112	10.9	111	8.36	127	28.2	156	38.2	-	-	-	-

* All permeances in [10^{-7} × mol·s^{-1}·m^{-2}·Pa]
**Average feed pressure
(1) Before calcination
(2) After calcination

The membrane in Figure 3.2 and all membranes listed in Table 3.3 are permeable to He and N_2 before calcination, which means that they are not defect-free. The corresponding defect permeances (P_d) of He and N_2 increase with pressure. The fact that defect permeance increases with pressure suggests that the first term in Equation (3.6) is not negligible. In other words, the transport through the defects must include the viscous flow, which is proportional to $p_h + p_l$. The defect permeance of He is higher than N_2, as indicated by the values obtained before calcination, which indicates that in addition to the viscous flow, there must also be Knudsen diffusion through the defects. As seen in Equation (3.6), the Knudsen diffusion favours the transport of the lighter He molecules over the heavier N_2 molecules. The ideal N_2/He selectivity slightly increases with feed pressure while remaining less than unity (hallow points in Figure 3.2 (b)). It is consistent with Equation (3.6), which indicates that the contribution of non-selective viscous flow to the total transport through the defects increases with an increase in $p_h + p_l$. On the other hand,

since Knudsen flow is independent of pressure, its contribution to the total flow must decrease with increasing p_h.

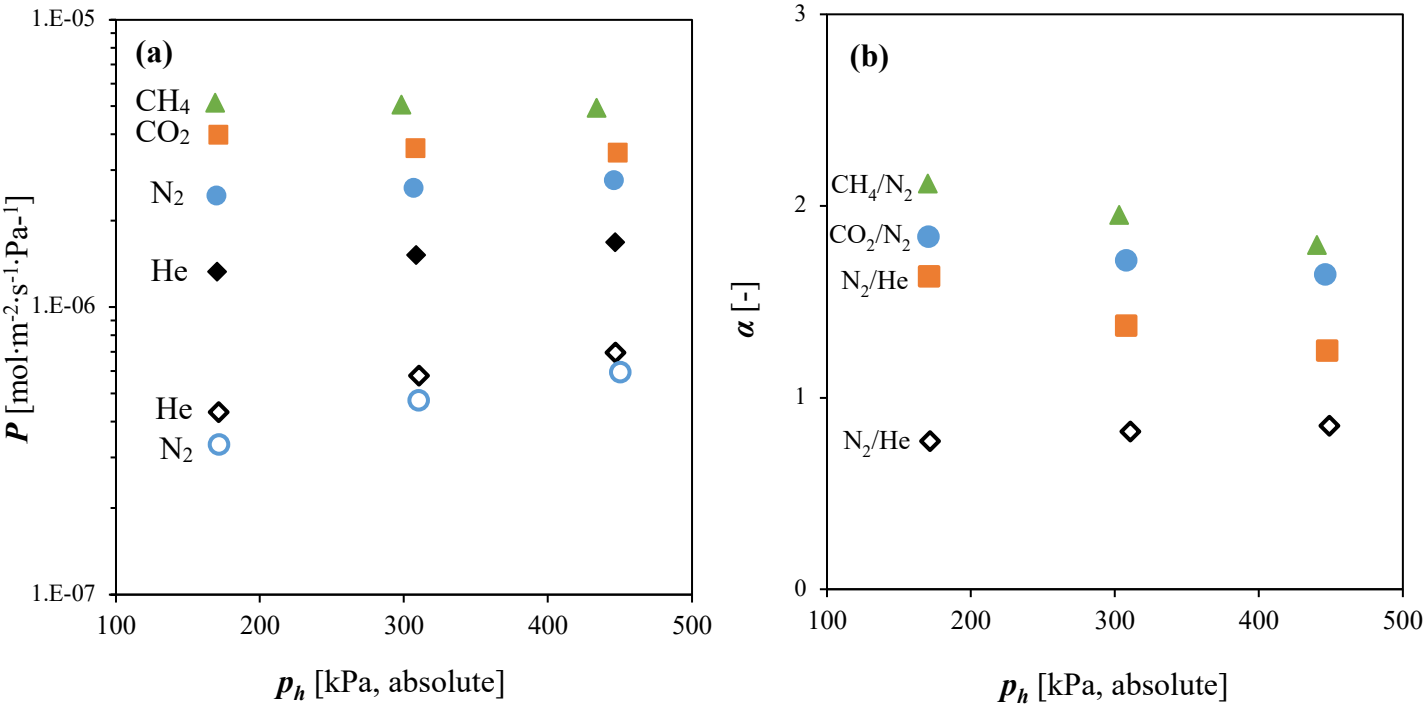

Figure 3.2. Summary of gas permeation experiments with membrane M1. **(a)** gas permeances, **(b)** ideal selectivities of selected pairs of gases. Hollow and filled points denote permeances (ideal selectivities) determined from permeation experiments conducted before and after membrane calcination respectively. All permeation experiments were conducted at a temperature of 295 ± 2 K. Membrane length and area were 6.0 ± 0.1 cm and 10.5 ± 0.1 cm^2, respectively.

As expected, He and N_2 permeances increase significantly after calcination. It is because calcination removes the template from the zeolite crystals, thus opening additional pathways for the transport of He and N_2 through the calcined membranes. As expected, the increase of N_2 permeance is much more significant than that of He. As a result, the calcined membranes become N_2-selective, i.e. the ideal N_2/He selectivity becomes greater than unity. Although He is smaller than N_2, it is practically not adsorbed by the silicalite crystals and its transport through the zeolite pores is limited to Knudsen flow. The fact that N_2 permeance of the calcined membranes is several times greater than that of the uncalcined membranes indicates that permeation through the calcined membranes is dominated by transport through the zeolite crystals.

Considering the effect of feed pressure on the ideal N_2/He selectivity of the uncalcined and calcined membranes, one can observe that the ideal N_2/He selectivity of the uncalcined membranes increases with feed pressure. In contrast, the opposite is the case for the calcined membranes. In both cases, the pressure dependence of the ideal selectivity results from an increasing contribution of non-selective viscous flow to the total transport at higher pressures. At higher feed pressures, more viscous flow occurs, which reduces the relative contribution of selective transport through zeolite channels. Although the trends are opposite, in both cases, the ideal selectivity at higher pressures is closer to unity than at the lower pressures.

CO_2 and CH_4 permeances of the calcined membranes are both higher than the N_2 permeance. Also, the CH_4 permeance is higher than the CO_2 permeance, which is in agreement with the findings of others in the literature [29,36–38]. It is interesting to note that unlike P_{N_2} of the calcined membrane, which increases with pressure, P_{CO_2} and P_{CH_4} are either approximately constant or decrease with p_h (Figure 3.2a). Moreover, the effect of feed pressure appears to be a little bit stronger for P_{CO_2} than for P_{CH_4}. These qualitative observations can be explained based on the transport mechanism through the pores of zeolite crystals. The transport of adsorbed gases such as N_2, CH_4 and CO_2 occurs by surface diffusion, in which the driving force is a surface occupancy difference across the membrane. In turn, the surface occupancy for a given gas is directly related to its adsorption isotherm. In the pressure range of interest, the N_2 isotherm is linear, while those of CO_2 and CH_4 are both concave. Moreover, the CO_2 isotherm is more concave than the CH_4 isotherm. If there were no viscous flow, P_{N_2} of the calcined membranes would be independent of pressure, while the P_{CO_2} and P_{CH_4} would decrease with increasing pressure. However, since calcination does not eliminate the contribution of viscous flow, P_{N_2} of the calcined membranes increases with pressure. Meanwhile, relatively constant P_{CO_2} and P_{CH_4} are influenced by the combined effects of a decreasing contribution of surface diffusion while there is an increasing viscous flow contribution with feed pressure.

Despite a higher affinity of CO_2 to silicalite crystals than CH_4, i.e. for a given feed pressure, the driving force for CO_2 diffusion is higher than that for CH_4, the permeance of CO_2 is less than the permeance of CH_4. This order of permeance can be attributed to the higher surface diffusion coefficient

of CH_4 in silicalite pores compared to CO_2, which is consistent with the data reported in the literature [19,29,36–39].

3.4.2. Quantification of the defect and zeolite transport

Table 3.4 summarizes the parameters characterizing the defect transport $x = \varepsilon_d/l_d$ and d_d, and the zeolite transport $y = \varepsilon_z/l_z$ and D_0. The procedure to calculate these parameters from the experimentally measured gas permeances was presented in Section 2. Each parameter was determined at three different pressures. In principle, the parameters should be independent of feed pressure. However, as shown in Table 3.4, they depend on pressure. The pressure dependence is particularly evident for the parameters characterizing the defect transport.

Table 3.4. Summary of experimentally determined model parameters, including corrected diffusivities of tested gases in silicalite-1 crystals.

Memb.	p_h* [kPa]	$x=\varepsilon_d/l_d$ [m^{-1}]	$d_d\times10^6$ [m]	$(y=\varepsilon_z/l_z)\times10^3$ [m^{-1}]	$D_{0,N2}\times10^8$ [$m^2\cdot s^{-1}$]	$D_{0,CO2}\times10^8$ [$m^2\cdot s^{-1}$]	$D_{0,CH4}\times10^8$ [$m^2\cdot s^{-1}$]
M1	171	0.57	2.1	9.63	8.28	1.79	7.01
	307	0.74	1.9	10.1	8.64	1.83	7.18
	445	0.94	1.6	10.6	9.07	1.92	7.19
M2	171	0.38	3.9	7.56	7.20	1.59	6.09
	310	0.61	3	7.63	7.72	1.71	6.24
	450	0.86	2.4	8.22	8.00	1.71	5.96
M3	171	0.33	2.4	11.8	7.83	1.48	6.21
	310	0.80	1.3	12.2	7.87	1.61	6.34
	450	0.95	1.2	13.1	8.30	1.60	6.38
M4	170	1.7	1.5	8.76	7.91	-	-
	309	1.1	2.1	9.56	7.70	-	-
	448	1.5	1.7	9.34	8.35	-	-
M5	171	1.3	1.5	12.6	6.37	-	-
	310	1.6	1.3	13.1	6.84	-	-
	447	2.3	1.0	13.4	7.68	-	-
M6	171	3.4	4.2	13.4	6.33	-	-
	309	5.8	2.7	14.0	7.01	-	-
	449	6.2	2.6	14.8	7.36	-	-
M7	171	1.7	1.5	17.1	6.24	-	-
	309	2.0	1.3	17.8	6.78	-	-
	444	3.0	1.0	18.4	7.15	-	-

*Average feed pressure

Except for the membrane M4, as the feed pressure increases, x increases while d_d decreases. According to Equation (3.6), an increase in either x or d_d increases P_d. Therefore, the opposite effect of the feed pressure on x and d_d may suggest that these two parameters are coupled. The values of d_d in Table 3.4 vary from 1.0 μm to 4.2 μm. Since the pore size of the active layer of the support provided by the manufacturer is 0.45 μm, the calculated d_d values appear to be very large. On the other hand, the pore size distribution of the active layer is unknown. It is possible that the active layer and small regular pores, may contain some large pores, which in turn would be difficult to plug during the hydrothermal synthesis.

The values of x in Table 3.4 vary from 0.33 m^{-1} to 6.2 m^{-1}. Assuming that l_d has a magnitude comparable to the thickness of the active layer, which has been found to be approximately 10 – 12 μm previously [19], the corresponding ε_d is in the order of 10^{-6} – 10^{-5}. In other words, according to the results reported in Table 3.4, the uncalcined membranes contain very few, but relatively large defects. In turn, this suggests that the vast majority of smaller pores in the active layer of the support were adequately plugged during the hydrothermal synthesis.

The values of x and d_d at a given feed pressure can be used to predict P_d of He and N_2 at the other feed pressures. Figure 3.3 presents the example of such predictions of P_d for He and N_2 in M1 at three different feed pressures. The predictions in this figure assume that regardless of the feed pressure, the permeate side is at atmospheric pressure. Figures similar to Figure 3.3 could be generated for each membrane listed in Table 3.4. It can be noticed that the highest N_2 permeance is predicted using x and d_d determined at the highest feed pressure. On the other hand, the lowest He permeance is predicted using x and d_d determined at the lowest feed pressure. However, there is no clear trend between the predicted P_d and the set of x and d_d used. Despite the variation of x and d_d with feed pressure, the predicted P_d using different sets of x and d_d are close to each other, confirming that x and d_d are coupled parameters.

The closeness of the predicted trendlines, regardless of the set x and d_d, represents the first validation of the proposed characterization method. In other words, the combination of x and d_d values adequately quantifies the defect transport through the membrane. A more detailed assessment of using x and d_d to predict P_d is presented in Table S.3.1 in the Appendix. The values of x and d_d determined at a given pressure are used to predict P_d at the other two pressures. The predicted P_d is then compared with the experimentally measured value, and the relative error in the predicted value to the measured value is reported. It is evident from Table S.3.1 that the relative error, which can be positive or negative, is

generally well below 10%. Also, the values of x and d_d determined at the medium and high feed pressures provide better predictions of P_d than the values determined at the low feed pressures

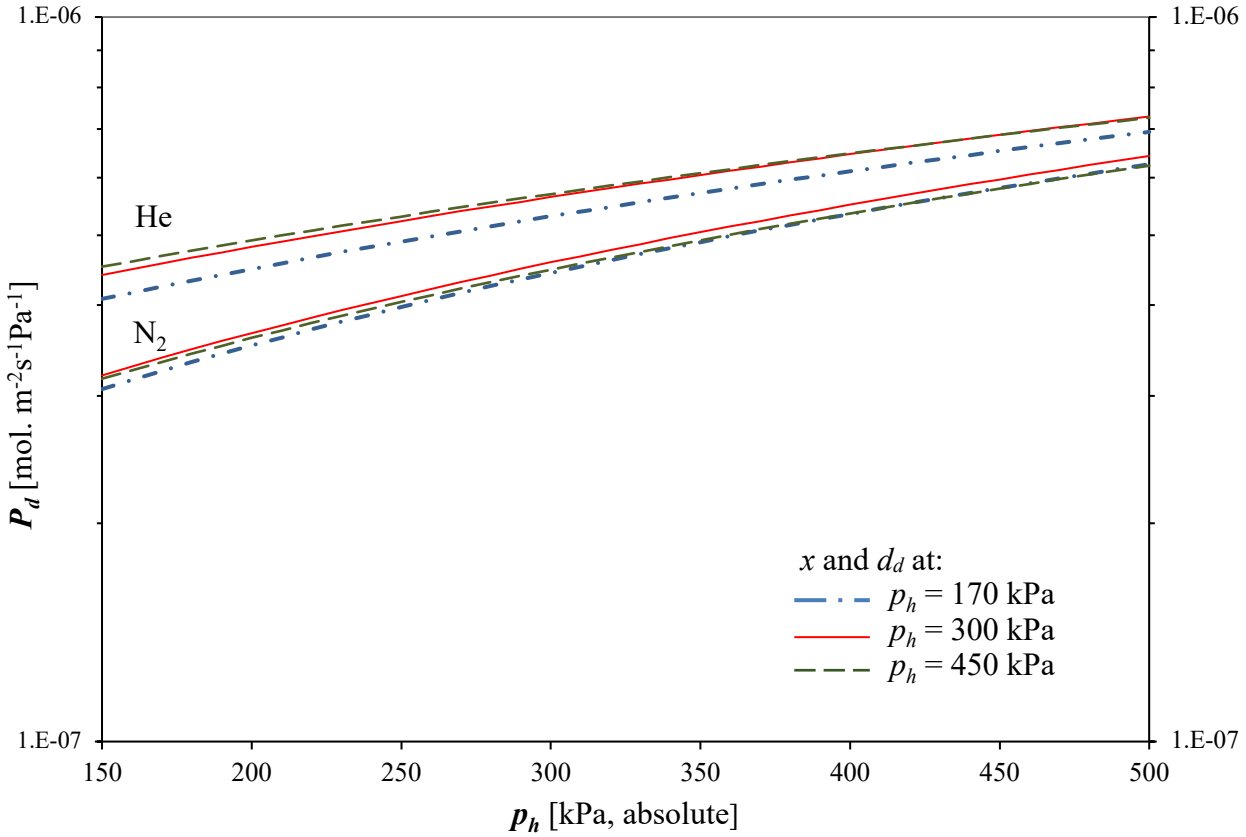

Figure 3.3. Effect of feed pressure on the predicted defect permeances of He and N_2 in the M1 membrane at 295 K and p_l=101.3 kPa. P_d calculated from Equation (3.6) using experimentally determined x and d_d at feed pressures of 170, 300 and 450 kPa.

In addition to x and d_d, which characterize the defect transport, Table 3.4 also summarizes $y = \varepsilon_z/l_z$ and D_0 for each membrane. Unlike x and d_d, which are coupled parameters, y and D_0 are not coupled. As explained in Section 2, using previously determined x and d_d, the y value is calculated from Equation (3.7), which is then used to calculate D_T from Equation (3.9). Finally, D_0 is calculated from Equation (3.10). The latter equation requires the knowledge of the adsorption isotherm. For M1-M3 membranes, D_0 is reported for N_2, CH_4 and CO_2, and M4-M7 membranes only for N_2.

It can be noticed that y and D_0 values of N_2 tend to increase with a feed pressure slightly. However, their dependence on feed pressure is much weaker than that of x and d_d. Moreover, there is hardly any dependence on the pressure of D_0 for CO_2 and CH_4. It is important to remember that similarly to x and d_d,

y is a characteristic parameter for a given membrane. On the other hand, D_0 should be independent of both the pressure and the given zeolite membrane.

As seen in Table 3.4, y varies from 7.56×10^3 m^{-1} to 18.4×10^3 m^{-1}. The variation in y is, therefore, much less than the variation in x. Also, y is a 4-orders magnitude higher than x; in contrast to ε_d, which depends on the quality of the membrane (the smaller the ε_d and d_d, the better membrane), ε_z depends on the type of zeolite crystals and the porosity of the active layer of the support. For zeolite crystals, the former is 0.15 [17], and the latter, according to the manufacturer of the porous support (TAMI), is approximately 0.23. The product of these two numbers (0.0345) provides the approximate value of ε_z. Consequently, since $y = \varepsilon_z/l_z$, l_z ranges from 1.9 μm to 4.5 μm. In other words, the effective path length for the transport in zeolite crystals is significantly smaller than the thickness of the active layer of the porous support, the pores of which are plugged during the hydrothermal synthesis.

Figure 3.4 presents a schematic representation of a defective pore (Figure 3.4a) and a selective pore (Figure 3.4b) in a pore-plugged membrane. In the limiting case, the pore of the active layer would be filled with zeolite crystals. However, as shown in Figure 3.4b, the complete pore-plugging is not necessary for the pore to be selective. The latter requires a continuous layer of zeolite crystals, which could be much thinner than the active layer of the membrane support. If there is a discontinuity in the zeolite layer (Figure 3.4a), the permeant molecules will bypass the zeolite crystals, even if there are many crystals in the pore. In this case, due to a tortuous pathway for the transport of permeating species, l_d would be greater than the thickness of the active layer. The schematic model presented in Figure 3.4 explains why l_z can be significantly smaller than l_d, or, more generally, the thickness of the active layer of the porous support.

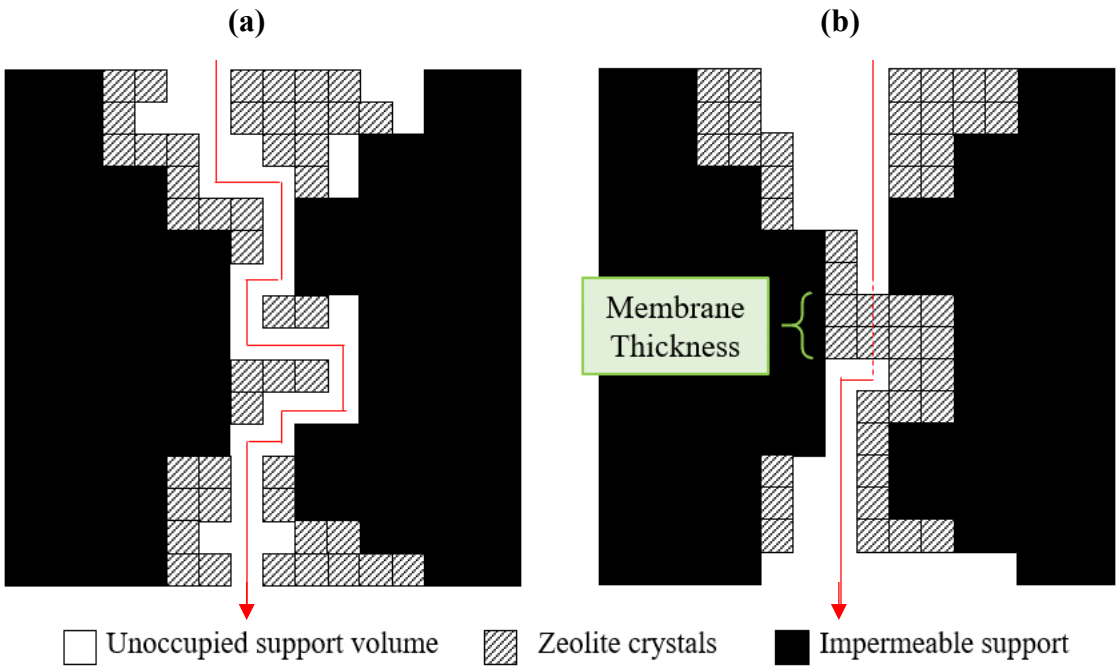

Figure 3.4.Schematic diagrams showing zeolite crystal occupancy configurations inside membrane support pores of pore plugged membranes. The line denotes the molecular pathway. Figure 3.4a shows a continuous defect pathway, and Figure 3.4b shows the pathway through a continuous zeolite layer made up of zeolite crystals, which can have a thickness less than the thickness of the active layer of the membrane support. Through the zeolite crystals, the molecular pathway line becomes dashed.

Considering D_0 of N_2, the minimum and the maximum values in Table 3.4 are 6.24 $\times 10^{-8}$ m^2/s and 9.07 $\times 10^{-8}$ m^2/s, respectively. The corresponding average and standard deviation values for D_0 of N_2 based 21 entries are 7.72 $\times 10^{-8}$ m^2/s and 0.76 $\times 10^{-8}$ m^2/s, respectively. In other words, for N_2, the standard deviation represents roughly 10% of the average value. For D_0 of CO_2, the average and standard deviation values are 1.69 $\times 10^{-8}$ m^2/s and 0.14 $\times 10^{-8}$ m^2/s, respectively, while for CH_4, these are 6.51 $\times 10^{-8}$ m^2/s and 0.48 $\times 10^{-8}$ m^2/s, respectively. Despite the smaller number of entries (9 versus 21), the standard deviation relative to the average value is 8.3% for CO_2 and 7.4% for CH_4.

Figure 3.5 presents the predicted total permeances of the calcined membrane M1 based on x, d_d, y, and D_0 values determined at three different pressures. Similarly to Figure 3.3, for a given gas, regardless of the set of the parameters used, predicted permeances are close to each other. However, they are not as

close as in Figure 3.3 for the uncalcined M1 membrane. This visual observation is further quantified in Table S.3.1 in the Appendix. The values of x, d_d, y, and D_0 determined at a given pressure are used to predict the total permeance at the other two pressures. The predicted permeance is then compared with the experimental value, and the relative error in the predicted value to the measured value is reported. Considering the predicted He and N_2 permeances, the relative error for He is generally less than that for N_2. The former is comparable to the relative error in the predicted permeances of the uncalcined membranes (up to 10%). The relative error in the predicted total N_2 permeances in Table S.3.1 is as high as 26%, but generally, it oscillates at ±10%. It is important to remember that the prediction of the He permeance requires only 3 parameters (x, d_d, y), but the prediction of the N_2 permeance requires all 4 parameters (x, d_d, y, D_0). Interestingly, although similarly to N_2, prediction of the CO_2 and CH_4 permeances also requires 4 parameters, the relative error in the predicted total CO_2 and CH_4 permeances in Table S.3.1 lower than for N_2.

For every gas in Figure 3.5, the highest predicted permeance is obtained using the set of characterization parameters determined at the highest feed pressure. The lowest predicted permeance is obtained using the set of characterization parameters determined at the lowest feed pressure. In other words, the order of the permeances follows the order of pressures at which the characterization parameters were determined. It might appear surprising that despite the fact x and d_d varied more considerably with pressure than y and D_0, the predicted permeances of the uncalcined membranes are closer to each other (Figure 3.3) than the predicted permeances of the calcined membranes (Figure 3.5). However, it should be remembered that, x and d_d are coupled, while y and D_0 are not coupled. In other words, the variation in x and d_d compensate each other when calculating the permeances of the uncalcined membranes. In contrast, the variation in y and D_0 independently contribute to the predicted permeance of the calcined membrane.

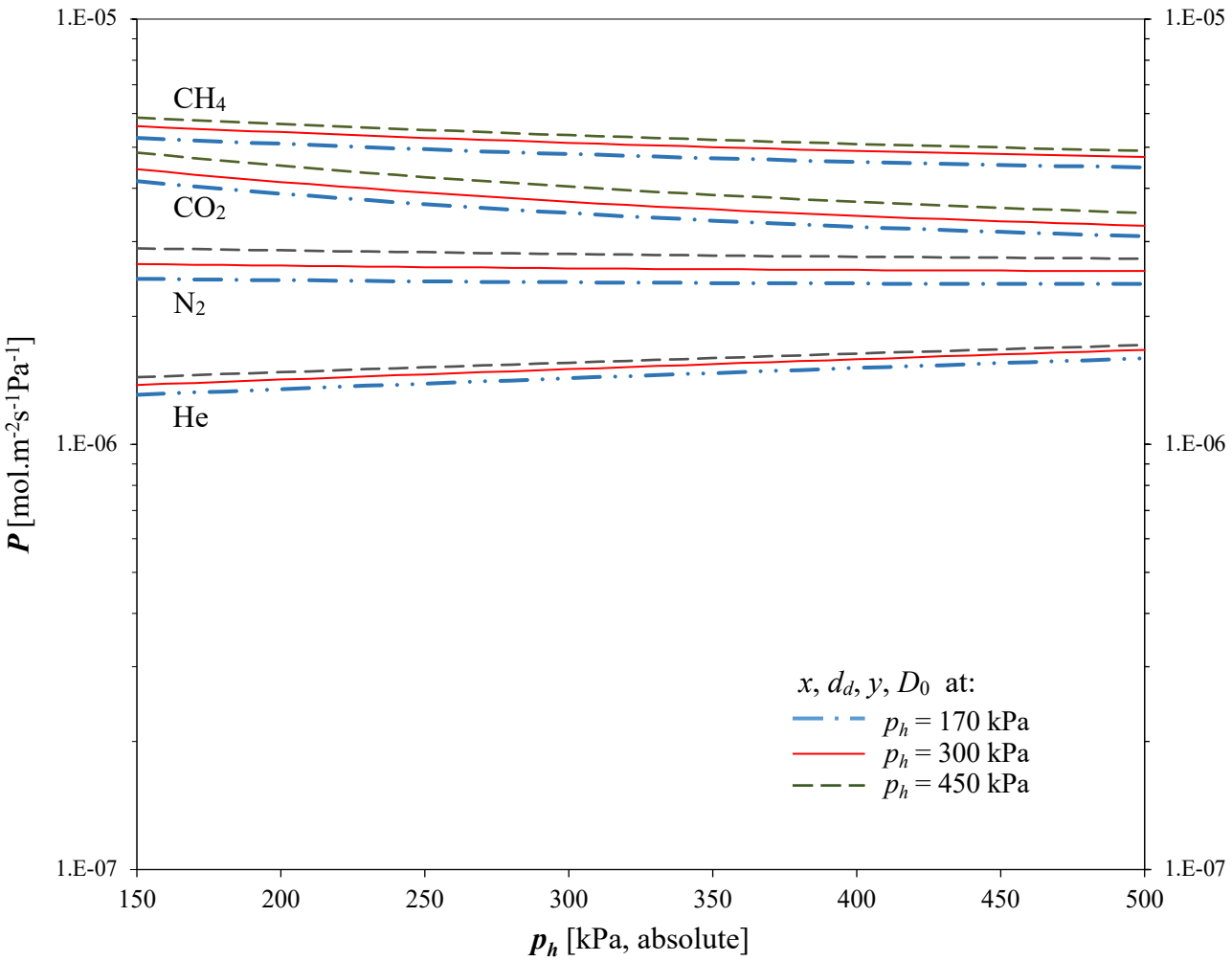

Figure 3.5. Effect of feed pressure on the predicted total permeances of He, N_2, CO_2, and CH_4 in the calcinated M1 membrane at 295 K and p_l = 101.3 kPa. The permeance of He calculated from Equation (3.7), and the permeance of N_2, CO_2 and CH_4 from Equation (3.9) using the experimental x, d_d, y, and D_0 determined at feed pressures of 170, 300 and 450 kPa.

3.5. DISCUSSION

There are different methods for determining the transport diffusivity of gases in zeolite membranes. These methods can be divided into two groups, i) microscopic techniques, and ii) macroscopic (permeation) techniques. The former include pulsed-field gradient nuclear magnetic resonance [40], quasi-elastic neutron scattering measurements [41], and micro-imaging by IR microscopy and optical interference microscopy [42,43]. In addition, some researchers also include atomistic molecular dynamics (MD) simulations in the category of microscopic methods [44].

The method proposed in this study falls into the category of permeation methods. The latter assume the applicability of Fick's first law to surface diffusion in zeolite crystals under non-equilibrium conditions. If surface diffusion were the only mode of gas transport through the zeolite membrane, the evaluation of transport diffusivity either from the steady-state gas flux or a time-lag would be straightforward [45]. However, apart from surface diffusion, gas transport in zeolite pores might take place also by Knudsen diffusion [16,29]. The situation becomes more complex when the zeolite membrane is not defect-free, i.e. when in addition to gas transport through zeolitic pores, there is also a parallel transport through the defects. Table 3.5 compares the average corrected diffusivities of N_2, CH_4, and CO_2 determined using the proposed method with the literature values of D_0 and D^0.

Table 3.5. Comparison of the corrected diffusivities of several gases in the silicalite-1 zeolite with the literature values.

Method	D_0 (or D^0) x 10^8 [m^2 s^{-1}]			Reference
	N_2	CO_2	CH_4	
Permeation[1]	7.72	1.69	6.51	This work
Permeation[2]	3.87	1.26	8.83	[17]
Permeation[2]	1.30	0.70	3.90	[29]
Quasi-Elastic Neutron Scattering (QENS)[1]	0.5 – 0.6	0.5 – 0.7	-	[44]
Molecular dynamics (MD)[1]	0.8	0.3 – 0.5	-	[44]
Molecular dynamics (MD)[1]	-	1.31	1.56	[46]
Infra-Red Micro-Imaging[1,3]	-	0.2 – 0.9	-	[47]

[1] D_0 = the corrected diffusivity; see Equation (3.10)
[2] D^0 = the limiting diffusivity; see Equation (3.10)
[3] Ref [47] reports D_T from which the current authors estimated D_0

In general, the corrected diffusivities in silicalite-1 evaluated using our method are higher than the values determined using microscopic methods. However, for a given gas, there is also a variation between different microscopic methods. For example, for CO_2, depending on the microscopic method, the corrected diffusivity ranges from 0.2 x 10^{-8} m^2 s^{-1} [47] to 1.31 x 10^{-8} m^2 s^{-1} [43]. Interestingly, our corrected diffusivities are closer to limiting diffusivities. They are between those reported by Zito et al. [17] and Bakker et al. [29]; the former are considerably higher than the latter. Although in both cases, gas transport in the silicalite-1 zeolite allows the coexistence of surface diffusion and Knudsen diffusion, Bakker et al.

[29] assumed that the two mechanisms occur in parallel. In contrast, Zito et al. [17] considered that gas molecules adsorbed inside the zeolite pores decrease the pore size and increase the tortuosity for Knudsen diffusion. As a result, Knudsen diffusion flux contributes more to the total flux in Bakker et al. [29] than in Zito et al. [17]. For the surface diffusion flux, the situation is the opposite, which is why the diffusivities reported by Zito et al. [17] are greater than those reported by Bakker et al. [29].

Our corrected diffusivities assume that gas transport in zeolite pores at ambient temperature occurs exclusively by surface diffusion; at the same time, our model allows for defect transport. As seen in Table 3.3, the contributions of the defect permanence to the total permeance are not negligible. For He, the defect permeance contributes from 19% to 63% to the total permeance. For N_2, the corresponding range is 6.4 % to 43%. By assuming defect-free membranes, the corrected diffusivities reported in Table 3.4 would not only be greater, but they would vary more with the feed pressure and the membrane. On the other hand, the corrected diffusivities in Table 3.4 might be overestimated because of the assumption of the exclusive transport by surface diffusion in the silicalite-1 zeolite. Since Knudsen diffusion of N_2 in silicalite-1 at ambient temperature is not negligible [17], this problem is likely most significant for the corrected diffusivities of N_2. On the other hand, this overestimation should be negligible for the corrected diffusivities of CH_4 and CO_2. It is important to emphasize that although neglecting possible Knudsen diffusion in zeolite pores introduces some uncertainty in the values determined by the proposed method, it greatly simplifies the mathematical analysis required to evaluate corrected diffusivities.

3.6. CONCLUSIONS

In this paper, we described and demonstrated a new method to characterize defect-containing zeolite membranes. More specifically, the method allows the determination of the following parameters:

1) ε_d/l_d, the ratio of the porosity resulting from the presence of the defects to the defect's length;
2) d_d, the effective pore size of the defects;
3) ε_z/l_z, the ratio of the porosity of the crystals in the selective layer of the membrane to the diffusion length in the crystal;
4) D_0, the corrected diffusivity of different adsorbed gases in the zeolite crystals.

The first two parameters characterize the defects; the smaller they are, the smaller the defect transport's contribution to total flux. The third parameter characterizes the selective layer; the greater it is, the greater

the surface diffusion flux. The last parameter represents the intrinsic properties of the zeolite crystals for different adsorbed gases. The proposed method requires two sets of permeation experiments with at least two gases, one not-absorbed gas (e.g. He), and the other an adsorbed gas (e.g. CO_2). The permeation tests are to be performed both before and after membrane calcination. Also, the method requires adsorption isotherm(s) of the gas(es) used in permeation experiments at the permeation experiment's temperature.

We demonstrated the new method's validity by successfully predicting the total gas permeation at different feed pressures when using the characteristic parameters determined at another feed pressure. Moreover, although gas permeation varied considerably from one membrane to another and with the feed pressure, the corrected diffusivities of N_2, CH_4 and CO_2 in silicalite-1 showed respective minimal variations. Compared to the literature values, our corrected diffusivities are higher than those determined using different microscopic techniques, but not more than an order of magnitude. On the other hand, they are more comparable (the same order of magnitude) to the limiting diffusivities of the respective gases, also determined by the different permeation methods. Since the proposed method assumes gas transport in zeolite crystals exclusively by surface diffusion, it is more suitable for determining the corrected diffusivities of strongly adsorbed gases such as CO_2.

3.7. ACKNOWLEDGEMENT

The authors gratefully acknowledge the financial support provided by the Natural Science and Engineering Research Council (NSERC) Canada.

3.8. DECLARATION OF COMPETING INTEREST

There are no conflicts of interest to declare.

3.9. NOMENCLATURE:

b	[Pa^{-1}]	Langmuir isotherm constant
d	[m]	Channel size

D_T	[$m^2 \cdot s^{-1}$]	Transport diffusivity
D^0	[$m^2 \cdot s^{-1}$]	Limiting diffusivity
D_0	[$m^2 \cdot s^{-1}$]	Corrected diffusivity
$E_{D,S}$	[$kJ \cdot mol^{-1}$]	Activation energy
J_d	[$mol \cdot m^{-2} \cdot s^{-1}$]	Defect flux
L	[m]	Membrane thickness
l	[m]	Effective length
M	[$kg \cdot mol^{-1}$]	Molecular weight
n	[-]	Number of defects per unit volume
P	[$mol \cdot m^{-2} \cdot s^{-1} \cdot Pa^{-1}$]	Permeance
P'	[$mol \cdot m^{-1} \cdot s^{-1} \cdot Pa^{-1}$]	Permeability
P_i	[$mol \cdot m^{-2} \cdot s^{-1} \cdot Pa^{-1}$]	Permeance of gas i
P_d	[$mol \cdot m^{-2} \cdot s^{-1} \cdot Pa^{-1}$]	Defect permeance
P_z	[$mol \cdot m^{-2} \cdot s^{-1} \cdot Pa^{-1}$]	Zeolite permeance
P_e	[$mol \cdot m^{-2} \cdot s^{-1} \cdot Pa^{-1}$]	Experimental permeance
p_h	[Pa]	Pressure at the high pressure side of the membrane
p_l	[Pa]	Pressure at the low pressure side of the membrane
q	[$mol \cdot kg^{-1}$]	Surface loading
q^s	[$mol \cdot kg^{-1}$]	Maximum surface loading
R	[$m^3 \cdot Pa \cdot K^{-1} \cdot mol^{-1}$]	Universal Gas constant
T	[K]	Temperature
x	[m^{-1}]	Lumped parameter describing defect porosity over defect effective length ε_d / l_d
y	[m^{-1}]	Lumped parameter describing zeolite porosity over zeolite effective length ε_s / l_s

Subscripts

i, j	Gas component identifier

d	Defect
v	Viscous flow
K	Knudsen flow
z	Zeolite

Greek letters

α	[-]	Ideal selectivity
ε	[-]	Volume fraction
μ	[$Pa \cdot s^{-1}$]	Dynamic viscosity
ρ	[$kg \cdot m^{-3}$]	Zeolite density

Abbreviations

CH_4	Methane
CO_2	Carbon dioxide
F-	Bubble flow metes
H_2	Hydrogen
H_2O	Water
He	Helium
M1, M2	Membrane identifiers
MFC-	Mass flow controller
MS	Maxwell-Stefan
N_2	Nitrogen
NaY	Sodium Y Zeolite
NSERC	Natural Sciences and Engineering Research Council of Canada
P-	Pressure transducer
PFD	Process flow diagram

SF_6	Sulfur Hexafluoride
SiO_2	Silica dioxide
T-	Thermocouple
TiO_2	Titanium dioxide
TPAOH	Tetra-propyl ammonium hydroxide

3.10. REFERENCES

[1] D.M. Ruthven, Principles of adsorption and adsorption processes, John Wiley and Sons, 1984.

[2] M. Pera-Titus, Porous inorganic membranes for CO_2 capture: Present and prospects, Chem. Rev. 114 (2014) 1413–1492. doi:10.1021/cr400237k.

[3] J.D. Figueroa, T. Fout, S. Plasynski, H. McIlvried, R.D. Srivastava, Advances in CO_2 capture technology - The U.S. Department of Energy's Carbon Sequestration Program, Int. J. Greenh. Gas Control. 2 (2008) 9–20. doi:10.1016/S1750-5836(07)00094-1.

[4] H. Maghsoudi, Defects of Zeolite Membranes: Characterization, Modification and Post-treatment Techniques, Sep. Purif. Rev. 45 (2016) 169–192. doi:10.1080/15422119.2015.1103270.

[5] G. Pecanac, J. Malzbender, F. Pauly, M.L. Fontaine, P. Niehoff, S. Baumann, T. Beck, L. Singheiser, Mechanical characterization of ceramics by means of a 3D defect analysis, Ceram. Int. 41 (2015) 2411–2417. doi:10.1016/j.ceramint.2014.10.055.

[6] S. Gourdin, L. Marcin, M. Podgorski, M. Cherif, L. Carroz, Effective elastic properties and residual stresses in directionally solidified eutectic Al_2O_3/YAG/ZrO_2 ceramics estimated by finite element analysis, J. Mater. Sci. 52 (2017) 13736–13747. doi:10.1007/s10853-017-1479-6.

[7] M. Drobek, J. Motuzas, M. van Loon, R.W.J. Dirrix, R. a. Terpstra, A. Julbe, Coupling microwave-assisted and classical heating methods for scaling-up MFI zeolite membrane synthesis, J. Memb. Sci. 401 (2012) 144–151. doi:10.1016/j.memsci.2012.01.045.

[8] C. Bai, M.-D. Jia, J.L. Falconer, R.D. Noble, Preparation and separation properties of silicalite composite membranes, J. Membr. Scien. 105 (1995) 79–87. doi:10.1016/0376-7388(95)00049-I.

[9] W. Xiao, J. Yang, J. Lu, J. Wang, A novel method to synthesize high performance silicalite-1 membrane, Sep. Purif. Technol. 67 (2009) 58–63. doi:10.1016/j.seppur.2009.03.007.

[10] J.B. Lee, H.H. Funke, R.D. Noble, J.L. Falconer, High selectivities in defective MFI membranes, J. Memb. Sci. 321 (2008) 309–315. doi:10.1016/j.memsci.2008.05.004.

[11] J. Van Den Bergh, M. Mittelmeijer-hazeleger, F. Kapteijn, Modeling Permeation of CO_2/CH_4, N_2/CH_4, and CO_2/Air Mixtures across a DD3R Zeolite Membrane, J. Phys. Chem. 114 (2010) 9379–9389. doi:10.1021/jp101075h.

[12] P.F. Lito, A.S. Santiago, S.P. Cardoso, B.R. Figueiredo, C.M. Silva, New expressions for single and binary permeation through zeolite membranes for different isotherm models, J. Memb. Sci. 367 (2011) 21–32. doi:10.1016/j.memsci.2010.10.034.

[13] R. Krishna, Describing the Diffusion of Guest Molecules Inside Porous Structures, J. Phys. Chem. 113 (2009) 19756–19781. doi:10.1021/jp906879d.

[14] T.Q. Gardner, J.L. Falconer, R.D. Noble, Adsorption and diffusion properties of zeolite membranes by transient permeation, Desalination. 149 (2002) 435–440. doi:10.1016/S0011-9164(02)00772-5.

[15] J. Kangas, L. Sandstrom, I. Malinen, J. Hedlund, J. Tanskanen, Maxwell–Stefan modeling of the separation of H_2 and CO_2 at high pressure in an MFI membrane, J. Memb. Sci. 435 (2013) 186–206. doi:10.1016/j.memsci.2013.02.026.

[16] A. Caravella, P.F. Zito, A. Brunetti, E. Drioli, G. Barbieri, Microporous and Mesoporous Materials A novel modelling approach to surface and Knudsen multicomponent diffusion through NaY zeolite membranes, Microporous Mesoporous Mater. 235 (2016) 87–99. doi:10.1016/j.micromeso.2016.07.049.

[17] P.F. Zito, A. Caravella, A. Brunetti, E. Drioli, G. Barbieri, Knudsen and surface diffusion competing for gas permeation inside silicalite membranes, J. Memb. Sci. 523 (2017) 456–469. doi:10.1016/j.memsci.2016.10.016.

[18] F. Jareman, J. Hedlund, D. Creaser, J. Sterte, Modelling of single gas permeation in real MFI membranes, J. Memb. Sci. 236 (2004) 81–89. doi:10.1016/j.memsci.2004.01.028.

[19] D. Kennedy, D. Carter, S. Wilson, B. Kruczek, F.H. Tezel, Pore plugging synthesis and characterization of silicalite-1 membranes using tubular TiO2 supports: Effect of support pore size on membrane performance., Can. J. Chem. Eng. 96 (2018) 1597–1611. doi:0.1002/cjce.23095.

[20] J. Kärger, D.M. Ruthven, D.N. Theodorou, Diffusion in Nanoporous Materials, John Wiley and Sons, 2012.

[21] R.W. Baker, Membrane Technology and Applications, 3rd ed., Wiley, 2012.

[22] J. Dong, Y.S. Lin, M. Hu, R. Peascoe, E.A. Payzant, Template-removal-associated microstructural development of porous ceramic-supported MFI zeolite membranes, Microporous Mesoporous Mater. 34 (2000) 241–253. doi:https://doi.org/10.1016/S1387-1811(99)00175-4.

[23] M.-D. Jia, K.-V. Peinemann, R.-D. Behling, Ceramic zeolite composite membranes., J. Memb. Sci. 82 (1993) 15–26. doi:10.1016/0376-7388(93)85089-F.

[24] J.M. Van De Graaf, F. Kapteijn, J.A. Moulijn, Permeation of weakly adsorbing components through a silicalite-1 membrane, Chem. Eng. Sci. 54 (1999) 1080–1092. doi:10.1016/S0009-2509(98)00326-1.

[25] X. Lin, J.L. Falconer, R.D. Noble, Parallel Pathways for Transport in ZSM-5 Zeolite Membranes, Chem. Mater. 10 (1998) 3716–3723. doi:10.1021/cm980484m.

[26] O. Talu, A.L. Myers, Reference potentials for adsorption of helium, argon, methane, and krypton in high-silica zeolites, Colloids Surfaces A Physicochem. Eng. Asp. 187 (2001) 83–93. doi:10.1016/S0927-7757(01)00628-8.

[27] R. Nagumo, H. Takaba, S. Suzuki, S. Nakao, Estimation of inorganic gas permeability through an MFI-type silicalite membrane by a molecular simulation technique combined with permeation theory, Microporous Mesoporous Mater. 48 (2001) 247–254. doi:10.1016/S1387-1811(01)00359-6.

[28] P. Malbrunot, D. Vidal, J. Vermesse, R. Chahine, T.K. Bose, Adsorbent Helium Density Measurement and Its Effect on Adsorption Isotherms at High Pressure, Langmuir. 13 (1997) 539–544. doi:10.1021/la950969e.

[29] W.J.W. Bakker, L.J.P. Van Den Broeke, F. Kapteijn, J. a Moulijn, Temperature Dependence of One-Component Permeation through a Silicalite-1 Membrane, AIChE J. 43 (1997) 2203–2214. doi:10.1002/aic.690430907.

[30] S. Miachon, E. Landrivon, M. Aouine, Y. Sun, I. Kumakiri, Y. Li, O.P. Prokopová, N. Guilhaume, a. Giroir-Fendler, H. Mozzanega, J. a. Dalmon, Nanocomposite MFI-alumina membranes via pore-plugging synthesis. Preparation and morphological characterisation, J. Memb. Sci. 281 (2006) 228–238. doi:10.1016/j.memsci.2006.03.036.

[31] M. Anderson, H. Wang, Y.S. Lin, Inorganic membranes for carbon dioxide and nitrogen separation, Rev. Chem. Eng. 28 (2012) 101–121. doi:10.1515/revce-2012-0001.

[32] L. Tosheva, B. Mihailova, V. Valtchev, J. Sterte, Silicalite-1 macrostructures - preparation and structural features, Microporous Mesoporous Mater. 39 (2000) 91–101. doi:10.1016/S1387-1811(00)00179-7.

[33] P. Li, F.H. Tezel, Pure and Binary Adsorption Equilibria of Carbon Dioxide and Nitrogen on Silicalite, J. Chem. Eng. Data. 53 (2008) 2479–2487. https://doi.org/10.1021/je700183y.

[34] P. Li, F.H. Tezel, Pure and Binary Adsorption Equilibria of Methane and Carbon Dioxide on Silicalite, Sep. Sci. Technol. 42 (2007) 3131–3153. doi:10.1080/01496390701512034.

[35] P. Li, F.H. Tezel, Pure and Binary Adsorption of Methane and Nitrogen by Silicalite, J. Chem. Eng. Data. 54 (2009) 8–15. doi:10.1021/je7005902.

[36] A.J. Burggraaf, Z. Vroon, K. Keizer, H. Verweij, Permeation of single gases in thin zeolite MFI membranes, J. Memb. Sci. 144 (1998) 77–86. doi:10.1016/S0376-7388(98)00036-2.

[37] C. Algieri, P. Bernardo, G. Golemme, G. Barbieri, E. Drioli, Permeation properties of a thin silicalite-1 (MFI) membrane, J. Memb. Sci. 222 (2003) 181–190. doi:10.1016/S0376-7388(03)00286-2.

[38] M. Noack, P. Kölsch, V. Seefeld, P. Toussaint, G. Georgi, J. Caro, Influence of the Si/Al-ratio on the permeation properties of MFI-membranes, Microporous Mesoporous Mater. 79 (2005) 329–337. doi:10.1016/j.micromeso.2005.01.004.

[39] D. Carter, D. Kennedy, F.H. Tezel, B. Kruczek, Characterization of Inorganic Silicalite - 1 Membrane to be used for the Separation of Greenhouse Gases, J. Fluid Flow Heat Mass Transf. 1 (2014) 43–47. doi:10.11159/jffhmt.2014.007.

[40] Kärger, J.; Ruthven, D. M. Diffusion in Zeolites and Other Porous Materials; Wiley-Interscience: New York, 1992. Rouquerol F.; Sing, K. S. W. Adsorption by Powders and Porous Solids; Academic Press: London, 1999.

[41] H. Jobic, J. Kärger, M. Bée, Simultaneous Measurement of Self- and Transport Diffusivities in Zeolites, Phys. Rev. Lett. 82 (1999) 4260–4263. https://doi.org/10.1103/PhysRevLett.82.4260.

[42] J. Kärger, T. Binder, C. Chmelik, F. Hibbe, H. Krautscheid, R. Krishna, J. Weitkamp, Microimaging of transient guest profiles to monitor mass transfer in nanoporous materials, Nat. Mater. 13 (2014) 333–343. https://doi.org/10.1038/nmat3917.

[43] D. Carter, F.H. Tezel, B. Kruczek, J. Kärger, D. Ruthven, C. Chmelik, "Determination of the adsorption isotherms and transport diffusivities of gases in mixtures inside zeolitic crystals using Infra-Red Micro-imaging," MethodsX 7 (2020) 100993, doi.org/10.1016/j.mex.2020.100993.

[44] G.K. Papadopoulos, H. Jobic, D.N. Theodorou, Transport diffusivity of N_2 and CO_2 in silicalite: Coherent quasi-elastic neutron scattering measurements and molecular dynamics simulations, J. Phys. Chem. B. 108 (2004) 12748–12756. doi:10.1021/jp049265g.

[45] J. Caro, Diffusion coefficients in nanoporous solids derived from membrane permeation measurements, Adsorpt. J. Int. Adsorpt. Soc. (2020), doi-org.proxy.bib.uottawa.ca/10.1007/s10450-020-00262-z

[46] R. Babarao, J. Jiang, Diffusion and separation of CO2 and CH4 in Silicalite, C168 schwarzite, and IRMOF-1: A comparative study from molecular dynamics simulation, Langmuir. 24 (2008) 5474–5484. https://doi.org/10.1021/la703434s.

[47] D. Carter, F.H. Tezel, B. Kruczek, J. Kärger, D. Ruthven, V.R.R. Marthala, C. Chmelik, "Equilibrium isotherms and transport diffusivities for CO2 and CO2/N2 mixtures in silicalite measured by Infra-Red Micro-imaging", Microporous and Mesoporous Materials" 300, (2020) 110172, doi.org/10.1016/j.micromeso.2020.110172.

3.11. SUPPLEMENTARY MATERIAL

Table S.3.1. Summary of the predicted permeances (P_p)* and the corresponding errors (e)** with respect to the experimentally measured permeances (P_e)* listed in Table 3.3.

Memb.	p_h***	$He^{(1)}$		$N_2^{(1)}$		$He^{(2)}$		$N_2^{(2)}$		$CH_4^{(2)}$		$CO_2^{(2)}$	
	[kPa]	P_p	e	P_p	e	P_p	e	P_p	e	P_p	e	P_p	e
M1	171	4.31	-	3.33	-	13.30	-	24.42	-	51.66	-	39.76	-
		4.64	8%	3.47	4%	14.02	5%	26.44	8%	55.06	7%	42.39	7%
		4.75	10%	3.42	3%	14.61	10%	28.75	18%	57.59	11%	46.29	16%
	307	5.45	-6%	4.60	-3%	14.46	-5%	24.10	-7%	47.76	-6%	33.57	-6%
		5.79	-	4.75	-	15.18	-	25.98	-	50.75	-	35.65	-
		5.84	1%	4.64	-2%	15.71	4%	28.02	8%	52.81	4%	38.58	8%
	445	6.62	-5%	5.94	0%	15.66	-7%	24.07	-13%	45.26	-9%	30.30	-12%
		6.96	0%	6.11	3%	16.40	-3%	25.83	-6%	47.93	-3%	32.05	-7%
		6.95	-	5.93	-	16.86	-	27.62	-	49.60	-	34.30	-
M2	171	7.72	-	6.75	-	14.72	-	21.12	-	42.25	-	33.01	-
		7.94	3%	6.58	-3%	15.00	2%	22.12	5%	42.96	2%	34.79	5%
		8.13	5%	6.44	-5%	15.76	7%	23.80	13%	43.66	3%	36.65	11%
	310	10.21	0%	9.59	4%	17.36	-1%	23.16	-3%	43.29	0%	31.48	-3%
		10.26	-	9.22	-	17.45	-	23.84	-	43.48	-	32.52	-
		10.32	1%	8.93	-3%	18.07	4%	25.20	6%	43.74	1%	33.68	4%
	450	13.15	2%	12.72	9%	20.28	-2%	25.47	-5%	45.64	1%	32.11	-3%
		13.00	1%	12.14	4%	20.18	-2%	25.84	-4%	45.32	0%	32.58	-2%
		12.89	-	11.67	-	20.62	-	26.89	-	45.16	-	33.22	-
M3	171	3.03	-	2.42	-	14.05	-	26.82	-	54.16	-	39.45	-
		3.16	4%	2.18	-10%	14.53	3%	27.51	3%	56.48	4%	43.69	11%
		3.25	7%	2.18	-10%	15.51	10%	30.99	16%	60.95	13%	46.61	18%
	310	3.88	2%	3.36	15%	14.91	-2%	25.89	-1%	48.88	-3%	32.78	-8%
		3.81	-	2.91	-	15.19	-	26.27	-	50.41	-	35.74	-

		3.89	2%	2.89	-1%	16.16	6%	29.45	12%	54.21	8%	37.99	6%
	450	4.72	4%	4.29	19%	15.81	-6%	25.20	-11%	45.41	-8%	29.02	-12%
		4.46	-1%	3.63	1%	15.89	-6%	25.27	-10%	46.24	-7%	31.04	-6%
		4.52	-	3.59	-	16.82	-	28.17	-	49.52	-	32.85	-
M4	170	8.06	-	5.72	-	16.23	-	24.05	-				
		7.84	-3%	6.02	5%	16.76	3%	25.46	6%				
		8.25	2%	6.03	5%	16.96	5%	26.64	11%				
	309	9.83	0%	7.74	-7%	18.04	-4%	24.76	-6%				
		9.86	-	8.33	-	18.81	-	26.39	-				
		10.17	3%	8.22	-1%	18.93	1%	27.36	4%				
	448	11.70	-4%	9.84	-6%	19.99	-5%	25.74	-9%				
		12.00	-2%	10.72	2%	21.05	0%	27.61	-3%				
		12.20	-	10.50	-	21.04	-	28.36	-				
M5	171	5.73	-	4.05	-	17.54	-	25.34	-				
		5.98	4%	4.09	1%	18.24	4%	27.81	10%				
		6.36	11%	4.07	1%	18.87	8%	31.25	23%				
	310	7.00	-3%	5.47	0%	18.84	-3%	25.15	-8%				
		7.21	-	5.46	-	19.48	-	27.38	-				
		7.49	4%	5.33	-2%	20.01	3%	30.41	11%				
	447	8.25	-4%	6.88	4%	20.17	-5%	25.27	-16%				
		8.43	-2%	6.83	4%	20.79	-2%	27.28	-9%				
		8.59	-	6.58	-	21.18	-	29.92	-				
M6	171	2.97	-	1.53	-	15.47	-	23.98	-				
		3.07	4%	1.45	-5%	16.13	4%	27.36	14%				
		3.12	5%	1.46	-4%	16.94	9%	30.28	26%				
	309	3.24	-1%	1.83	9%	15.75	-3%	22.49	-12%				
		3.26	-	1.67	-	16.32	-	25.51	-				
		3.31	1%	1.68	0%	17.13	5%	28.19	10%				
	449	3.51	0%	2.12	13%	16.04	-7%	21.22	-19%				

		3.46	-1%	1.89	0%	16.54	-5%	23.90	-9%				
		3.50	-	1.89	-	17.33	-	26.36	-				
M7	171	7.39	-	5.20	-	23.32	-	33.37	-				
		7.64	3%	5.21	0%	24.22	4%	37.06	11%				
		8.11	10%	5.17	0%	25.24	8%	39.91	20%				
	309	8.99	-2%	7.01	1%	25.04	-3%	33.07	-9%				
		9.18	-	6.95	-	25.85	-	36.37	-				
		9.51	4%	6.76	-3%	26.74	3%	38.80	7%				
	444	10.63	-3%	8.83	6%	26.76	-5%	33.17	-13%				
		10.76	-2%	8.70	4%	27.53	-3%	36.15	-5%				
		10.94	-	8.36	-	28.24	-	38.21	-				

* All permeances in [$10^7 \times mol \cdot s^{-1} \cdot m^{-2} \cdot Pa$]

** $e = \left[\left(P_p\text{-}P_e\right)/P_e\right] \times 100\%$

***Average feed pressure

(1) Before calcination

(2) After calcination

Chapter 4

Modification of In-Situ Characterization Model

S. Al-Akwaa, D. Carter, J. Penny, B. Kruczek, F.H. Tezel
University of Ottawa, Department of Chemical and Biological Engineering
161 Louis Pasteur, Ottawa, Ontario, CANADA, K1N 6N5

Abstract

Inorganic membranes have great advantages in separation of gases compared to others, due to their low energy demand and maintenance requirements. However, their main disadvantage is the presence of defects within the selective layer. Therefore a characterization model is used to isolate the effect of defects to further understand the quality of the membranes synthesized. The model relies on knowledge of the adsorption isotherms and the results of single gas permeation experiments. It investigates the quality of the membranes by quantifying the flow through the defects and providing structural parameters of the membrane. Consequently, allowing for better assessment of the membranes' performance and obtaining reliable diffusivity values for silicalite-1.

Nevertheless, the seal used to connect the membrane to the housing module plays an important role in such analysis. In this study, ten membranes are tested using two types of sealants. One of these sealants had a higher permeance than the other one, indicating the presence of defects in the seal. Accordingly, the original model was modified to distinguish the defect source and provide parameters that describe the defects in the membrane alone. 2 out of 10 membranes gave reasonable physical parameters.

Keywords: Zeolite, silicalite, Membranes, Characterization, Diffusivity, Gas separations

HIGHLIGHTS:

- Distinguishing the defects present in the membrane from the seal
- Quantifying membrane defects

4.1. INTRODUCTION

Gas separation processes include cryogenic distillation, membrane separation, adsorption and amine absorption. Most of these processes have large demands for energy and maintenance. Membranes have been extensively studied over the past years for gas separation applications. Zeolite membranes being robust and thermally stable can be used in harsh environments. Specifically, silicalite-1 membranes deposited on various supports have been studied for their selective adsorption and precise pore size distribution. It shares an MFI framework with zeolite ZSM-5 [1], which has an average pore size of 5.5 Å [2]. The two can be distinguished by their Si/Al ratio where silicalite's ratio is greater than 1000 [3]. This low number of cations in its framework makes it hydrophobic [4]. The pore size of silicalite-1 promotes its use for gases such as CO_2, CH_4 and N_2 as they can permeate with a reasonable flux.

Membranes are placed in housing modules that separate the feed and permeate flow. Tubular and disk shapes are the most common for zeolite membranes. Depending on the shape, the housing module is designed accordingly. Zeolite membranes are commonly deposited on porous stainless steel (SS) or ceramic supports. Before membrane synthesis, SS supports can be welded onto non-porous parts that seal the module [5]. However due to the large thermal expansion differences between the SS support and silicalite, cracks can be introduced during calcination [6]. For tubular ceramic supports, an epoxy seal can be used to attach SS tubes that extend to the module as shown in Figure 4.1 (a). Or, the support ends are coated with an impermeable substance to seal the ends and O-rings are placed when the membrane is installed as shown in Figure 4.1 (b) to separate the streams. In literature, for tubular membranes, the ends of the side surface and axial surfaces of the membrane are coated using glass enamel [7][8] or ceramic glaze Duncan GL 611A [9][10]. Whereas O-rings commonly used are made out of graphite [7][8][9] or silicon rubber [5][10][11].

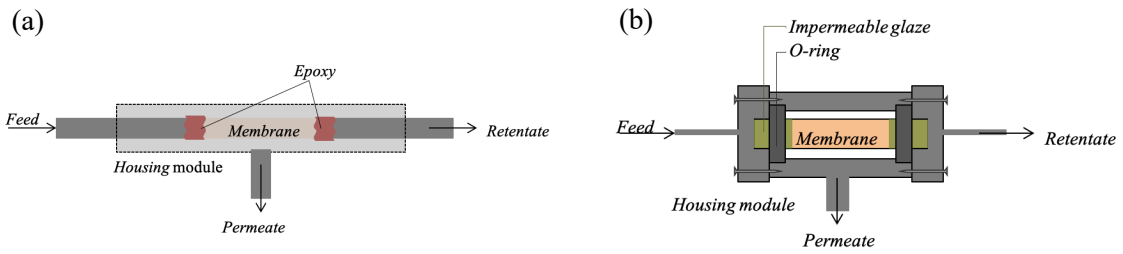

Figure 4.1. Types of modules (a) using epoxy and (b) using an impermeable glaze at the membrane ends and O-rings.

In this work, different types of modules and sealants were studied. A summary of the housing modules, the compression fittings or O-rings, place of connection and sealant are provided in Table 4.1. Three types of SS modules were prepared in our labs:

Module 1 - with Teflon ferrules on stainless steel tubing and epoxy connecting membrane to SS tubes as shown in Figure 4.1 (a).

Module 2 - with Teflon ferrules on ceramic membrane support with impermeable coating to seal ends and without epoxy.

Module 3 - with graphite gaskets (O-ring) on ceramic membrane support with impermeable coating to seal ends as shown in Figure 4.1 (b).

Two sealants were used for the first module, general epoxy (Devcon, Danvers, MA, USA and Solon, OH, USA) and torrseal epoxy (Agilent, Santa Clara, CA, USA) that is suitable for vacuum conditions. The second module requires an impermeable coating at the two ends of the side surface and axial surfaces of the ceramic tubular support. For that, Aremco 617 (Aremco Products Inc, Valley Cottage, NY), Aremco 617 with silicon rubber coating, Minwax Polycrylic (Sherwin Williams, Cleveland, OH, USA) and Tremclad (Rust-Oleum, Vernon Hills, IL, USA) were tested. Both Minwax and Tremclad have been proven to emit VOCs that would likely poison the membrane. Silicon rubber was used with Aremco 617 to block any viscous flow between the Teflon ferrules and the membrane. However, due to the compressive stress from the Teflon ferrules the impermeable layer was scraped. More information can be found on these trials in D. Carter's work [12]. Even though Aremco 617 is thought to degrade in basic solutions such as the precursor solution used in silicalite membrane's synthesis [13][14], it is proven to be the best at sealing as it does not off-gas

and can withstand the high temperatures required for calcination and regeneration. Curing of Aremco 617 is done at 875℃, which could affect the thermal stability of silicalite [15], thus the supports are glazed before synthesis. However, multiple coatings are applied to reduce the effect of degradation and to ensure the results obtained are reproducible. Therefore, for the final module (module 3) with compressible graphite gaskets, Aremco 617 is used. In this study two modules are used to test the same membrane. At first Aremco 617 is applied and module 3 is used, then Torrseal epoxy is applied and module 1 is installed. Torrseal melts at 120℃ thus it can only be applied after calcination. After that, regeneration can only be performed by purging helium gas through the membrane. Despite its low melting point, Torrseal remains the best at sealing the ends and withstanding high pressures required for this study.

Table 4.1. Summary of module design, fittings and sealants used in this study.

Module	Compression fitting	Compression fitting connecting	Sealant used on membrane
1	Teflon	SS tubing to housing module	• Generic epoxy • Torrseal
2	Teflon	Ceramic support to housing module	• Aremco 617 • Aremco 617 and silicon rubber • Minwax • Tremclad
3	Graphite gaskets	Ceramic support to housing module	• Aremco 617

In this paper, the characterization model is applied to the results obtained using these two modules. After observing a change in the permeance with different seals it is assumed that the difference is due to non-selective openings in the seal we call defects. We try to model these defects to obtain physically reasonable parameters that compare to known values. Thus, allowing us to distinguish the defects that are within the membrane from those in the seal for better assessment of the membranes.

4.2. THEORETICAL BACKGROUND

Gases permeating through the membrane by three types of mass transfer mechanisms: viscous flow, Knudsen diffusion and surface diffusion. The gases can travel within the membrane through crystal channels and through defects. Consequently, the governing transport depends on the permeating gas and the passageway. In order to quantify the type of transport that takes place, a characterization model developed by Carter [12] is used. The model contains structural parameters and diffusivity values for the zeolite, which are calculated using single gas permeation experiments. For all permeating species, the permeance prior to calcination is by viscous flow and Knudsen diffusion solely through defects. However, after calcination, when the crystal pores are opened, non-adsorbed gases permeate by Knudsen diffusion, whereas adsorbed gases permeate by surface diffusion.

Viscous flow is commonly referred to as Poiseuille flow, which is a non-selective flow that depends on the pressure difference across the pore. Whereas, Knudsen diffusion is selective and proportional to the inverse square root of the molecular weight of the permeating specie. It usually occurs when the free mean path is equal to or larger than the pore diameter, and the movement of the molecules happens as they collide with the pore wall. On the other hand, surface diffusion happens in the adsorbed phase and greatly depends on the adsorbate molecule's affinity towards the adsorbent. This transport depends on the slope of the adsorption isotherm, which represents the change in quantity adsorbed over pressure gradient at constant temperature. Transport by this mechanism has been illustrated as molecules hopping from one adsorption site to another. Surface diffusion is an activated process [16]. In the model that is developed, the three transport mechanisms are expressed and are summed up to provide the total permeance through the membrane.

Langmuir isotherm is used to model the adsorption isotherm data collected by Kennedy et al. for silicalite-1 adsorbent for nitrogen, methane and carbon dioxide gases [17] and the model parameters are reported in Table 4.2. Langmuir model is based on the assumption that adsorption is monolayer and the energy of adsorption is the same for all sites. The model is shown in Equation (4.1) where q_{sat} is the quantity adsorbed at saturation (mmol/g), K is the Langmuir adsorption coefficient (atm^{-1}) and p is the pressure (atm).

$$q = \frac{q_{sat} K p}{1 + K p} \tag{4.1}$$

Table 4.2. Langmuir isotherm parameters for silicalite-1 using data collected by Kennedy et al. [17]

	N_2	CH_4	CO_2
q_{sat} (mmol/g)	1.371	1.986	3.28
K (atm^{-1})	0.128	0.268	0.723

For silicalite-1, Helium is considered not adsorbed whereas nitrogen is, with a relatively linear adsorption isotherm. For both adsorbed and not adsorbed gas species before calcination, the model consists of viscous and Knudsen flow through defects as shown in Equation (4.2). Where $\mathcal{P}_i$ is the total permeance, $\mathcal{P}_{v,d}$ and $\mathcal{P}_{K,d}$ are the permeances due to viscous flow and Knudsen diffusion through the defects, respectively, d_d is the defect diameter assuming them to be straight cylinders, x_d is a parameter equal to $\frac{\varepsilon_d}{l_d}$ (void fraction over the effective length of the defects), p_h and p_l are the pressures at the high and low pressure sides, respectively, μ_i is the viscosity of the gas, R is the gas constant, T is the absolute temperature and M_i is the molecular weight of the permeating gas.

$$\mathcal{P}_i = \mathcal{P}_{v,d} + \mathcal{P}_{k,d} = x_d d_d^2 \frac{(p_h + p_l)}{64 \mu_i RT} + x_d d_d \frac{1}{3} \sqrt{\frac{8}{\pi M_i RT}} \tag{4.2}$$

After calcination, gases that are not-adsorbed such as helium, permeate through crystal channels by Knudsen diffusion. Therefore, for these gases, another Knudsen term is applied to the model with parameters that describe the crystal pores as shown in Equation (4.3). Where y is equal to $\frac{\varepsilon_z}{l_z}$ (the void fraction over the effective length for the zeolite crystal) and d_z is the average zeolite crystal pore size, which is taken as 5.5 Å [2].

$$\mathcal{P}_i = \mathcal{P}_{v,d} + \mathcal{P}_{k,d} + \mathcal{P}_{k,z} = x_d d_d^2 \frac{(p_h + p_l)}{64 \mu_i RT} + x_d d_d \frac{1}{3} \sqrt{\frac{8}{\pi M_i RT}} + y d_z \frac{1}{3} \sqrt{\frac{8}{\pi M_i RT}} \tag{4.3}$$

For gases that are adsorbed, the transport mechanism in zeolite crystals is mainly by surface diffusion, which depends on transport diffusivity and adsorption affinity as shown in

Equation (4.4), where, q_h and q_l are the quantity adsorbed at the high and low pressure sides, ρ is the density of silicalite-1 and D_T is the transport diffusivity.

$$\mathcal{P}_i = \mathcal{P}_{v,d} + \mathcal{P}_{k,d} + \mathcal{P}_{SD,z} = x_d d_d^2 \frac{(p_h + p_l)}{64\mu_i RT} + x_d d_d \frac{1}{3}\sqrt{\frac{8}{\pi M_i RT}} + y\left(\frac{q_h - q_l}{p_h - p_l}\right)\rho D_T \tag{4.4}$$

Transport diffusivity, D_T is a proportionality constant for molar flux and it greatly depends on the conditions of the experiment. However, by applying fundamental equations, corrected transport diffusivity constant is obtained, which is considered to be more independent of concentration or loading compared to transport diffusivity [3]. It is donated as D_0 and is specific to the adsorbent and adsorbate pair. The logarithmic slope of the isotherm relates the two diffusivities as shown in Equation (4.5):

$$D_T = D_0 \frac{\ln p_h - \ln p_l}{\ln q_h - \ln q_l} \tag{4.5}$$

After testing the same tubular membrane in module 1 with torrseal over Aremco 617 coating and in module 3 with just Aremco 617, it was observed that the measured permeances were higher for module 3, signifying the presence of leaks within the seal in module 3. It looks like the torrseal sealed the defects in the Aremco seal. Two sources of defects are present in module 3 with just Aremco: 1) defects in the selective layer within membrane 2) defects in the membrane seal. Even though defects through the seal would be considered negligible for industrial cases when compared to defects in the active layer of the membrane, for characterization purposes, the source of the defects need to be differentiated to better evaluate the parameters. There are three important points to consider as follows:

- Prior to calcination the permeance observed is solely due to defects.
- After calcination and testing with module 3 with Aremco, all defects and crystal channels are open.
- After applying torrseal for module 1, the defects in the seal are blocked. The permeance is due to the defects and crystal channels through the membrane's selective layer only.

This led to a simple mathematical model of isolating the flow through the seal and eliminating it from the pre-calcined results. As mentioned earlier, torrseal cannot be

applied prior to calcination for thermal stability reasons. The system of equations is briefly stated below:

$$\mathcal{P}_{GC} - \mathcal{P}_{TC} = \mathcal{P}_{SL} \tag{4.6}$$

$$\mathcal{P}_{GD} - \mathcal{P}_{SL} = \mathcal{P}_{RD} \tag{4.7}$$

Where $\mathcal{P}_{GC}$ is the permeance calculated when the **c**alcined membrane is installed in module 3 (Aremco 617 seal with **g**raphite), $\mathcal{P}_{TC}$ is the permeance when the **c**alcined membrane is installed in module 1 (**t**orrseal with Teflon), $\mathcal{P}_{SL}$ is the calculated permeance of the **l**eak in the **s**eal. $\mathcal{P}_{GD}$ permeance of the **d**ried/uncalcined membrane installed in module 3 (with **g**raphite), $\mathcal{P}_{RD}$ is the calculated corrected permeance for when the membrane is dried/uncalcined. Removing the effect of the leak is thought to improve the parameters obtained from the model. However, in order to proceed with these calculations an assumption must be made, that all the permeances used are calculated at the same pressure differential. This is not the case as the permeate pressure was linked to the feed pressure due to the backpressure in the system as discussed in section 4.4.3.

Two defect sources were presented to the main characterization model using the same theory. Figure 4.2 shows the different types of channels available at different stages of testing. The shaded portions represent the blocked channels. Equation (4.8) to Equation (4.12) represent the modified model that includes the distinction of the defect sources.

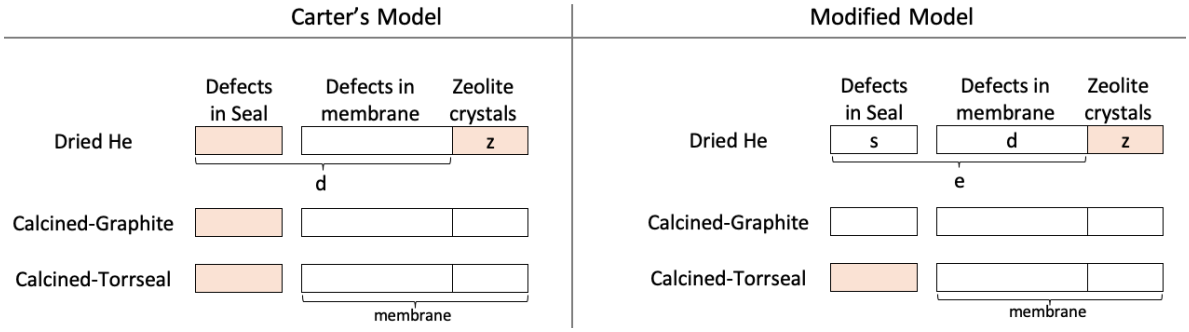

Figure 4.2. Schematic illustration of open and closed channels. The shaded blocks in solid color are considered closed where d represents defects through membrane, z represents pores in the zeolite crystals, s represents leaks through the seal and e represents the total defects.

When the membrane is dried and tested with module 3 (Aremco with graphite), flow can bypass the membrane and go through the defects in the seal (s) and through the membrane defect (d), since their pores are much larger. The parameters x_e and d_e represent the total defects (e) as shown in Figure 4.2 under modified model. The numerical values are the same as x and d reported in the previous chapter using the original model by Carter [18]. x_e represents the ratio of the total defect's void fraction to the effective length of the defects; and d_e represents the defect pore size average in the membrane and seal. The crystal parameters y and D_T are calculated similar to the original model. The new step is to calculate the membrane's defect parameters x_d and d_d using the data with module 1 (with torrseal). y and D_T values are used to calculate the defect parameters x_d and d_d.

Before Calcination

With module 3:

$$\mathcal{P}_i = \mathcal{P}_{v,e} + \mathcal{P}_{k,e} = x_e d_e^2 \frac{(p_h + p_l)}{64\mu_i RT} + x_e d_e \frac{1}{3}\sqrt{\frac{8}{\pi M_i RT}} \tag{4.8}$$

After Calcination

With module 3:

For a non-adsorbed gas

$$\mathcal{P}_i = \mathcal{P}_{v,e} + \mathcal{P}_{k,e} + \mathcal{P}_{K,z} = x_e d_e^2 \frac{(p_h + p_l)}{64\mu_i RT} + x_e d_e \frac{1}{3}\sqrt{\frac{8}{\pi M_i RT}} + y d_z \frac{1}{3}\sqrt{\frac{8}{\pi M_i RT}} \tag{4.9}$$

For an adsorbed gas

$$\mathcal{P}_i = \mathcal{P}_{v,e} + \mathcal{P}_{k,e} + \mathcal{P}_{SD,z} = x_e d_e^2 \frac{(p_h + p_l)}{64\mu_i RT} + x_e d_e \frac{1}{3}\sqrt{\frac{8}{\pi M_i RT}} + y\left(\frac{q_h - q_l}{p_h - p_l}\right)\rho D_T \tag{4.10}$$

With module 1:

For a non-adsorbed gas

$$\mathcal{P}_i = \mathcal{P}_{v,d} + \mathcal{P}_{k,d} + \mathcal{P}_{k,z} = x_d d_d^2 \frac{(p_h + p_l)}{64\mu_i RT} + x_d d_d \frac{1}{3}\sqrt{\frac{8}{\pi M_i RT}} + y d_z \frac{1}{3}\sqrt{\frac{8}{\pi M_i RT}} \tag{4.11}$$

For an adsorbed gas

$$\mathcal{P}_i = \mathcal{P}_{v,d} + \mathcal{P}_{k,d} + \mathcal{P}_{SD,z} = x_d d_d^2 \frac{(p_h + p_l)}{64\mu_i RT} + x_d d_d \frac{1}{3}\sqrt{\frac{8}{\pi M_i RT}} + y\left(\frac{q_h - q_l}{p_h - p_l}\right)\rho D_T \quad (4.12)$$

More models were postulated and are presented in the Appendix II. Those models used the same concept explained in this section but were unfortunately not successful. There is an implicit assumption made to generate all the models, which assumes that the defects remain the same before and after calcination. Even though, at higher temperatures the differences in thermal expansion between the zeolite crystals and support become more prominent.

4.3. EXPERIMENTAL

4.3.1. Synthesis

Silicalite-1 membranes were synthesized by pore-plugging method on TAMI Industries' (Nyons, France) tubular ceramic supports. The supports have an active layer made of titanium oxide and zirconium oxide, which would prevent the leeching of aluminum ions from the body of the support to the zeolite layer (selective layer). The tubular supports are 6 cm long, 1 cm in diameter with a thickness of 0.2 cm. In this synthesis the crystals are deposited on the inner surface of the support. The active layer, which is ~11 μm in depth had pores that are 0.45 μm in size, which were plugged with silicalite during its synthesis. It undergoes a hydrothermal process that has been explained in great detail previously by Carter [12]. The precursor solution contains SiO_2:0.45 TPAOH:27.8 H_2O in mole ratio. They are synthesized in a Teflon lined stainless steel autoclave, which is placed in a programmable oven. The heating program consists of a break for 12 hours that allows the solution to seep back into the pores for further crystal growth.

For permeation experiments, the membranes undergo a preparation step before hydrothermal synthesis. The membrane ends are coated with Aremco 617 (Aremco Products Inc, Valley Cottage, NY, USA) solution. The axial faces and 1 cm of the outer surfaces at both ends are glazed 5 times with this solution to prevent bypassing of gases. The support enters a heating program that goes up to 875℃. This temperature is unsafe to work on after silicalite is deposited since its crystals are unstable at such high temperatures

[15]. However, there are speculations that Aremco glaze gets degraded during synthesis due to the presence of the template, TPAOH. Once the membrane is synthesized it is dried and tested with helium and nitrogen. The permeation test demonstrates the amount of defects present in the membrane. Next, the membrane is calcined at 500℃ to remove the TPAOH bonded to the crystal pores. This opens up the zeolite crystal channels allowing for a faster and more selective permeation through the membrane. To study the leak in the seal, Torrseal (Agilent, Santa Clara, CA, USA), an epoxy used for vacuum conditions is used to attach SS tubes to the membrane. The tubes extend the membrane and connect to the housing module. Torrseal melts at 120℃ and after it is applied to the membrane, it cannot be removed. Therefore, it is only used after the membrane is calcined. The membranes are tested with helium and nitrogen after drying, calcination and applying torrseal on the membrane. Carbon dioxide and methane tests are performed only after calcination.

Four membrane batches are used with different autoclave fill-levels. Since we are characterizing the membranes, we expect a change in the structural parameters of the defects and therefore this should not affect our results in this chapter. However for the diffusivity of silicalite-1 we expect them to be similar within experimental and modeling error.

4.3.2. Backpressure

During this study the set-up underwent an update to decouple the permeate pressure from the feed pressure. This is due to backpressure on the permeate side that occurs when the flow rate is large at high feed pressures. Since the tubing and connections were narrow, the resistance to flow was high at such conditions. Therefore, the tube diameter after the membrane cell was changed from $^1/_{16}{}''$ to $^1/_4{}''$ including all the valves. Another factor that contributes to this is the long tubing on the permeate side. Which ran through the gas chromatograph (GC), which is used during binary experiments. To overcome this, a three-way valve was added to direct the flow to the bubble flow meter without passing through the GC. Even after the upgrade, the permeate side experienced backpressure when the permeance was high. Thus the permeate line was redirected straight to the bubble flow

meter. This attempt is made to ensure the permeate pressure is kept constant at all times. The bubble flow meter is connected to the fume hood and the pressure gauges at the feed and permeate side are calibrated daily. Overall, this caused a slight variation with the previous experiments done with the old system. For the previous system the permeate side would be set to 1 psig which would not be maintained at high pressures. However with the new system it is set at 0 psig and maintained as such. The pressure differential is kept the same for both systems but the feed pressure changed by 1 psi. This would not affect the permeance of gases with linear adsorption isotherm, but for rectangular isotherms such as CO_2 it could have a slight effect.

4.4. RESULTS AND DISCUSSION

4.4.1. Modified Characterization model

After testing many membranes with the two seals available, it was evident that the permeance is lower with torrseal in module 1. In the appendix the permeances of 10 membranes are listed for four gases He, N_2, CH_4 and CO_2. And in 9 cases of 10 membranes tested with torrseal this was the case. M9 was the only membrane that showed interchangeable results with the graphite+Aremco and torrseal. It is important to add that from membranes M9 and onwards the membranes are tested with the updated system that eliminated the backpressure. However, the abnormal results with M9 are not related to the sealant effect. It could be associated to the successful closure of defects between Aremco 617 glaze and the compressible graphite gaskets or the minimal effect of Aremco 617 degrading during synthesis.

The simple mathematical model that is presented in the theoretical background as Equation (4.6) and (4.7) is applied and the results are shown in Table 4.3 for M5 and M3 and for all membranes in Appendix I. For M5 the method worked and reasonable values for the corrected uncalcined permeances were obtained for helium and nitrogen. On the other hand, for M3 the permeance of the leak is greater than the uncalcined permeance found experimentally, which is infeasible, therefore two explanations were put forward.
First, remaining residual of TPAOH has not been removed during the drying process as a result it could be blocking some of the defect channels but then is gradually pushed out of

the pores during high feed pressure experiments. This idea was reinforced by observing the trends for x_e and d_e for a number of membranes. With the increase in pressure, the average defect pore size, d_e decreases. Indicating that the defects that are blocked by the template are of smaller size, which explains why it is harder for the template molecules to escape. As for x_e which is the defect void fraction divided by the defect length, it increases with increase in pressure. Since the defect length is estimated as the length of the support's active layer, which is constant, the increase in the void fraction means that more pores are opening up by the increase in pressure differential. Second, this model is very sensitive to the slightest variation in pressure. Therefore the assumption that the pressure differential is the same for all experiments is not satisfied, especially with backpressure involved. Overall, for uncalcined membranes 4 out of 9 membranes, excluding M9, gave physically viable corrected permeances.

Table 4.3. Results of measured permeances for membrane M5 and M3 when uncalcined, calcined and torrsealed. With the calculated leak through the seal and corrected uncalcined permeance.

Permeance[1]			$\mathcal{P}_{GC}$	$\mathcal{P}_{TC}$	$\mathcal{P}_{SL}$	$\mathcal{P}_{GD}$	$\mathcal{P}_{RD}$
M5	Δp_{low}	N_2	25.3	22.4	2.96	4.05	1.09
		He	17.5	14.5	3.02	5.73	2.71
	Δp_{medium}	N_2	27.4	23.7	3.70	5.46	1.76
		He	19.5	15.8	3.66	7.21	3.55
	Δp_{high}	N_2	29.9	25.3	4.60	6.58	1.98
		He	21.2	17.3	3.86	8.59	4.73
M3	Δp_{low}	N_2	26.8	21.8	5.02	2.42	$\mathcal{P}_{SL} > \mathcal{P}_{GD}$
		He	14.0	9.49	4.51	3.03	$\mathcal{P}_{SL} > \mathcal{P}_{GD}$
	Δp_{medium}	N_2	26.3	22.2	4.07	2.91	$\mathcal{P}_{SL} > \mathcal{P}_{GD}$
		He	15.2	9.58	5.62	3.81	$\mathcal{P}_{SL} > \mathcal{P}_{GD}$
	Δp_{high}	N_2	28.2	22.0	6.20	3.59	$\mathcal{P}_{SL} > \mathcal{P}_{GD}$
		He	16.8	9.67	7.13	4.52	$\mathcal{P}_{SL} > \mathcal{P}_{GD}$

[1] All permeances in [$10^{-7} \times mol \cdot s^{-1} \cdot m^{-2} \cdot Pa$]

Furthermore, the first explanation was put to test by investigating the presence of TPAOH residual and whether it would affect the permeance. A new uncalcined membrane was used and tested with helium. The test involved measuring the permeance in the order of low, medium, high, medium, low pressure differentials. Each of these 5 tests is performed as single experiments. If TPAOH is remaining, the final test done should be greater than the first, as more pores are available for permeation. Figure 4.3 shows the results of this trial. The first permeance measured is actually 2% greater than the one taken at the end. This difference is within experimental error and the explanation is proven false.

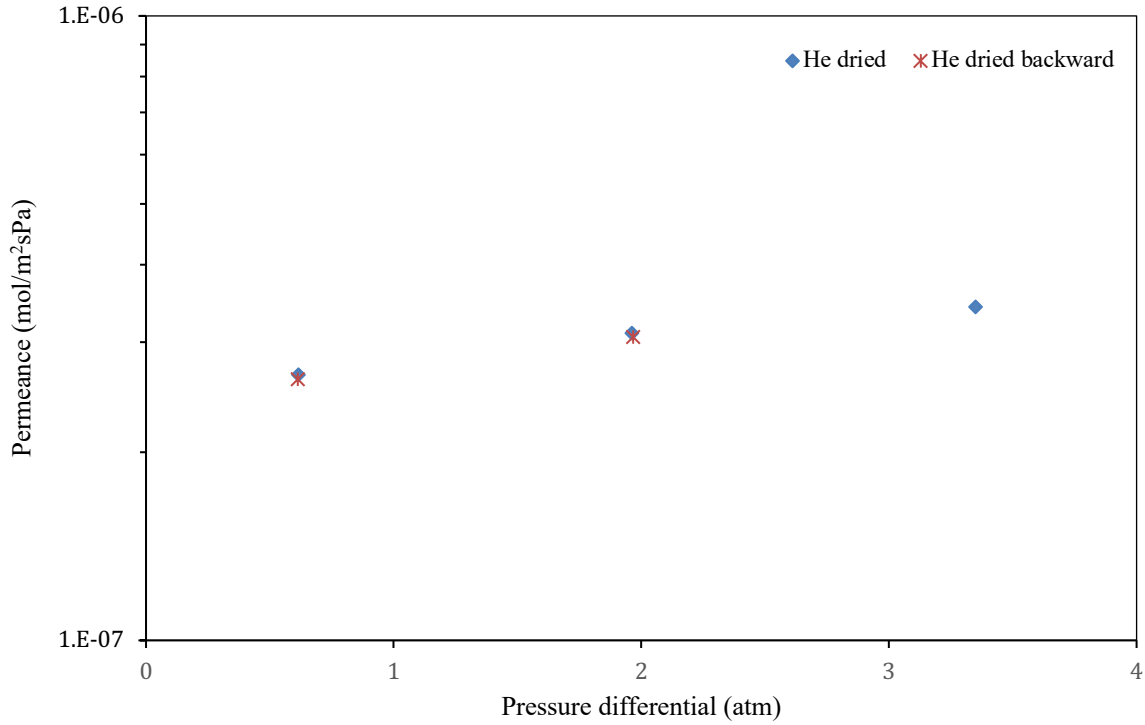

Figure 4.3. Pure helium permeance versus pressure differential of a new membrane prior to calcination. The blue rhombus points represent data obtained by increasing the pressure differential and the red crosses represent the data obtained by decreasing the pressure differential.

Accordingly, more importance is given to the second explanation that states that the simplified model is highly sensitive to pressure differences between experiments. It means that the pressure difference for the uncalcined, calcined with Aremco 617 and with torrseal must be the same. This is not the case when backpressure is present, especially at

high permeation rates that occur at high feed pressures and with highly permeating gas species such as CO_2 and CH_4.

By applying the simplified model ideology to the characterization model using Equations (4.8) to (4.12), the membrane defect parameters, x_d and d_d, will be calculated using the data obtained from the membranes tested with torrseal.

Table 4.4 shows the viable results obtained for two membranes. The rest of the membranes gave negative results, which is physically insignificant. To understand whether these values have physical significance, the defect diameter d_d is compared to the support's pore size. The support's active layer has a pore size of 0.45 μm as reported by the manufacturer. Therefore, any predicted values around 0.45 μm would be meaningful. Better results were expected with the upgraded system where both the feed and permeate pressure are controlled. However both M9 and M10 did not give feasible results. Thus, the modified characterization model was further examined.

Table 4.4. Modified model parameters obtained for M5 and M7.

Pressure differential	Parameters	M5	M7
Δp_{low}	$x_d[m^{-1}]$	27	0.20
	$d_d[\mu m]$	0.058	2.7
Δp_{medium}	$x_d[m^{-1}]$	6.0	0.16
	$d_d[\mu m]$	0.29	2.7
Δp_{high}	$x_d[m^{-1}]$	21	6.2
	$d_d[\mu m]$	0.12	0.29

When Equations (4.11) and (4.12) are solved simultaneously for x_d and d_d, Equations (4.13) and (4.14) are obtained. By analyzing Equation (4.13) it is understood that three conditions must be satisfied to obtain feasible parameters, avoiding negative numbers.

$$d_d = \frac{\frac{1}{3}\sqrt{\frac{8}{\pi M_{He} RT}}\left(\mathcal{P}_i - \mathcal{P}_{SD,z}\right)\Big|_{N_2} - \frac{1}{3}\sqrt{\frac{8}{\pi M_{N_2} RT}}\left(\mathcal{P}_i - \mathcal{P}_{K,z}\right)\Big|_{He}}{\left(\frac{\left(\mathcal{P}_i - \mathcal{P}_{K,z}\right)\big|_{He}}{\mu_{N_2}} - \frac{\left(\mathcal{P}_i - \mathcal{P}_{SD,z}\right)\big|_{N_2}}{\mu_{He}}\right)\frac{(p_h + p_l)}{64\,RT}} \tag{4.13}$$

$$x_d = \frac{\left(\mathcal{P}_i - \mathcal{P}_{K,z}\right)\big|_{He}}{{d_d}^2 \frac{(p_h + p_l)}{64 \mu_{He} RT} + d_d \frac{1}{3}\sqrt{\frac{8}{\pi M_{He} RT}}} \tag{4.14}$$

The experimentally found permeance for nitrogen and helium in module 1 must be greater than the calculated permeance through the crystals; $\left(\mathcal{P}_i > \mathcal{P}_{SD,z}\right)\big|_{N_2}$ and $\left(\mathcal{P}_i > \mathcal{P}_{k,z}\right)\big|_{He}$. This was not the case, since the calculated permeance of nitrogen by surface diffusion $\mathcal{P}_{SD}$ was usually overestimated. This is because the characterization model does not take into account the sorbate-sorbate interactions, which, in reality lowers the value of the corrected transport diffusivity and consequently $\mathcal{P}_{SD}$ [19]. In addition, nitrogen flow through the crystals is possible by Knudsen flow, which is not accounted for in the model. The third condition is shown in Equation (4.15) and expressed in terms of permeances in Equations (4.16); where the left-hand term is the ratio of the permeances of helium to nitrogen by Knudsen diffusion, the right-hand term is the ratio of permeances by viscous flow and the term in the center is the ratio of permeances through the defects.

$$\frac{\frac{1}{3}\sqrt{\frac{8}{\pi M_{He} RT}}}{\frac{1}{3}\sqrt{\frac{8}{\pi M_{N_2} RT}}} > \frac{\left(\mathcal{P}_i - \mathcal{P}_{K,z}\right)\big|_{He}}{\left(\mathcal{P}_i - \mathcal{P}_{SD,z}\right)\big|_{N_2}} > \frac{\frac{(p_h + p_l)}{64\,\mu_{N_2} RT}}{\frac{(p_h + p_l)}{64\,\mu_{He} RT}} \tag{4.15}$$

$$\frac{\mathcal{P}_{k,d}\big|_{He}}{\mathcal{P}_{k,d}\big|_{N_2}} > \frac{\left(\mathcal{P}_{v,d} + \mathcal{P}_{k,d}\right)\big|_{He}}{\left(\mathcal{P}_{v,d} + \mathcal{P}_{k,d}\right)\big|_{N_2}} = \frac{\mathcal{P}_d|_{He}}{\mathcal{P}_d|_{N_2}} > \frac{\mathcal{P}_{v,d}\big|_{N_2}}{\mathcal{P}_{v,d}\big|_{He}} \tag{4.16}$$

Equation (4.15) is simplified to give Equation (4.17), where the ratio of $(\mathcal{P}_i - \mathcal{P}_{K,z})\big|_{He}$ to $(\mathcal{P}_i - \mathcal{P}_{SD,z})\big|_{N_2}$ should be less than the square root of the molecular weight of nitrogen over helium and greater than the viscosity ratio of nitrogen over helium. For membrane M7 and M5 both conditions are satisfied as shown in Table 4.5.

$$\sqrt{\frac{M_{N_2}}{M_{He}}} > \frac{(\mathcal{P}_i - \mathcal{P}_{K,z})\big|_{He}}{(\mathcal{P}_i - \mathcal{P}_{SD,z})\big|_{N_2}} > \frac{\mu_{N_2}}{\mu_{He}} \tag{4.17}$$

Table 4.5. Characterization model's condition compared to membrane M5 and M7.

	$(\mathcal{P}_i > \mathcal{P}_{k,z})\big\|_{He} \cdot 10^{-6}$	$(\mathcal{P}_i > \mathcal{P}_{SD,z})\big\|_{N_2} \cdot 10^{-6}$	$\sqrt{\frac{M_{N_2}}{M_{He}}} > \frac{(\mathcal{P}_i > \mathcal{P}_{k,z})\big\|_{He}}{(\mathcal{P}_i > \mathcal{P}_{SD,z})\big\|_{N_2}} > \frac{\mu_{N_2}}{\mu_{He}}$
M5	$1.5 > 1.2$	$2.2 > 2.1$	$2.6 > 2.5 > 0.89$
M7	$1.8 > 1.6$	$3.0 > 2.8$	$2.6 > 1.2 > 0.89$

4.4.2. Sensitivity Analysis

Sensitivity analysis is performed to further investigate the problem and to check if it is a problem of accuracy. Four uncertainty levels were chosen 5, 10, 15 and 30%. The experimental permeances were varied according to these levels and the corresponding parameters were studied. If the parameters calculated were positive, they are validated and shown as ✓ in Table 4.6. An increase of 30% in the permeance of helium with module 1 gave reasonable parameters for M2. Similarly, a decrease of 15% in the permeance of nitrogen tested with module 3 gave valid results for M4. A summary of these results for other membranes is shown in Table 4.6. However, since only 3 out of 8 membranes gave valid results, the problem does not seem to be an issue of accuracy.

Table 4.6. Summary of sensitivity analysis performed at 4 levels

Membrane	Module	Permeance varied	Uncertainty			
			5%	10%	15%	30%
M2 (calcined)	1	$\mathcal{P}_{He} \uparrow$	-	-	-	✓
	3	$\mathcal{P}_{He} \downarrow$	-	✓	✓	✓
M4 (calcined)	3	$\mathcal{P}_{N_2} \downarrow$	-	-	✓	-
M8 (calcined)	1	$\mathcal{P}_{He} \uparrow$	-	✓	✓	✓
	3	$\mathcal{P}_{He} \downarrow$	✓	✓	✓	✓
M8 (dried)	3	$\mathcal{P}_{N_2} \downarrow$	-	✓	✓	✓

4.4.3. Backpressure

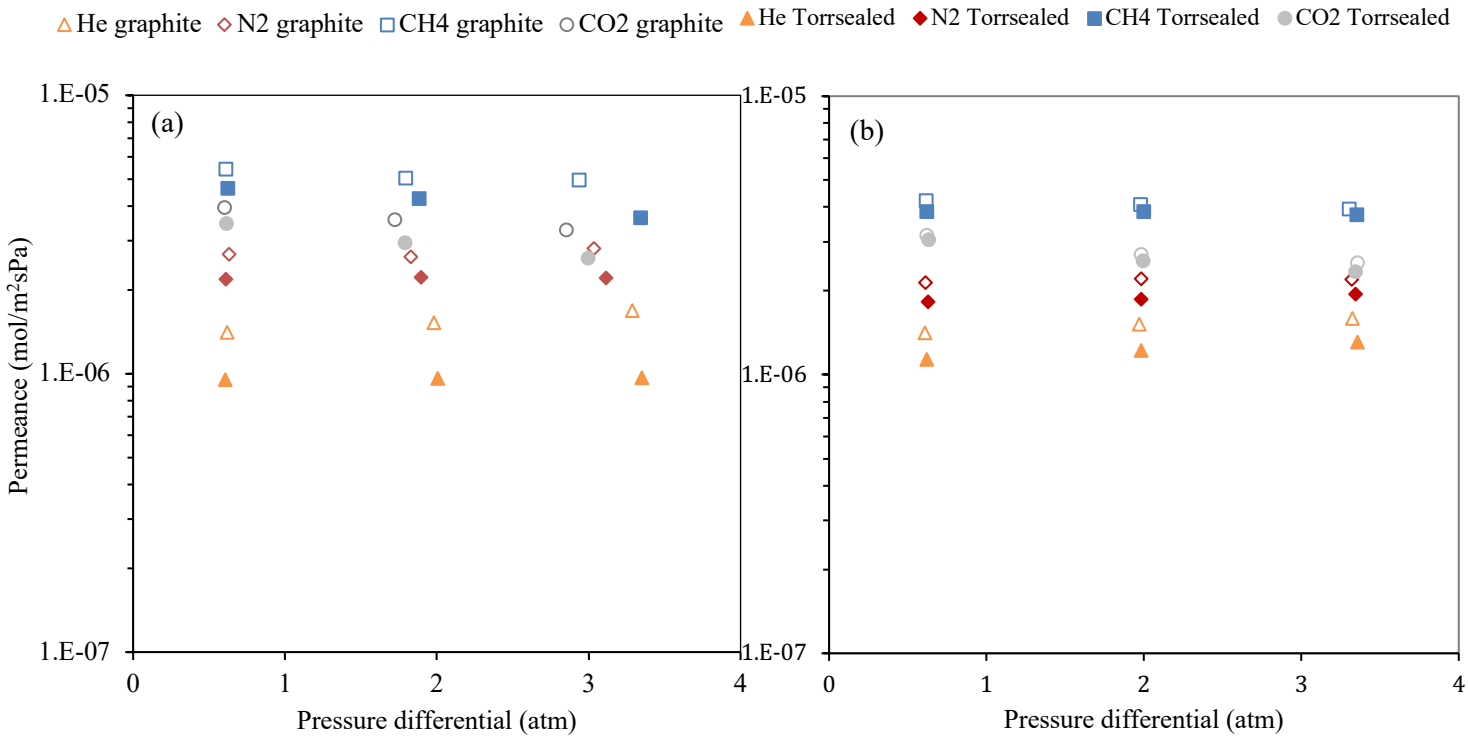

Figure 4.4. Pure permeation experimental results of two membranes (a) M3 tested with the old system and (b) M10 tested with the updated system using both module 1 (Torrsealed) and module 3 (graphite).

When calculating the parameters for the characterization model, it was understood that it is very sensitive to the data given. This step was believed to give better results, as permeate pressure is a controlled variable and should be constant throughout all experiments. Providing better input to the model would give more consistent diffusivities for silicalite-1. Membrane M10 was tested with the updated set-up and the results compared with a membrane tested with the old set-up as shown in Figure 4.4. Pure permeation experiments of He, N_2, CH_4 and CO_2 were performed on both calcined membranes. The results from the updated system show uniformity of the pressure differential for all points. This is the outcome of eliminating backpressure and making sure that the permeances are evaluated at the same conditions. The shift seen in the pressure differential in Figure 4.4 (a) is explained by the larger resistance experienced by the permeating specie in the old system on the permeate side. The backpressure results in a higher permeate pressure and consequently a lower pressure gradient. In addition, since Aremco 617 seal has some defects the gas can bypass the membrane, decreasing the selectivity and lowering the pressure differential.

4.5. CONCLUSIONS

After permeation experiments were done using torrseal, 9 out of 10 membranes show a decrease in permeance. This signified the presence of a leak in the graphite-Aremco 617 junction. Thus the defect parameters obtained from the original model represent the defects from two sources. Numerically x_e and d_e are the same as x and d in the original model evaluated in chapter 3. y and D_0 on the other hand are structural and diffusivity parameters for the crystal and therefore should not vary much. Once the membrane is torrsealed, the defects through the Aremco seal are blocked. Then the defects through the membrane are reevaluated using torrseal experimental data to give the true values of x_d and d_d. These parameters describe the defects solely in the membrane. However, in most of the cases, these values are negative which is physically not reasonable. For the positive values obtained, the defect diameters within the membranes were within reasonable values.

The reasons for the failure of the modified characterization model was investigated. In many cases, the calculated flow through the crystals is greater than the experimental permeance. This proves that the model is overestimating the flow through the crystals. For

nitrogen, this could be due to two reason; the corrected diffusivities are higher than reality, as sorbate-sorbate interactions are not taken into account. And that Knudsen flow could occur within the crystals which is not accounted for in the model. Sensitivity analysis results showed that the failure of the model is not due to experimental error.

The permeation results obtained before and after the updated system were compared. And the permeate pressure was successful controlled yielding to constant pressure differential for all experiments, regardless of the membrane's condition.

4.6. NOMENCLATURE

d	$[m]$	Diameter
D_T	$[m^2.s^{-1}]$	Transport diffusivity
D_0	$[m^2.s^{-1}]$	Corrected diffusivity
ε	$[-]$	Void fraction
K	$[atm^{-1}]$	Langmuir adsorption coefficient
l	$[m]$	Length
M	$[kg.mol^{-1}]$	Molecular weight
$\mathcal{P}_i$	$[mol \cdot m^{-2} \cdot s^{-1} \cdot Pa^{-1}]$	Permeance
p	$[kPa]$	Pressure differential
Δp_i	$[Pa]$	Partial pressure differential
$\Delta \boldsymbol{P_{low}}$	$[kPa]$	Partial pressure at low pressure differential
$\Delta \boldsymbol{P_{medium}}$	$[kPa]$	Partial pressure at medium pressure differential
$\Delta \boldsymbol{P_{high}}$	$[kPa]$	Partial pressure at high pressure differential
ρ	$[kg.m^{-3}]$	Zeolite density
q	$[mmol \cdot g^{-1}]$	Quantity of amount adsorbed
q_{sat}	$[mmol \cdot g^{-1}]$	Saturation adsorption capacity
R	$[Pa.m^3.K^{-1}mol^{-1}]$	Gas constant
T	$[K]$	Temperature
μ	$[Pa.s^{-1}]$	Viscosity
x	$[m^{-1}]$	Lumped parameter of porosity over effective length of defect

y	$[m^{-1}]$	Lumped parameter of porosity over effective length of zeolite

Subscripts

d	Defect
e	Total defects
h	At high pressure side
i,j	Component
k	Knudsen flow
l	At low pressure side
v	Viscous flow
z	Zeolite crystal

Abbreviations

CH_4	Methane
CO_2	Carbon Dioxide
GC	Gas Chromatograph
He	Helium
MFI	Mordenite Framework Inverted
N_2	Nitrogen
SS	Stainless Steel
TPAOH	Tetra Propyl Ammonium Hydroxide

4.7. REFERENCE

[1] M. Matsukata, K. Sawamura, Y. Sekine, Review on Prospects for Energy Saving in Distillation Process with Microporous Membranes, 1st ed., Elsevier B.V., 2011. https://doi.org/10.1016/B978-0-444-53728-7.00008-2.

[2] L.B. McCusker, D.H. Olson, C. Baerlocher, Atlas of Zeolite Framework Types, in: C. Baerlocher, W.M. Meier, D.H.B.T.-A. of Z.F.T. Olson (Eds.), Atlas Zeolite Framew. Types, Elsevier, Amsterdam, 2007: pp. 184–185. https://doi.org/10.1016/B978-0-444-53064-6.X5186-X.

[3] J. Kärger, D.M. Ruthven, D.N. Theodorou, Diffusion in Nanoporous Materials, Hoboken: John Wiley & Sons, Weinheim, 2012.

[4] J. Caro, M. Noack, Zeolite membranes - Recent developments and progress, Microporous Mesoporous Mater. 115 (2008) 215–233. https://doi.org/10.1016/j.micromeso.2008.03.008.

[5] M. Hong, S. Li, J.L. Falconer, R.D. Noble, Hydrogen purification using a SAPO-34 membrane, J. Memb. Sci. 307 (2008) 277–283. https://doi.org/10.1016/j.memsci.2007.09.031.

[6] C. Kong, J. Lu, J. Yang, J. Wang, Preparation of silicalite-1 membranes on stainless steel supports by a two-stage varying-temperature in situ synthesis, J. Memb. Sci. 285 (2006) 258–264. https://doi.org/10.1016/j.memsci.2006.08.027.

[7] J. Motuzas, R. Mikutaviciute, E. Gerardin, A. Julbe, Controlled growth of thin and uniform TS-1 membranes by MW-assisted heating, Microporous Mesoporous Mater. 128 (2010) 136–143. https://doi.org/10.1016/j.micromeso.2009.08.014.

[8] S. Miachon, E. Landrivon, M. Aouine, Y. Sun, I. Kumakiri, Y. Li, O.P. Prokopová, N. Guilhaume, A. Giroir-Fendler, H. Mozzanega, J.A. Dalmon,

Nanocomposite MFI-alumina membranes via pore-plugging synthesis. Preparation and morphological characterisation, J. Memb. Sci. 281 (2006) 228–238. https://doi.org/10.1016/j.memsci.2006.03.036.

[9] H.H. Funke, M.G. Kovalchick, J.L. Falconer, R.D. Noble, Separation of hydrocarbon isomer vapors with silicalite zeolite membranes, Ind. Eng. Chem. Res. 35 (1996) 1575–1582. https://doi.org/10.1021/ie950495e.

[10] J.C. Poshusta, V.A. Tuan, E.A. Pape, R.D. Noble, J.L. Falconer, Separation of light gas mixtures using SAPO-34 membranes, AIChE J. 46 (2000) 779–789. https://doi.org/10.1002/aic.690460412.

[11] T. Mohammadi, S. Asarehpour, M. Samei, Effects of Synthesis Temperature and Support Material on CO2 and CH4 Permeation through SAPO-34 Membranes, Sep. Sci. Technol. 47 (2012) 2320–2330. https://doi.org/10.1080/01496395.2012.677924.

[12] D. Carter, Fabrication and Characterization of Silicalite-1 Membranes for the Separation of the Greenhouse Gases, (2019).PhD Thesis, University of Ottawa, Ottawa

[13] L.L. Hench, Characterization of glass corrosion and durability, J. Non. Cryst. Solids. 19 (1975) 27–39. https://doi.org/10.1016/0022-3093(75)90067-8.

[14] R.W. DOUGLAS, T.M.M. EL-SHAMY, Reactions of Glasses with Aqueous Solutions, J. Am. Ceram. Soc. 50 (1967) 1–8. https://doi.org/10.1111/j.1151-2916.1967.tb14960.x.

[15] S.P. Zhdanov, N.N. Feoktistova, N.I. Kozlova, M.M. Piryutko, Silicalites and their thermal stability, Bull. Acad. Sci. USSR Div. Chem. Sci. 34 (1985) 2467–2472. https://doi.org/10.1007/BF00953007.

[16] M. Ponzi, J. Papa, J.B.P. Rivarola, G. Zgrablich, On the surface diffusion of adsorbable gases through porous media, AIChE J. 23 (1977) 347–352.

[17] D.A. Kennedy, D. Carter, S. Wilson, B. Kruczek, F.H. Tezel, Pore plugging synthesis and characterization of silicalite-1 membranes using tubular TiO2 supports: Effect of support pore size on membrane performance, Can. J. Chem. Eng. 96 (2018) 1597–1611. https://doi.org/10.1002/cjce.23095.

[18] S. Al Akwaa, D. Carter, F.H. Tezel, B. Kruczek, The new characterization method of defect-containing zeolite membranes, Journal of Membrane Science. (n.d.).

[19] G.K. Papadopoulos, H. Jobic, D.N. Theodorou, Transport diffusivity of N2 and CO2 in silicalite: Coherent quasielastic neutron scattering measurements and molecular dynamics simulations, J. Phys. Chem. B. 108 (2004) 12748–12756. https://doi.org/10.1021/jp049265g.

Chapter 5

Conclusions, Contributions to Original Knowledge, And Recommendations For Future Work

5.1. CONCLUSIONS

Silicalite-1 zeolite, deposited on porous ceramic support with an active layer having a pore size of 0.45 μm was synthesized, tested and characterized. The membranes were fabricated using the pore-plugging method, placing the selective layer within the ceramic support's active layer. To assess the quality of the new membranes, gas permeation experiments were performed using He, N_2, CH_4 and CO_2 gases. The measured permeation rates were used in a characterization model that allowed the determination of the membrane's structural parameters and the corrected diffusivity of the tested gases, the latter representing intrinsic properties of the silicalite-1 crystals.

We investigated the effect of varying the autoclave fill-level during hydrothermal synthesis on the synthesized membranes' quality. We considered different levels ranging from 94% to 99%. Table 5.1 shows the relative ideal selectivity after the membranes were calcined. The largest increase in selectivity after calcination is observed at 98% autoclave fill-level. This can be explained by examining the selectivity when the membranes are dried. A low selectivity implies the greater contribution of the selective mode of transport, Knudsen diffusion. Implying that the defect pores are smaller and thus the presence of more zeolite crystals filling the pores. Therefore, at 98% fill-level, the performance of the membranes was relatively the highest.

Table 5.1. Permeance and ideal selectivity of nitrogen over helium for dried and calcined membranes synthesized at four different autoclave fill-levels.

Autoclave Fill-level	Dried	Calcined	$\frac{\alpha_{N_2/He}^*}{\alpha_{N_2/He}}$
	$\alpha_{N_2/He}$	$\alpha_{N_2/He}^*$	
94%	0.85±0.06	1.38±0.06	1.6±0.2
97%	0.67±0.11	1.45±0.07	2.3±0.5
98%	0.57±0.04	1.36±0.13	2.4±0.3
99%	0.8±0.0	1.75±0.10	2.2±0.2

We updated the membrane characterization model proposed by Carter (2019) [1] by focusing on the corrected, rather than transport diffusivities of tested gases in silicalite-1 crystals. The updated model does not rely on dynamic adsorption experiments. It only requires equilibrium isotherms of the gases on zeolite crystals and experimentally measured gas permeances before and after calcination. The calculated corrected diffusivities of N_2, CH_4 and CO_2, did not vary with feed pressure and the membrane. This indicates an intrinsic nature of the corrected diffusivities. Compared to the literature values obtained using different microscopic methods, our corrected diffusivities were generally higher, but not more than an order of magnitude. Compared to different microscopic and macroscopic characterization techniques, our method is more straightforward and does not require sophisticated equipment. A summary of the calculated corrected diffusivity as well as some averaged values obtained from the characterization model is shown in Table 5.2. The parameters obtained were compared to physically known values to validate the model. The volume fraction calculated for the selective layer is between 10^{-5} and 10^{-6} which is very small compared to the value reported by the porous support's manufacturer. This conveys that most of the pores are filled with silicalite-1 crystals. The pore diameter and effective pore length help us understand the way the pores are plugged. The pore size distribution is larger after synthesis, since larger pores are more difficuilt to plug, they remain open and yield to larger values. Comparing the effective pore length of the selective layer and porous support, the pores are partially plugged. Therefore, the selective layer is thin which is a great advantage, as it helps balance the trade-off between selectivity and permeance.

Table 5.2. Summary of experimentally determined model parameters.

Characteristic parameter								
Volume fraction [-]		Pore diameter [μm]		Effective pore length [μm]		$D_0 .10^8$ [$m^2 s^{-1}$]		
Selective layer	Porous Support	Selective layer	Porous Support	Selective layer	Porous Support	N_2	CO_2	CH_4
$10^{-5} – 10^{-6}$	0.23	1.0 - 4.2	0.45	1.9 – 4.5	11[2]	7.72	1.69	6.51

To further improve our characterization method, we considered the possibility of defects in sealed ends of the membrane, which were attached to the membrane module. We quantified these defects' contribution to the total gas transport by sealing the membrane with Torrseal and comparing gas permeation of the calcined membrane with that of the non-Torrsealed calcined membrane. However, the difference in membrane performance before and after Torrsealing led to physically impossible negative structural parameters. One possible reason for the negative structural parameters is the assumption that gas transport of nitrogen in silicalite-1 crystals takes place explicitly by surface diffusion. In reality, the contribution of Knudsen diffusion in silicalite-1 crystals might not be negligible for nitrogen. Besides, Torrsealed membranes did not exhibit a consistent improvement of the ideal selectivity of the membrane. In some cases, the difference in the Torrsealed and non-Torrsealed membrane performance was withing a statistical error.

Furthermore, we improved the experimental gas permeation system by eliminating back pressure on the permeate side. It allows better control of the experiments without the necessity of modelling backpressure as a function of feed pressure and the testing gas. This led to more consistent experimentally determined total gas permeances. However, because of lockdown due to COVID19, we could not take full advantage of the upgraded system in this research project.

5.2. CONTRIBUTION TO ORIGINAL KNOWLEDGE

- The updated characterization model allows determining the corrected transport diffusivity, an intrinsic parameter for zeolite crystals, using defect-containing zeolite membranes.
- We recognized the possible contribution of Knudsen diffusion of nitrogen in silicalite-1 crystals at ambient temperature.
- Elimination of backpressure in gas permeation experiments allowing more reliable structural parameters of zeolite membranes.
- Systematically studied the effect of autoclave fill-level on membrane performance.

5.3. FUTURE RECOMMENDATIONS

- Replace N_2 by CO_2 as an adsorbed gas in the proposed characterization method. Unlike N_2, CO_2 permeates through zeolites only by surface diffusion.
- Further validation of the characterization method by determining the corrected transport diffusivities of gases using silicalite-1 membranes with more defects: to examine the model's ability to isolate permeance through the defects.
- Quantification of Knudsen diffusion of nitrogen in silicalite-1 zeolite crystals at ambient temperature by using the ratios of transport diffusivities of CO_2 and N_2 reported by Kennedy et al. (2018) [2]. This will help us understand the contribution of Knudsen diffusion and surface diffusion through the zeolite cystal channels for N_2 gas.
- Determination of the activation energy and the limiting diffusivities in silicalite-1 crystals by applying the characterization method at different temperatures.
- Application of experimentally determined corrected diffusivities of CO_2 and N_2 in silicalite-1 crystals to determine the Maxwell-Stefan exchange diffusivities from gas separation experiments using different CO_2/N_2 gas mixtures.
- Application of sorbate-sorbate interactions to the corrected diffusivities in the characterization model, to obtain more realistic values.
- Application of the proposed characterization method for other zeolite membranes. To obtain corrected transport diffusivities for other zeolites.
- To obtain thermodynamic data for TPAOH to further investigate the effect of autoclave fill-level on the silicalite-1 crystals' growth during hydrothermal synthesis.
- To find an airtight seal that can withstand high calcination temperatures (500 °C).

5.4. REFERENCES

[1] D. Carter, Fabrication and Characterization of Silicalite-1 Membranes for the Separation of the Greenhouse Gases, (2019).Ph.D. thesis, University of Ottawa, Ottawa

[2] D.A. Kennedy, D. Carter, S. Wilson, B. Kruczek, F.H. Tezel, Pore plugging synthesis and characterization of silicalite-1 membranes using tubular TiO2 supports: Effect of support pore size on membrane performance, Can. J. Chem. Eng. 96 (2018) 1597–1611. https://doi.org/10.1002/cjce.23095.

[3] P.F. Zito, A. Caravella, A. Brunetti, E. Drioli, G. Barbieri, Knudsen and surface diffusion competing for gas permeation inside silicalite membranes, J. Memb. Sci. 523 (2017) 456–469. https://doi.org/10.1016/j.memsci.2016.10.016.

APPENDIX I -Tabulated permeances of all pure gases

Table A.1. Summary of experimentally determined permeances and calculated leak and corrected permeances for He gas.

Memb.	Permeance of He									
	p_{h}^{**} *[kPa]*	p_l *[kPa]*	$\mathcal{P}_{GD} \cdot 10^7$	p_l *[kPa]*	$\mathcal{P}_{GC} \cdot 10^7$	p_l *[kPa]*	$\mathcal{P}_{TC} \cdot 10^7$	*% Leak*	$\mathcal{P}_{SL} \cdot 10^7$	$\mathcal{P}_{RD} \cdot 10^7$
M1	171	108	4.31	109	13.3	109	8.62	-35%	4.68	
	308	109	5.79	112	15.2	109	9.08	-40%	6.12	
	446	115	6.95	122	16.9	112	9.33	-45%	7.57	
M2	171	110	7.72	109	14.7	108	8.70	-41%	6.00	1.72
	309	109	10.3	113	17.5	109	8.79	-50%	8.71	1.59
	449	123	12.9	125	20.6	112	8.96	-57%	11.6	1.26
M3	171	109	3.03	108	14.0	109	9.49	-32%	4.51	
	311	108	3.81	110	15.2	108	9.58	-37%	5.62	
	453	109	4.52	117	16.8	111	9.67	-42%	7.13	
M4	171	108	8.06	109	16.2	108	9.86	-39%	6.34	1.72
	310	109	9.86	112	18.8	109	11.2	-40%	7.60	2.26
	449	113	12.2	122	21.0	113	11.9	-43%	9.10	3.10
M5	171	109	5.73	109	17.5	109	14.5	-17%	3.00	2.73
	310	109	7.21	112	19.5	110	15.8	-19%	3.70	3.51
	447	110	8.59	122	21.2	118	17.3	-18%	3.90	4.69
M6	171	108	2.97	109	15.5	109	13.0	-16%	2.50	0.47
	309	108	3.26	111	16.3	109	13.4	-18%	2.90	0.36
	448	108	3.50	118	17.3	115	14.1	-18%	3.20	0.30
M7	170	109	7.39	108	23.3	108	18.2	-22%	5.07	2.32
	309	109	9.18	116	25.9	112	18.9	-27%	7.01	2.17
	445	112	10.9	127	28.2	120	21.2	-25%	6.98	3.92
M8	170	108	8.67	108	16.6	109	11.8	-29%	4.80	3.87
	308	108	12.0	112	18.7	109	12.0	-36%	6.70	5.30
	448	116	14.7	122	21.2	113	12.1	-43%	9.10	5.60
M9	163	101	4.23	101	17.5	101	14.7	-16%	2.75	1.48
	302	101	4.81	101	16.3	101	14.9	-9%	1.41	3.40
	440	101	5.27	101	18.0	102	15.6	-13%	2.38	2.90
M10	164	101	2.34	101	14.2	101	11.4	-20%	2.85	
	302	101	2.54	101	15.2	101	12.3	-19%	2.90	
	439	101	2.73	101	16.0	101	13.1	-18%	2.83	

*Colored cells represent negative values

**Average feed pressure of all experiments

Table A.2. Summary of experimentally determined permeances and calculated leak and corrected permeances for N_2 gas.

Memb.	Permeance of N_2									
	p_h** *[kPa]*	p_l *[kPa]*	$\mathcal{P}_{GD} \cdot 10^7$	p_l *[kPa]*	$\mathcal{P}_{GC} \cdot 10^7$	p_l *[kPa]*	$\mathcal{P}_{TC} \cdot 10^7$	% *Leak*	$\mathcal{P}_{SL} \cdot 10^7$	$\mathcal{P}_{RD} \cdot 10^7$
M1	171	108	3.32	108	24.4	108	20.4	-16%	3.95	
	308	109	4.75	127	26.0	121	20.6	-21%	5.37	
	446	116	5.93	152	27.6	137	20.5	-26%	7.11	
M2	171	109	6.75	108	21.1	109	17.5	-17%	3.63	3.12
	309	109	9.22	124	23.8	118	17.6	-26%	6.24	2.98
	449	121	11.7	150	26.9	132	17.8	-34%	9.05	2.65
M3	171	108	2.42	109	26.8	108	21.8	-19%	5.00	
	311	109	2.91	122	26.3	118	22.2	-16%	4.10	
	453	109	3.59	144	28.2	133	22.0	-22%	6.20	
M4	171	109	5.72	108	24.1	109	15.4	-36%	8.70	
	310	107	8.33	123	26.4	114	16.2	-39%	10.2	
	449	115	10.5	145	28.4	126	16.6	-42%	11.8	
M5	171	108	4.05	108	25.3	108	22.4	-11%	2.90	1.15
	310	108	5.46	123	27.4	120	23.7	-14%	3.70	1.76
	447	109	6.58	146	29.9	139	25.3	-15%	4.60	1.98
M6	171	109	1.53	108	24.0	108	21.7	-10%	2.30	
	309	109	1.67	121	25.5	118	22.4	-12%	3.10	
	448	108	1.89	140	26.4	135	23.3	-12%	3.10	
M7	170	108	5.20	108	33.4	108	30.0	-10%	3.36	1.84
	309	109	6.95	130	36.4	126	31.3	-14%	5.07	1.88
	445	111	8.36	156	38.2	148	31.7	-17%	6.48	1.88
M8	170	108	7.03	108	23.0	108	20.9	-9%	2.10	4.93
	308	108	10.1	121	25.4	118	21.4	-16%	4.00	6.10
	448	120	13.0	144	28.3	133	22.2	-22%	6.10	6.90
M9	163	101	2.42	101	20.2	101	21.4	-	-	
	302	101	2.87	101	20.8	101	22.0	-	-	
	440	101	3.27	102	24.8	102	22.2	-10%	2.54	
M10	163	101	1.21	101	21.4	101	18.3	-15%	3.12	
	302	101	1.39	101	22.1	101	18.7	-15%	3.42	
	439	101	1.54	102	22.0	102	19.5	-11%	2.50	

*Colored cells represent negative values

**Average feed pressure of all experiments

Table A.3. Summary of experimentally determined permeances and calculated leak and corrected permeances for CH_4 gas.

Memb.	Permeance of CH_4						
	p_h** [kPa]	p_l [kPa]	$\mathcal{P}_{GC} \cdot 10^7$	p_l *[kPa]*	$\mathcal{P}_{TC} \cdot 10^7$	*% Leak*	$\mathcal{P}_{SL} \cdot 10^7$
M1	171	110	51.7				
	308	135	50.7				
	446	165	49.6				
M2	171	109	42.3	109	36.8	-13%	5.46
	309	135	43.5	126	35.9	-17%	7.56
	449	164	45.2	145	33.4	-26%	11.8
M3	171	109	54.2	109	46.3	-15%	7.89
	311	131	50.4	126	42.6	-16%	7.82
	453	157	49.5	144	36.3	-27%	13.2
M4	171			108	30.4		
M5	171			108	44.7		
	310			128	49.2		
	447			151	45.8		
M6	171			108	44.0		
	309			126	44.2		
	448			149	44.3		
M7							
M8	170			109	43.5		
	308			125	42.7		
	448			145	40.9		
M9	163	101	43.0	101	43.8	-	-
	302	102	45.4	102	42.6	-6%	2.81
	440	102	43.7	102	40.7	-7%	2.99
M10	164	101	42.2	101	38.5	-9%	3.79
	302	102	40.9	102	38.6	-6%	2.29
	439	102	39.4	102	37.6	-5%	1.86

**Average feed pressure of all experiments

Table A.4. Summary of experimentally determined permeances and calculated leak and corrected permeances for CO_2 gas.

Memb.	Permeance of CO_2						
	p_h** [kPa]	p_l [kPa]	$\mathcal{P}_{GC} \cdot 10^7$	p_l *[kPa]* [kPa]	$\mathcal{P}_{TC} \cdot 10^7$	*% Leak*	$\mathcal{P}_{SL} \cdot 10^7$
M1	171	112	39.8				
	308	140	35.7				
	446	173	34.3				
M2	171	110	33.0	109	27.9	-15%	5.09
	309	137	32.5	126	24.0	-26%	8.47
	449	171	33.2	144	21.2	-36%	1.20
M3	171	110	39.4	109	34.6	-12%	4.77
	311	133	35.7	127	29.5	-17%	6.24
	453	158	32.8	144	26.0	-21%	6.78
M4	171			109	23.1		
M5	171			109	34.9		
	310			129	31.3		
	447			152	29.5		
M6	171			109	34.1		
	309			128	30.4		
	448			148	27.7		
M7							
M8				108	32.4		
				126	28.9		
				144	26.1		
M9	163	101	35.7	101	33.6	-6%	2.13
	302	102	31.7	101	29.4	-7%	2.26
	440	102	29.2	102	26.0	-11%	3.21
M10	164	101	31.8	101	30.5	-4%	1.28
	302	102	27.1	102	25.7	-5%	1.36
	439	102	25.2	102	23.4	-7%	1.84

**Average feed pressure of all experiments

APPENDIX II- Postulated modified characterization models

Model 3

	Defects in Seal	Defects in membrane		Crystals
Dried	c	b	a	z
Calcined-Graphite				
Calcined-Torrseal				

Before Calcination

With module 3:

He:

$$P_{He} = P_{d,b} + P_{d,c} = \left\{ x_b d_{d,b}^2 \frac{\left(p_h + p_l\right)}{64\mu_{He} RT} + x_b d_{d,b} \frac{1}{3}\sqrt{\frac{8}{\pi M_{He} RT}} \right\} + \left\{ x_c d_{d,c}^2 \frac{\left(p_h + p_l\right)}{64\mu_{He} RT} + x_c d_{d,c} \frac{1}{3}\sqrt{\frac{8}{\pi M_{He} RT}} \right\}$$

N_2:

$$P = P_{d,b} + P_{d,c} = \left\{ x_b d_{d,b}^2 \frac{\left(p_h + p_l\right)}{64\mu RT} + x_b d_{d,b} \frac{1}{3}\sqrt{\frac{8}{\pi MRT}} \right\} + \left\{ x_c d_{d,c}^2 \frac{\left(p_h + p_l\right)}{64\mu RT} + x_c d_{d,c} \frac{1}{3}\sqrt{\frac{8}{\pi MRT}} \right\}$$

After Calcination

With module 3:

He:

$$P_{He} = P_{He,d} + P_{He,z} = \left\{ x_a d_{d,a}^2 \frac{\left(p_h + p_l\right)}{64\mu_{He} RT} + x_a d_{d,a} \frac{1}{3}\sqrt{\frac{8}{\pi M_{He} RT}} \right\} + \left\{ x_b d_{d,b}^2 \frac{\left(p_h + p_l\right)}{64\mu_{He} RT} + x_b d_{d,b} \frac{1}{3}\sqrt{\frac{8}{\pi M_{He} RT}} \right\} +$$

$$\left\{ x_c d_{d,c}^2 \frac{\left(p_h + p_l\right)}{64\mu_{He} RT} + x_c d_{d,c} \frac{1}{3}\sqrt{\frac{8}{\pi M_{He} RT}} \right\} + y d_z \frac{1}{3}\sqrt{\frac{8}{\pi M_{He} RT}}$$

N_2:

$$P = P_d + P_z = \left\{ x_a d_{d,a}^2 \frac{\left(p_h + p_l\right)}{64\mu_{He} RT} + x_a d_{d,a} \frac{1}{3}\sqrt{\frac{8}{\pi M_{He} RT}} \right\} + \left\{ x_b d_{d,b}^2 \frac{\left(p_h + p_l\right)}{64\mu_{He} RT} + x_b d_{d,b} \frac{1}{3}\sqrt{\frac{8}{\pi M_{He} RT}} \right\} +$$

$$\left\{ x_c d_{d,c}^2 \frac{\left(p_h + p_l\right)}{64\mu_{He} RT} + x_c d_{d,c} \frac{1}{3}\sqrt{\frac{8}{\pi M_{He} RT}} \right\} + y\left(\frac{q_h - q_l}{p_h - p_l}\right)\rho D_T$$

With module 1:

He:

$$P_{He} = P_{He,d} + P_{He,z} = \left\{ x_a d_{d,a}^2 \frac{\left(p_h + p_l\right)}{64\mu_{He} RT} + x_a d_{d,a} \frac{1}{3}\sqrt{\frac{8}{\pi M_{He} RT}} \right\} + \left\{ x_b d_{d,b}^2 \frac{\left(p_h + p_l\right)}{64\mu_{He} RT} + x_b d_{d,b} \frac{1}{3}\sqrt{\frac{8}{\pi M_{He} RT}} \right\}$$

$$+ y d_z \frac{1}{3}\sqrt{\frac{8}{\pi M_{He} RT}}$$

N_2:

$$P = P_d + P_z = \left\{ x_a d_{d,a}^2 \frac{\left(p_h + p_l\right)}{64\mu_{He} RT} + x_a d_{d,a} \frac{1}{3}\sqrt{\frac{8}{\pi M_{He} RT}} \right\} + \left\{ x_b d_{d,b}^2 \frac{\left(p_h + p_l\right)}{64\mu_{He} RT} + x_b d_{d,b} \frac{1}{3}\sqrt{\frac{8}{\pi M_{He} RT}} \right\}$$

$$+ y\left(\frac{q_h - q_l}{p_h - p_l}\right)\rho D_T$$

Model 4

Combining Defects b and c as a lumped defect parameter e

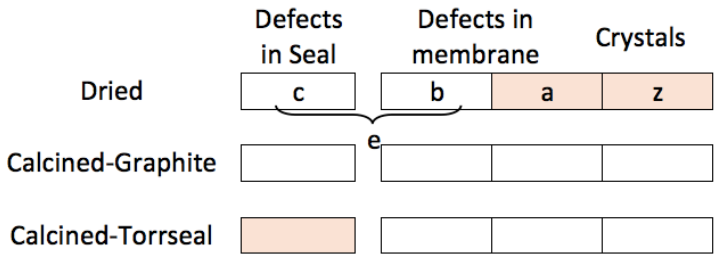

Before Calcination

With module 3:

He:

$$P_{He} = P_{d,e} = \left\{ x_e d_{d,e}^2 \frac{\left(p_h + p_l\right)}{64\mu_{He} RT} + x_e d_{d,e} \frac{1}{3}\sqrt{\frac{8}{\pi M_{He} RT}} \right\}$$

N_2

$$P = P_{d,e} = \left\{ x_e d_{d,e}^2 \frac{\left(p_h + p_l\right)}{64\mu RT} + x_e d_{d,e} \frac{1}{3}\sqrt{\frac{8}{\pi M RT}} \right\}$$

After Calcination

With module 3:

He:

$$P_{He} = P_{He,d} + P_{He,z} = \left\{ x_a d_{d,a}^2 \frac{\left(p_h + p_l\right)}{64\mu_{He} RT} + x_a d_{d,a} \frac{1}{3}\sqrt{\frac{8}{\pi M_{He} RT}} \right\} + \left\{ x_e d_{d,e}^2 \frac{\left(p_h + p_l\right)}{64\mu_{He} RT} + x_e d_{d,e} \frac{1}{3}\sqrt{\frac{8}{\pi M_{He} RT}} \right\}$$

$$+ y d_z \frac{1}{3}\sqrt{\frac{8}{\pi M_{He} RT}}$$

N_2:

$$P = P_d + P_z = \left\{ x_a d_{d,a}^2 \frac{\left(p_h + p_l\right)}{64\mu_{He} RT} + x_a d_{d,a} \frac{1}{3}\sqrt{\frac{8}{\pi M_{He} RT}} \right\} + \left\{ x_e d_{d,e}^2 \frac{\left(p_h + p_l\right)}{64\mu_{He} RT} + x_e d_{d,e} \frac{1}{3}\sqrt{\frac{8}{\pi M_{He} RT}} \right\} + y\left(\frac{q_h - q_l}{p_h - p_l}\right)\rho D_T$$

With module 1:

He:

$$P_{He} = P_{He,d} + P_{He,z} = \left\{ x_a d_{d,a}^2 \frac{\left(p_h + p_l\right)}{64\mu_{He} RT} + x_a d_{d,a} \frac{1}{3}\sqrt{\frac{8}{\pi M_{He} RT}} \right\} + \left\{ x_b d_{d,b}^2 \frac{\left(p_h + p_l\right)}{64\mu_{He} RT} + x_b d_{d,b} \frac{1}{3}\sqrt{\frac{8}{\pi M_{He} RT}} \right\} + yd_z \frac{1}{3}\sqrt{\frac{8}{\pi M_{He} RT}}$$

N_2:

$$P = P_d + P_z = \left\{ x_a d_{d,a}^2 \frac{\left(p_h + p_l\right)}{64\mu_{He} RT} + x_a d_{d,a} \frac{1}{3}\sqrt{\frac{8}{\pi M_{He} RT}} \right\} + \left\{ x_b d_{d,b}^2 \frac{\left(p_h + p_l\right)}{64\mu_{He} RT} + x_b d_{d,b} \frac{1}{3}\sqrt{\frac{8}{\pi M_{He} RT}} \right\} + y\left(\frac{q_h - q_l}{p_h - p_l}\right)\rho D_T$$

Model 5

Speculations were put that some of the Aremco 617 glazing is eaten up and replaced by TPAOH during synthesis at such high temperatures. The remaining TPAOH blocks the defects in the seal and some of the defects within the membrane. If torrseal remains after drying it is assumed to be removed during the first permeation test with helium. Therefore, in this model only the data obtained from the highest pressure differential is used.

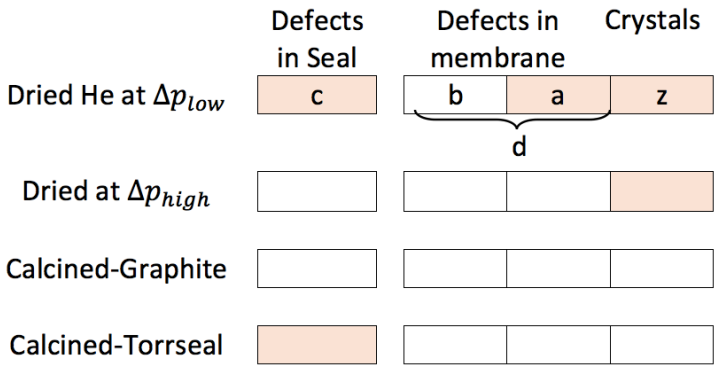

Before Calcination

With module 3:

He

$$P_{He} = P_{d,d} = \left\{ x_d d_{d,d}^2 \frac{\left(p_h + p_l\right)}{64\mu_{He} RT} + x_d d_{d,d} \frac{1}{3}\sqrt{\frac{8}{\pi M_{He} RT}} \right\}$$

N_2

$$P = P_{d,d} = \left\{ x_d d_{d,d}^2 \frac{\left(p_h + p_l\right)}{64\mu_i RT} + x_d d_{d,d} \frac{1}{3}\sqrt{\frac{8}{\pi M_i RT}} \right\}$$

After Calcination

With module 3:

He:

$$P_{He} = P_{He,d} + P_{He,z} = \left\{ x_d d_{d,d}^2 \frac{\left(p_h + p_l\right)}{64\mu_{He} RT} + x_d d_{d,d} \frac{1}{3}\sqrt{\frac{8}{\pi M_{He} RT}} \right\} + \left\{ x_c d_{d,c}^2 \frac{\left(p_h + p_l\right)}{64\mu_{He} RT} + x_c d_{d,c} \frac{1}{3}\sqrt{\frac{8}{\pi M_{He} RT}} \right\} + yd_z \frac{1}{3}\sqrt{\frac{8}{\pi M_{He} RT}}$$

N_2:

$$P = P_d + P_z = \left\{ x_d d_{d,d}^2 \frac{\left(p_h + p_l\right)}{64\mu_i RT} + x_d d_{d,d} \frac{1}{3}\sqrt{\frac{8}{\pi M_i RT}} \right\} + \left\{ x_c d_{d,c}^2 \frac{\left(p_h + p_l\right)}{64\mu_i RT} + x_c d_{d,c} \frac{1}{3}\sqrt{\frac{8}{\pi M_i RT}} \right\} + y\left(\frac{q_h - q_l}{p_h - p_l}\right)\rho D_T$$

With module 1:

He:

$$P_{He} = P_{He,d} + P_{He,z} = \left\{ x_d d_{d,d}^2 \frac{\left(p_h + p_l\right)}{64\mu_{He} RT} + x_d d_{d,d} \frac{1}{3}\sqrt{\frac{8}{\pi M_{He} RT}} \right\} + yd_z \frac{1}{3}\sqrt{\frac{8}{\pi M_{He} RT}}$$

N_2:

$$P = P_d + P_z = \left\{ x_d d_{d,d}^2 \frac{\left(p_h + p_l\right)}{64\mu_{He} RT} + x_d d_{d,d} \frac{1}{3}\sqrt{\frac{8}{\pi M_{He} RT}} \right\} + y\left(\frac{q_h - q_l}{p_h - p_l}\right)\rho D_T$$

APPENDIX III- Process hazard analysis

Table A.5. Process hazards, risks and recommendations

	Risk	**Recommendation**
High Pressure	-High pressure build-up in autoclave during synthesis	-Do not overfill autoclave
	- Off-gassing of volatile components during synthesis	-During synthesis place autoclave in an oven positioned inside a fume hood to prevent
	-Handling gas cylinders	-Wear protective eyewear
	-Leakage from gas cylinders	-Systematic testing of leaks after replacement of any parts in the system
	-Handling flammable gases	-Ensure gas detectors are active and connect outlet to fume hood
High Temperature	-During glazing, synthesis, drying and calcination of the membranes in oven	-Wear heat resistant gloves
High Flow	-Leak in the system	-Close gas cylinder in use